UNIVERSITE DE LIMOGES

ECOLE DOCTORALE SIMMEA
Sciences et Ingénierie en Matériaux, Mécanique, Energétique et Aéronautique

Faculté des Sciences et Techniques de Limoges

Laboratoire Sciences des Procédés Céramiques et Traitements de Surface

Thèse N° [-----]

Thèse

pour obtenir le grade de

DOCTEUR DE L'UNIVERSITÉ DE LIMOGES

Discipline / Spécialité : **Sciences des Matériaux**

Aleksandra Małachowska

Le 22 mars 2016

Analysis of the cold gas spraying process and determination of selected properties of metallic coatings on polymers

Thèse dirigée par Andrzej Ambroziak et co-encadrée par Lech Pawłowski

Président du jury		
Wojciech ZORAWSKI	Professeur	Université de Technologie de Kielce (Pologne)
Rapporteurs		
Thomas LAMPKE	Professeur	Université de Technologie de Chemnitz (Allemagne)
Didier CHICOT	Professeur	Université Lille 1 Sciences et Technologies (France)
Tomasz CHMIELEWSKI	Professeur	Université de Technologie de Varsovie (Pologne)
Membres du jury		
Andrzej AMBROZIAK	Professeur	Université de Technologie de Varsovie (Pologne)
Lech PAWLOWSKI	Professeur	Université de Limoges (France)
Jerzy NOWACKI	Professeur	Université de Technologie de Poméranie Occidentale (Pologne)

Wrocław University of Technology

Université de Limoges

Analysis of the cold gas spraying process and determination of selected properties of metallic coatings on polymers

PhD Thesis

by Aleksandra Małachowska, MSc, Eng

Tutors: Prof. Andrzej Ambroziak and Prof. Lech Pawłowski

Additional tutor: dr Tomasz Piwowarczyk

Wroclaw University of Technology (Poland) and University of Limoges (France)

December 2015

List of contents

List of figures

List of tables

List of symbols

A - cross-sectional flow area at given point [m^2]

A_t - cross-sectional flow area of the throat of the nozzle [m^2]

A_{pp} - outside area of the particle [m^2]

c - velocity of sound [m/s]

C_p - specific heat at constant pressure [J/kg/K]

C_v - specific heat at constant volume [J/kg/K]

C_D - drag coefficient

d_p - particle diameter [m]

F_d - drag force [N]

F_x - acceleration term [N]

F_1 - mechanical calibration (for cold spray 1.2), Schmidt model [1]

F_2 - thermal calibration (for cold spray 0.3), Schmidt model [1]

F_H - force at which the coating detached from the surface [N]

h - gas enthalpy

I - current [A]

k - heat transfer coefficient of gas[$W/m^2/K$]

l - distance between measuring probes [m]

m_p - particle mass [kg]

M - Mach number

M_p - particle Mach number

Nu - Nusselt number

p_0 - gas stagnation temperature [K]

p^* - gas pressure at throat [Pa]

p_i - inlet pressure [Pa]

p - gas pressure at given point [Pa]

p_s - shock pressure [Pa]

p_e - ambient pressure [Pa]

Pr - Prandl number

r - resistivity [Ωm]

R - specific gas constant [J/kg/K]

Re_p - particle Reynolds number

R_H - bond strength [MPa]

S_r - Cross-section of the conductive layer [m^2]

S - surface area of sample [mm^2]

T_m - Material melting point [K]

T_i - impact temperature [K]

T_R - reference temperature

T - gas temperature at given point [K]

T_i - gas temperature at the inlet of the nozzle [K]

T_0 - gas stagnation temperature [K]

T^* - gas temperature at throat [K]

T_p - particle temperature at given point [K]

T_{p0} - initial temperature of particle [K]

U - voltage [V]

V - gas velocity at given point [m/s]

V_i - gas velocity at the inlet of the nozzle [K]

V_p - particle velocity at given point [m/s]

v_{cr} - critical velocity [m/s]

v_i - particle impact velocity [m/s]

v_{er} - erosion velocity[m/s]

λ - thermal conductivity [W/m/K]

ρ - density [kg/m^3]

σ_u - yield strength [MPa]

σ_{TS} - tensile strength [MPa]

η - quality parameter equal to v_i/v_{cr}

γ - ratio of specific heat equal to C_p/C_v

ρ - density [kg/m^3]

ρ_p - particle density [kg/m^3]

ρ_0 - gas stagnation density [kg/m^3]

ρ^* - gas density at throat [kg/m^3]

μ - viscosity[kg/m/s]

μ_R - reference viscosity of gas [kg/m/s]

G - material constant [MPa]

D - material constant [MPa]

H - material constant [MPa]

Q - material constant [MPa]

ω - inelastic work fraction generating the heat

c - specific heat capacity

ϑ - Poisson's ratio

Ω - temperature-dependent scalar function

π - temperature-dependent scalar function

α_{th} - thermal expansion coefficient,

Subscripts

e, ve, p - elastic, viscoelastic, plastic

1. Thermal spraying methods.

Following its definition (DIN EN 657), thermal spraying is a process in which molten, semi molten or solid particles are deposited on a substrate while the surfaces to be coated are not molten. The layer is built up by superposition of the particles [2]. This technology is believed to be invented by Switzerland's engineer Schoop in early 1900s. The legend said that this discovery was made during observation of children shooting Flobert guns. He noticed that small lead balls formed splats after hitting the wall [3]. Since then, it is constantly under development and the new techniques are introduced.

Currently used thermal spray methods may be classified by considering the type of heat source (Fig. 1). The flame and electric arc spray processes are used as a cheap solution for parts with low technical requirements as the porosity and oxygen contents is higher than in other methods. Plasma spraying is usually applied for ceramic coatings [4] and HVOF process for producing metal and cermet coatings [5]. Cold spray method is used to deposit mostly metallic and composite coatings. The only requirements is the ductility of the powder [4, 6].

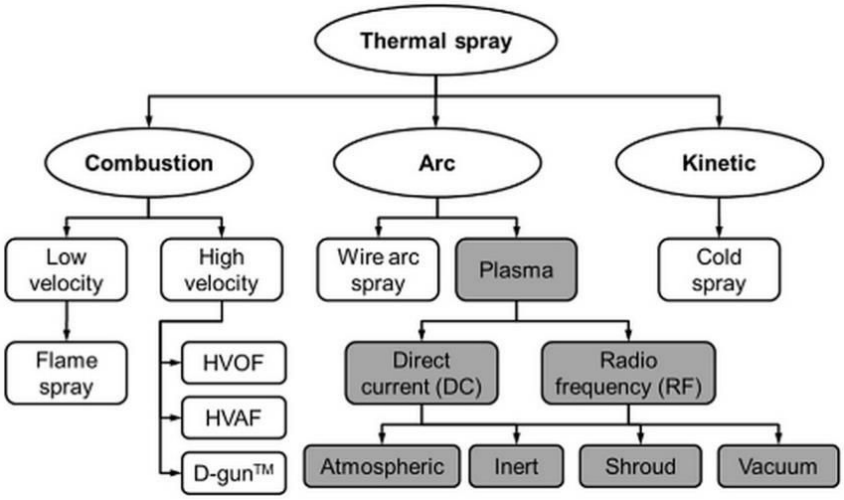

Fig. 1 Classification of thermal spray method [7]

There are two basic process parameters which may be modified during spraying to obtain adherent coating, namely temperature and velocity [4, 8]. In traditional thermal spraying methods i.e. flame spray, the feedstock material must be rendered molten or semi molten in order to achieve coating. The structure of consolidated deposit is composed of unmelted or incompletely melted particles, fully melted splats, certain level of porosity and varying amount of inclusions resulted from oxidation during spraying. The exact structure depends on type of the used process, selected operating conditions and material

being sprayed [9]. It was observed that higher particles velocity results in higher bond strength, density of the coating and lower oxide content due to less in-flight reaction with atmosphere [10, 11]. Therefore, the trend in thermal spraying goes towards increasing it. The particles velocity increased from circa 150 m/s in flame spray to about 1200 m/s and above i.e. in cold spray (Fig. 2) [12]. At the same time it is possible to reduce temperature of the process [4].

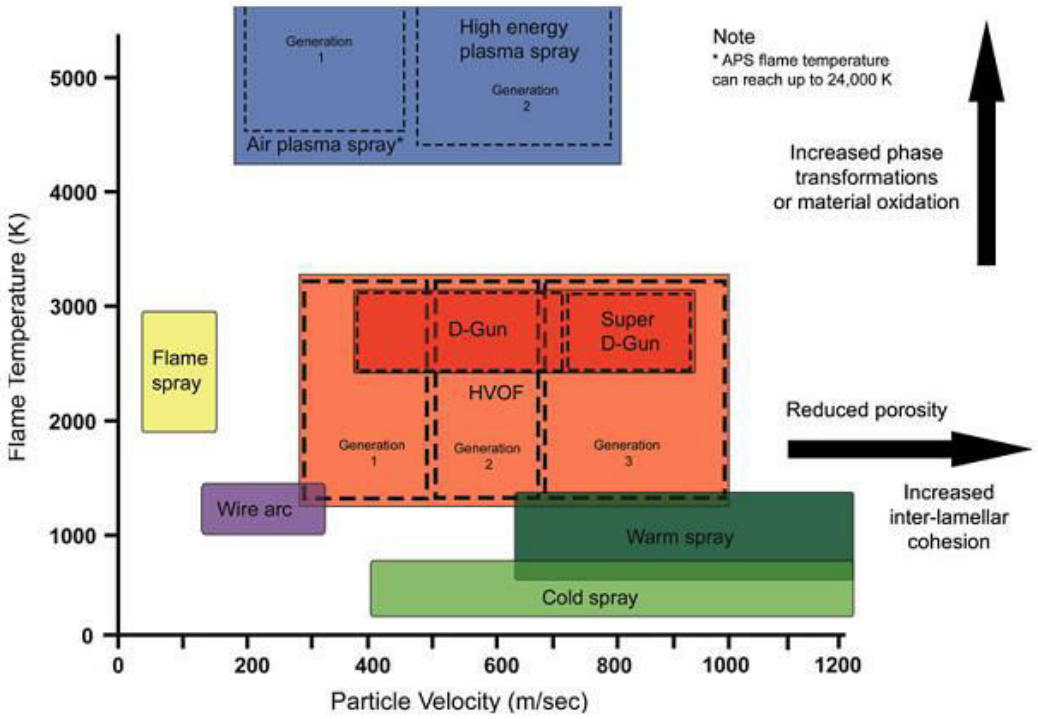

Fig. 2 Classification of thermal spray processes in terms of velocity and temperature [13]

The most important advantages of thermal spraying are [14]:

- variety of material - virtually any coating material can be used (metals, ceramics, cermets, plastics)
- low thermal stress on substrate parts
- local and reinforced coatings possible
- processes are available as field services
- nearly any substrate material can be coated
- high deposition rates (coating thickness from 20µm to several millimeters)

2. Cold spray method.

Cold spray method was invented by scientists from Institute of Theoretical and Applied Mechanics of the Siberian Branch of the Russian Academy of Sciences (ITAM of RAS) in Novosibirsk, Russia in the mid-1980s [15]. It uses high kinetic energy of powder particles to achieve a bonding with a substrate. Highly pressurized hot gas (Air, He, N) is accelerated inside usually convergent-divergent nozzle [16, 17]. But applying different shape i.e. convergent-barrel, convergent-divergent-barrel is also possible [4, 18]. The powder is fed into the gas flow through a separate line and accelerated due to drag force before striking the substrate.

The formation of coating is related to velocity of powder particles. Each material may be defined by critical velocity v_{cr} above which the particles are sufficiently plastically deformed and adhere to the substrate, forming a coating. Below v_{cr} mostly erosion and particles rebounding occur [4, 17]. The deposition efficiency and bond strength increases with particles velocity until reaching erosion velocity v_{er} when again erosion appears. This scheme is only valid for ductile materials. In case of ceramic erosion is prevalent regardless the velocity [16]. The other important parameters influencing bonding formation are: particles oxidation, particles size, particles temperature, substrate and coating material properties [17, 19, 20]. Numerous numerical and experimental studies have been done to explain the nature of the bonding between metal particles and substrates. Nowadays, it is commonly believed that the microscopically detectable adiabatic shears bands occur in highly deformed region when particles velocity exceeds critical one. Thermal softening of material plays also important role [16, 21, 22].

The low and high pressure cold spray devices are available. The devices differ by type of working gas, its pressure and, by the way of powder feeding [4, 23]. Depending of the process parameters (gas temperature and pressure, powder particle size, shape of the nozzle and spraying distance) and applied gas the powder particles impact velocity reaches 200-1200 m/s or even more [24]. The powder size varies from 5 to 150 μm [24].

2.1. High pressure system

In high pressure cold spray (HPCS) usually nitrogen or helium under pressure up to 5 MPa and temperature reaching 1373 K (Impact Spray System 5/11) is used. This allows obtaining velocities up to 1200 m /s and depositing wide range of materials such as Al, Cu, Cu-Sn, Ni, NiCr, Ni-Al, Ta, or Ti. The operating principle of HPCS system is shown at

Fig. 3. The highly pressurized gas is heated and supplied to the convergent-divergent type of nozzle which accelerates the gas to the supersonic velocity while reducing its temperature. The powder is usually fed axially through a separate carrier gas line to the gas stream before the nozzle throat. It gains the velocity from the gas and after leaving the nozzle impact at the substrate. Whole process is control through a control unit [4].

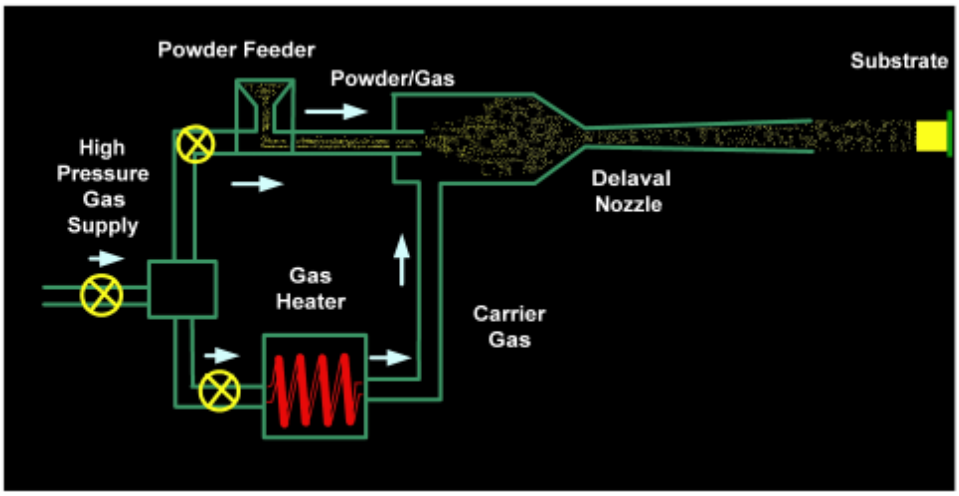

Fig. 3 Schematic presentation of HPSC system [25]

2.2. Low pressure system (LPCS)

The low pressure cold spray method (LPCS) (Fig. 4) is the process in which the pressure usually does not exceed 1 MPa and the temperature varies between room temperature and 873 K [26]. As spray gas usually air or nitrogen is used. Due to relatively low powder particles velocity the range of spraying materials is limited to low strength material Sn, Zn, Al, Cu and Ni. Typically to increase deposition efficiency of the process as well as bond strength some addition of ceramic powder (usually Al_2O_3 or SiC) is added [27–29]. Apart from gas pressure HPCS and LPCS method have different powder feeding solution. In the latter powder is fed radially, usually through underpressure. There is also different solution for gas preheating which in LPCS system is done only by heater placed in spraying gun. Although the powder feed rates in LPCS method are lower than in HPSC, particle concentration in gas stream is higher. This is due to normal shock wave layer with a higher concentration of powder particles. The particles which rebound from the substrate surface collide with particles from the powder jet and decreasing their velocity, which affect strongly deposition efficiency [4, 29]

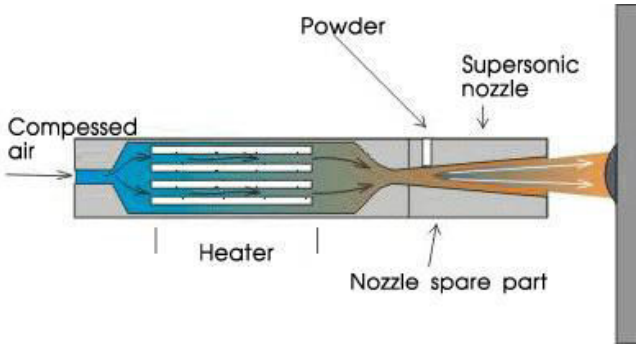

Fig. 4 Schematic presentation of LPCS system [30]

The main advantages of the LPCS method are much lower cost of equipment purchase, as well as the cost of process gases, and the mobility of the system. The main difference between HPCS and LPCS process are presented in Tab. 1

Tab. 1 Comparison of HPCS and LPCS system [4].

Parameter	**HPCS**	**LPCS**
Process gas	N_2, He, mixture	Air, N_2
Gas pressure [MPa]	1-5	0.1-1
Gas temperature [K]	293-1373	293-873
Gas flow rate [m3/h]	0,85-2,5 (N2), max. 4,2 (He)	0,3-0,4
Powder feed rate [kg/h]	4,5-13,5	0,3-3
Spraying distance [mm]	10-50	5-15

3. Coating building

The preliminary condition to form a coating is exceeding critical velocity (v_{cr}) by powder particles [31]. Formation of the coating is presented in Fig. 5. It may be divided in two basic stages: spraying of the first layer of particles on a substrate and subsequent buildup of the coating. During first stage arriving particles activate the surface by removing the oxide layer and increasing its roughness. Some of the particles leave attached to the surface what additionally decrease activation energy of the particle-substrate interaction. It was observed that adhesion of first particles leads to a rapid increase of subsequent attached particles. This may be observed in form of delay time before forming a coating [32].

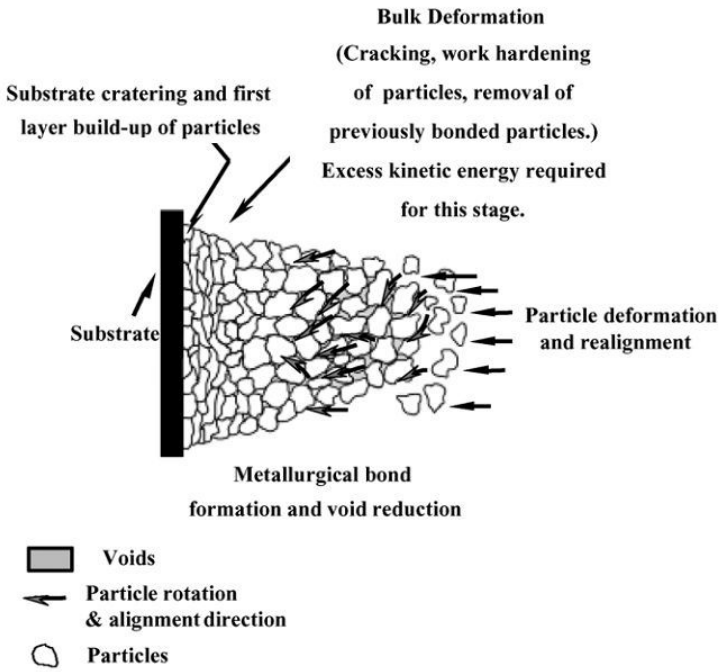

Fig. 5 Formation of coating in cold spray process [32]

The first stage is related to particle and substrate properties (roughness, hardness etc.) as well as on the state of the surface which is changing during bombarding process [24]. The first stage is responsible for adhesion strength the second one for cohesion inside the coating [33]. In the second stage the particles stick to the first layer, deform and build up multilayer coating. During further spraying process void reduction and metallic bonding occur as a result of hammering already deposited particles by upcoming ones. The peening process may lead to the hardening of the coating and formation of compressive type of stress in it [34]. At the same time, there is a grit blasting process during all the stages which coexist with deposition process and is particularly visible when the particles velocity is low. The particles that not stick clean and roughen the substrate so the thick coating is built only when more particles stick than is rebounded [32]. Coating formation process is reflected in its structure (Fig. 6.) The densest area is situated near substrate material due to peening effect.

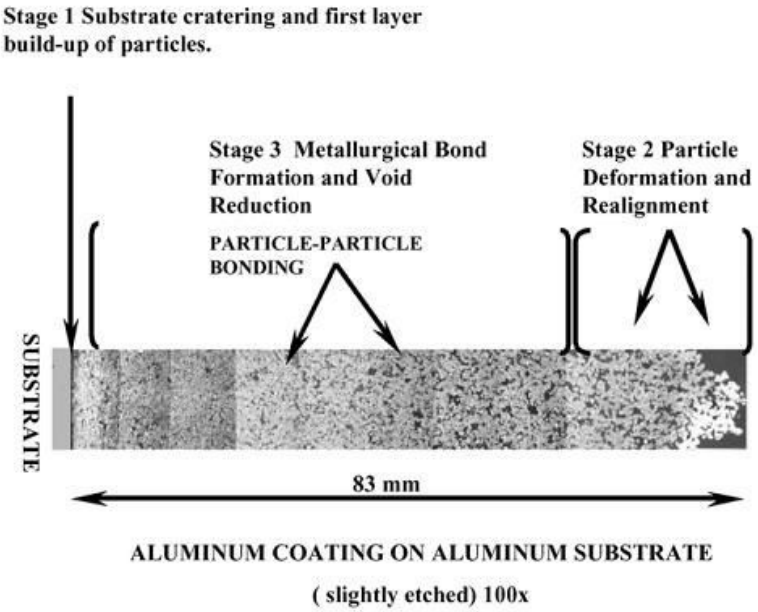

Fig. 6 Optical photo of Al sample prepared at 588 K illustrating coating formation process [32]

In case of spraying metal-ceramic mixtures "activating" role of ceramic particles increase deposition efficiency [35]. Particularly for aluminium-alumina and copper-alumina powder mixtures deposition occurred at significantly lower gas temperature and pressure than in case of pure metallic powders. These results were used in low-pressure cold spray method.

3.1. Critical velocity

Critical velocity is a key concept in cold spray method [36]. It is defined as velocity that an individual particle of powder muss attain in order to deposit after impact with the substrate (Fig. 7) [4] This definition is valid for ductile material, brittle material like ceramic will cause erosion for any velocity at temperature below their melting temperature [16]. Critical velocity depends mostly on sprayed material mechanical properties but varies also with particle size, particle morphology, particle impact temperature or powders oxidation [1, 21, 37].

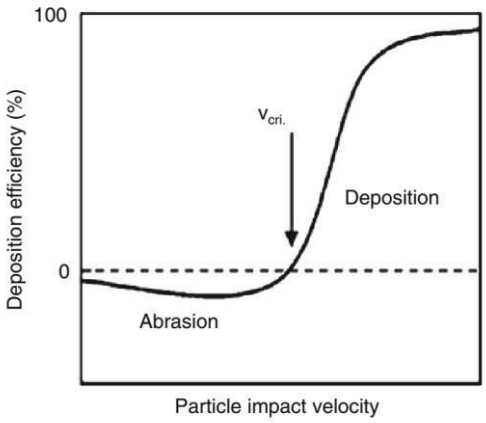

Fig. 7 Schematic of the correlation between particle velocity and deposition efficiency. The transition between abrasion and deposition defines the critical velocity Vcr [38]

Assadi et al [21] developed numerical model for copper particles and extended it to other materials. The effect of various material property was summarized in form of equation [21]:

$$v_{cr} = 667 - 0.014\rho + 0.08(T_m - T_R) + 10^{-7}\sigma_u - 0.4(T_i - T_R) \quad (1)$$

Where: ρ – density, σ_u – Yield strength, T_m – Melting point, T_i – Impact temperature, T_R – Reference temperature (293 K).

More advanced model was proposed by Schmidt at all [1]. It takes into account specific heat, tensile strength, mechanical and thermal calibration and it is given by equation [1]:

$$v_{cr} = \sqrt{\frac{F_1 \cdot 4 \cdot \sigma_{TS} \cdot \left(1 - \frac{T_i - T_R}{T_m - T_R}\right)}{\rho} + F_2 \cdot C_{pp} \cdot (T_m - T_i)} \quad (2)$$

Where: ρ – density, σ_{TS} – tensile strength, T_m – Melting point, T_i – Impact temperature, T_R – Reference temperature (293 K), c_p – specific heat of particle, F_1 – Mechanical calibration (for cold spray 1.2), F_2 – Thermal calibration (for cold spray 0.3).

This equation does not take into account particle size which is important factor. With decrease in particle size critical velocity increase. The possible reason for higher critical velocity of small particles may be higher content of oxides or adsorbents hindering the bonding. Usually powder contains a mixture of particles with various diameters. In such case critical velocity is calculate for larger particles due to fact that smaller

particles achieve higher velocity [1].Calculated critical velocities for different metals are presented in Fig. 8.

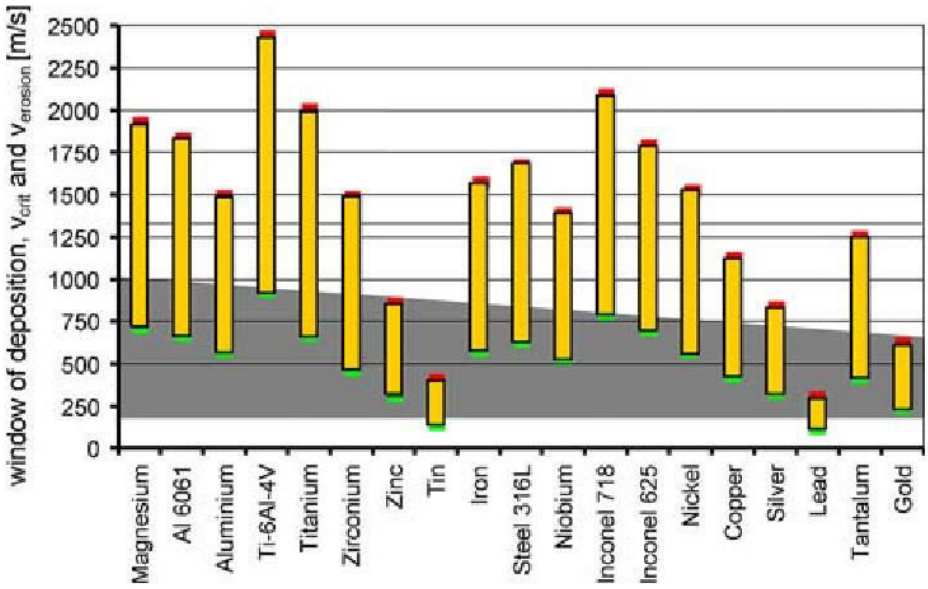

Fig. 8 Calculated critical velocities and widows of deposition for selected metals. The calculation were performed for and impact temperature 293 K[16]

Assadi et al [39] introduce also a concept of η ratio with is given as v_i/v_{cr}, where v_i -impact velocity, v_{cr} – critical velocity. This coefficient allows predicting deposition efficiency and mechanical properties of the coating i.e. bond strength (Fig. 9).

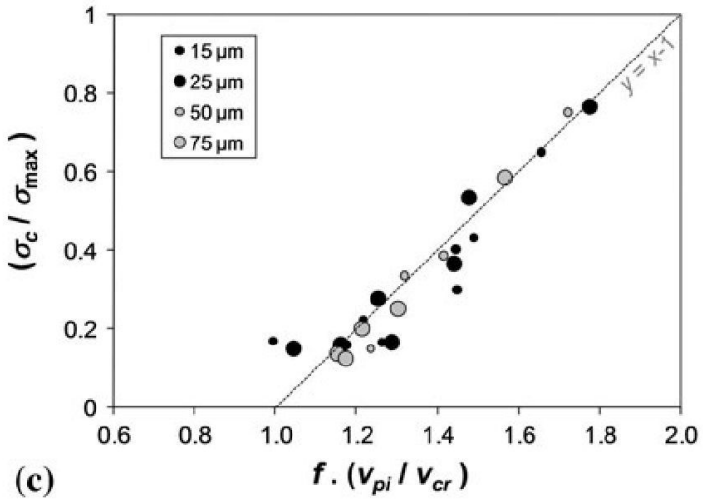

Fig. 9 Measured values of cohesive strength of cold sprayed copper coatings normalized with respect to a reference value of 300 MPa (tensile strength of highly deformed bulk copper in a TCT test) in function of η coefficient [39]

The dependence between bond strength and η ratio results from the fact, that the higher the impact velocity in relation to the critical velocity the higher is the bonding area between

particle and substrate (Fig. 10). When this area reaches 100 % of contact surface the maximum bond strength is obtained equal even to the strength of bulk material [40]. However it should be mentioned that the increase in the particles velocity is possible only to the certain value above which there is no positive effect on deposition efficiency and properties of the coating and erosive effect start to occur due to excessive deformation [16].

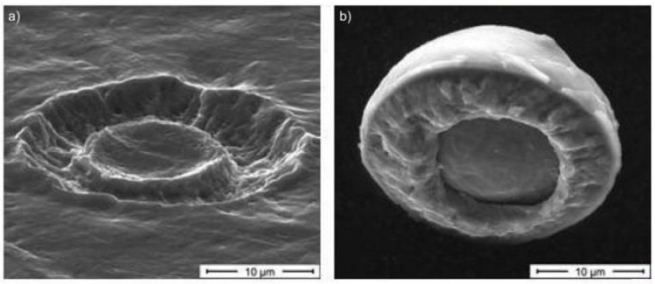

Fig. 10 Crater after detached Ti-6Al-4V particle on Ti (parameters T = 1053 K, p = 3,8 MPa, nitrogen) (a) and the particle (b) [40]

This second threshold velocity is called erosion velocity, v_{er}. It is usually two or three times higher than critical velocity [16]. The area between v_{cr} and v_{er} for given particle impact temperature is called window of deposition (Fig. 11). In case of ductile material at certain velocity deposition begins. A further increase in velocity improve deposition efficiency until reaching saturation point, at which optimum coating properties may be expected. Afterwards decrease in deposition efficiency with increasing velocity is observed due to erosive effect caused by hydrodynamic penetration of the substrate by the particles. At the point where deposition changes to erosion, the erosion velocity is defined [16].

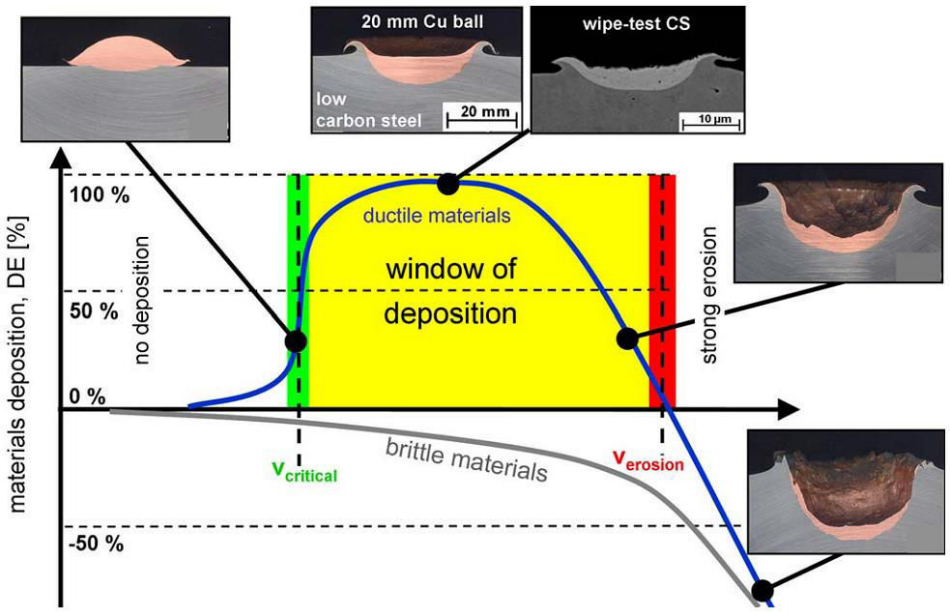

Fig. 11 Correlation between particle velocity, deposition efficiency and impact effects for a constant impact temperature [16].

The erosion velocity is strongly depended on the particle size [41]. Wu et al [41] presented critical and erosion velocity in function of particle size by comparing the adhesion velocity to the rebound energy (Fig. 12). For larger particle the erosion velocity become as low as critical velocity, therefore there is no deposition window and big particles can not be deposited on the substrate with any impact velocity [41].

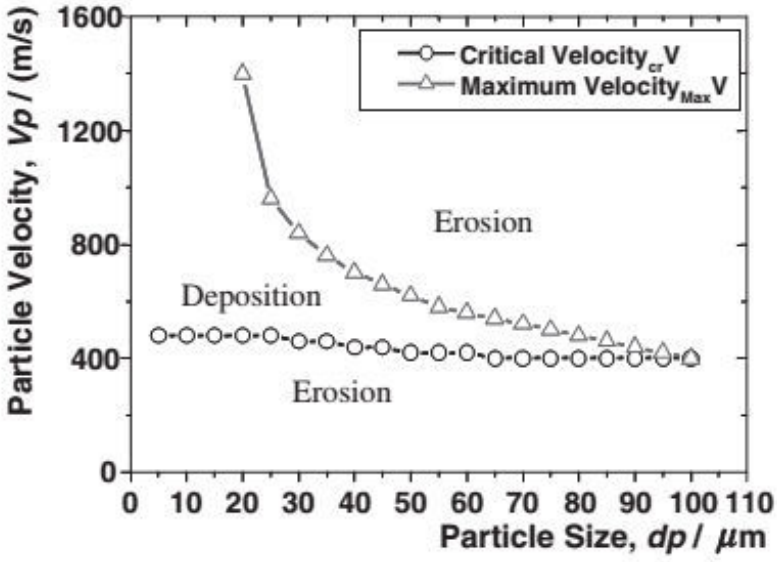

Fig. 12 Calculated critical velocity and maximum velocity for Al-Si feedstock containing particles with different diameters onto mild steel substrate [41]

3.2. Bonding formation

Although impact phenomena have been studied both numerically and experimentally the actual bonding mechanism is still not completely clear. It is commonly believe that particles and substrate undergo extensive localized plastic deformation due to impact. It enables to remove oxide layer and hence intimate contact of clean metallic surfaces [22, 32, 42–44]. The impact stress applied to the particle, when the velocity was sufficient, is generally higher than its yield stress hence the deformation is plastic. In case of isotherm conditions there is a monotonic increase of flow stress with plastic strain. However, upon impact, high-plastic strain rates occurs in the particle/substrate contact zone and due to the very short time of acting, result in adiabatic heating [22, 45]. Grujicic et al [22] estimated that more than 90% of impact energy is converted into heat which causes local softening of the material [22]. Additionally, in real materials there are fluctuation in stress, strain, temperature, microstructure and strain softening which result in plastic flow (shear) localization. Consequently, softening become highly localized, shearing and heating in surrounding material area practically stop and the flow stress drops to zero (Fig. 13) [22].

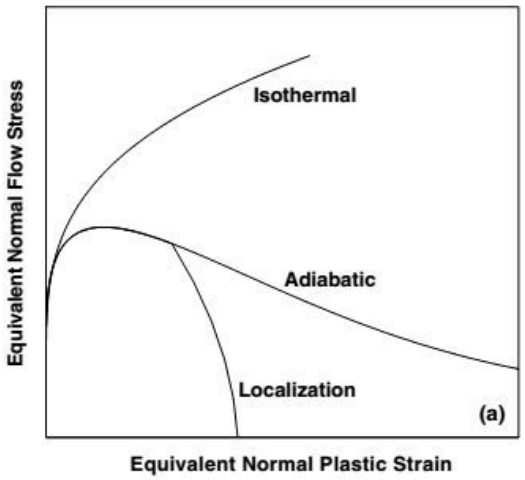

Fig. 13 Stress-strain curves in a solid for isothermal, adiabatic, and localized deformation [22]

These phenomena were studied deeper using numerical simulation using Lagrangian [1, 16, 22], Eulerian [46] or SPH (smoothed particle hydrodynamics) [47] principle. Schmitdt et al [1] observed that in the beginning of the particle impact strong pressure field propagates spherically from the point of contact. The pressure gradient at the gap between particle and substrate generates a shear load which accelerates material laterally and by that causes localized shear straining. When the impact pressure is high enough, this shear straining leads to adiabatic shear instabilities [1]. Consequently, as was described, rapid rise in strain and temperature occur and immediate breakdown of

stress [1, 22]. Material starts to flow viscously in the contact region and form a jet (Fig. 14). At the highly deformed interface, oxide layers are broken, heated material are pressed together and hence bonding is possible [1]. The evidence of ruptured oxide layer was found experimentally i.e. in aluminum coating [48].

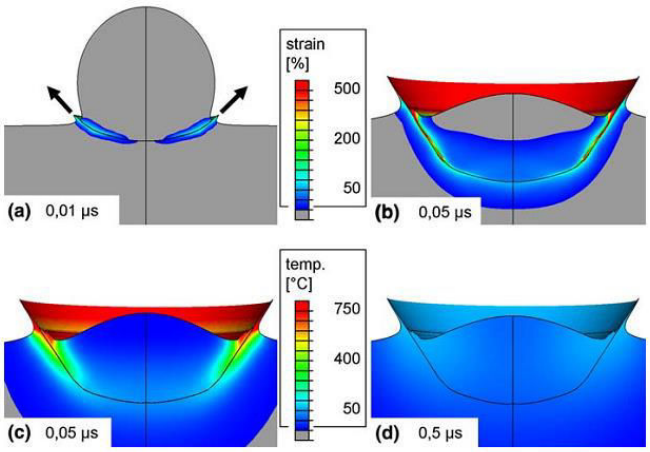

Fig. 14 Impact of a 25 µm Cu particle to a Cu substrate with 500 m/s at an initial temperature of 20° C. Strain field (a,b) and temperature field (c, d) [16].

Schmidt at al [1] claimed that for bonding strength the cooling rate is very important factor. From one side it should be low to promote shear instability, from the other one high enough to enable interface solidification before the particle bounces back. Additionally bond strength should be high enough to prevent particle detachment by elastic 'spring-back' forces [1].

The experimental confirmation of metal bonding was the presence of diffusion areas and intermetallic phases reaching several hundred of nanometers in areas where highest temperature was predicted by numerical simulations [49, 50].

The bonding phenomena is cold spray is also prescribed to other mechanism. The most contributing seems to be mechanical interlocking [44, 51]. Hussain et al [51] used the formation of intermetallic phases during annealing as indicator of surface area where oxide film was removed during spraying and metal-to-metal contact is possible. This principle was first introduced by Prince et al [52]. It turned out that intermetallic area fraction was strongly depended on the substrate preparation and together with increase of this area there was an increase in bond strength. Apart from metal bonding strong influence of mechanical interlocking was observed [53].

3.3. Numerical simulation

The sudden rise in temperature curves from simulation, indicating critical shear instabilities, is used for determining critical velocity. The threshold value amounts 60% of the material melting temperature as this is minimum interface temperature for bonding [16]. Value of critical velocity varies with particle size (Fig. 15).

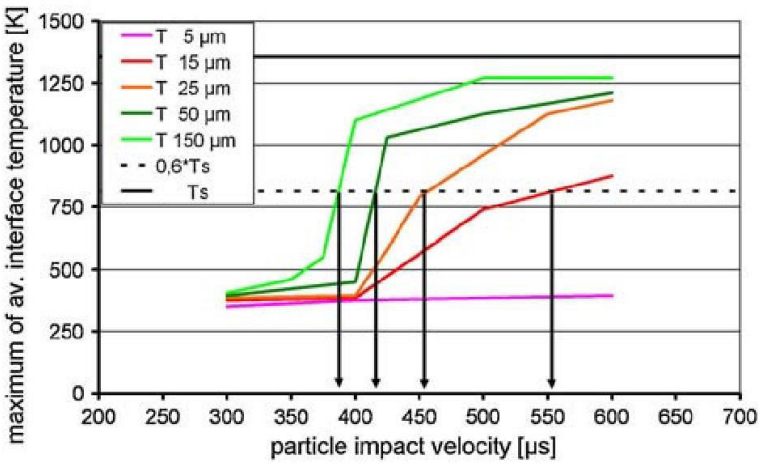

Fig. 15 Maximum interface temperature in function of impact velocity, plotted for different particle sizes [16]

Values of critical velocity decrease with the mesh size for the same material. It turned out that for different materials they tend to be in the range 300-400 m/s, including even high strain materials i.e. In718 alloy [54] which is much lower than previously reported values [1, 22]. Additionally, according to [55] strong dependence of critical velocity on the oxidation state of Cu particles exist i.e. for low oxidized Cu particles the critical velocity amounts only ~ 300 m/s. This dependence was confirmed for Al powder by Kang et al [56]. Therefore it was suggested by Li et al [57] that values of critical velocity previously calculated by Assadi et al [21] and Grujicic [22] at all are in coincidence with experimental results for powders with certain oxygen content.

It was proved that numerical simulation give results in good agreement with metallographic examination (Fig. 16) [49].

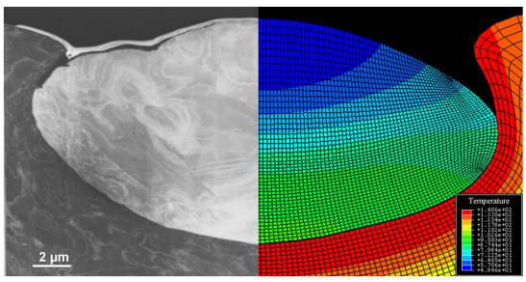

Fig. 16 Comparison of final deformation of copper particle from TEM (left) and simulation (right) [49]

3.4. Particle and/or substrate preheating

Higher temperature of the gas apart from increasing particle velocity leads also to higher particles temperature [58, 59]. The deposition efficiency tends to increase when particle/substrate temperature increase due to thermal softening which is beneficial for bonding [1, 21]. In was shown for Cu particles deposited on Cu substrate that preheating enlarge so called thermal softening zone, defined as region in which temperature is greater than 0.5 T_m, thermal softening and work hardening coexist and intensive deformation may be expected. If it sufficiently high thermal softening zone may be even spread to whole particle. Additionally, in case of high-temperature particles, a more prominent metal jet is formed at the rim [60]. Consequently preheated particle is more likely to deposit on the substrate and the deposited coating is characterized by lower hardness due to eliminating of work hardening [60]. It was demonstrated by Kim at al [61] that powder preheating facilitates deposition of WC-12%Co coatings. In cold spray system the particles may be heated separately from the spray gas due to heating carrier gas. A gas heater is usually added downstream of the powder feeder, possibly close to the injector [45, 61].

There are also disadvantages of preheating of particles. If they are heated to much they become sticky, start sticking to interior walls of nozzle. In consequence control of powder mass flow is difficult and nozzle clogging may occur. Additionally surface oxidation may increase especially when air is used as spray gas [45].

3.5. Particle Oxidation

It was shown that [55, 56] that critical velocity increases significantly with increase in oxygen content in the feedstock material. In case of Cu powder the critical velocity amounted ~300 m/s for oxygen content 0.02 wt.% and ~600m/s for oxygen content 0.38 wt. %. This effect was also observed for Monel alloy and 316L stainless steel powder [62]. The reason is hindering of deformation of particle by brittle and hard oxide. It was shown by Li et al [43] that although oxide layer has little influence on compression ratio of Al particles it affects maximum effective plastic strain. Additionally with increasing oxide thickness formation of jet becomes difficult. Oxide layer crashed during impact could not be cleared fully in central region of interference [63] and the parts of it may be incorporated into the coating [43]. In both cases the bonding is weakened.

3.6. Impacting Angle

Impacting angle is an important factor regarding spraying efficiency in cold spray method [36, 64]. It decreases sharply with decrease in the impacting angle. It can be noted for lower angles that metal jet is formed only at one side of deformed particle (Fig. 17).

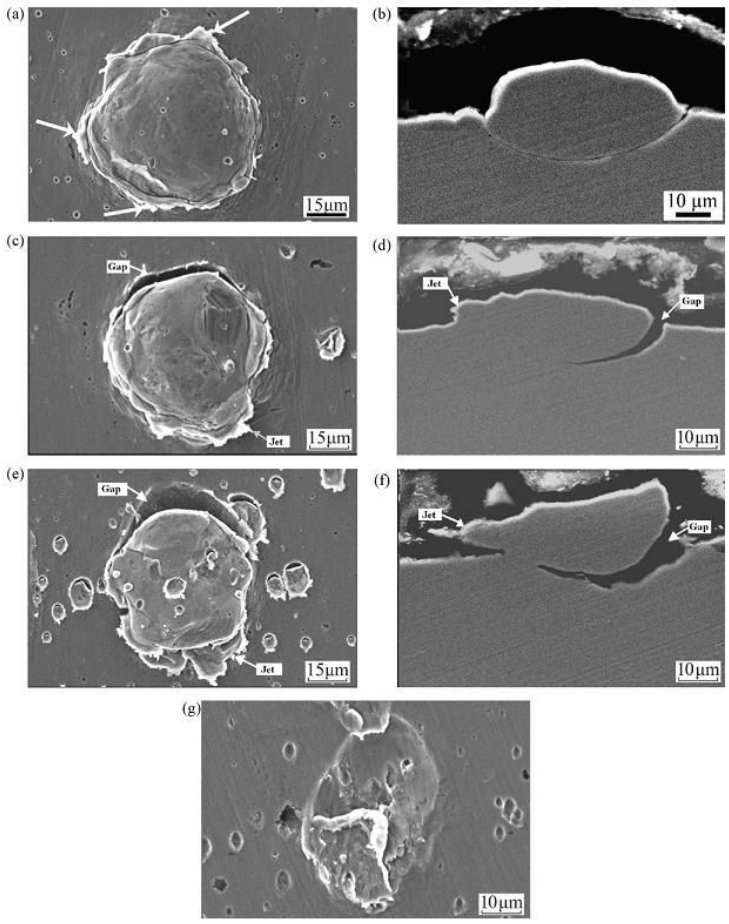

Fig. 17 Results of individual deposited copper particles on polished copper surface. Surface (a) and cross-section (b) for incident angle of 90°; surface (c) and cross-section (d) for incident angle of 70°; surface (e) and cross-section (f) for incident angle of 50°; surface (g) for incident angle 30° [65]

Additionally the tangential movement of the particle may be observed which could lead to the gap between particle and substrate and deteriorating the bonding. Li et al [66] estimated that the drop of relative efficiency is important below 70° (Fig. 18). For angles lower than 30 ° in case of spraying copper, only cratering was observed [65]. On the other side the maximum deposition efficiency may be not present at the normal angle as in some angle range deposition efficiency may be promoted by shear friction [65].

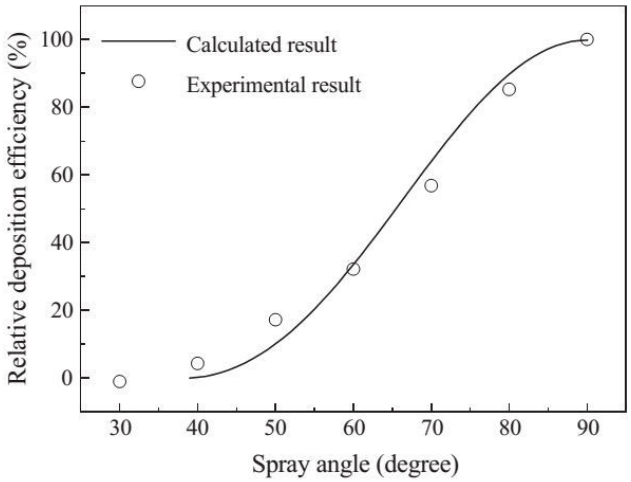

Fig. 18 Relative deposition efficiency calculated theoretically with those measured under nitrogen operated at the inlet pressure of 2 MPa and temperature of 613 K in function of spray angle [66]

3.7. Loading effect

The thickness of the coating may be controlled among other by varying the mass flow rate of feedstock. The dependence between mass flow rate and coating thickness is linear until maximum powder mass flow rate is reached for which too many particles impact the surface causing delamination of coating (Fig. 19). This effect may be reduced by increasing the taverse speed of the substrate or increasing gas temperature [67]. Although it is known that increasing amount of the powder in the gas stream reduces particles velocity Taylor et al [67] shown that this effect is too small to explain peeling of the coating. The majority of the particles should be able to reach and maintain velocity higher than critical one. Consequently this phenomena may be clarified by residual stresses caused by excessive surface bombardment per unit area of substrate [67].

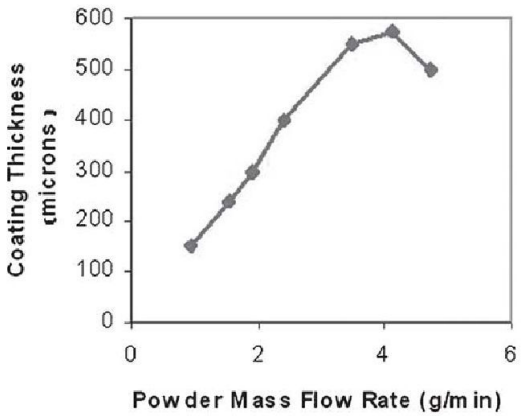

Fig. 19 Coating thicknesses as function of the powder mass flow rate [67]

3.8. Substrate effect

Substrate hardness with respect to that of impacting particles plays important role in the deposition process i.e. 316L particles hardly deform on aluminum substrate and copper particles can hardly form craters in steel substrate [68, 69]. Vlcek at al [69] distinguished three possibility of particle/substrate interaction and concluded that with decreasing deformability of substrate increase ease of bonding:

- Substrate material with higher deformability – in this case powder particles penetrate to a certain degree into substrate and their deformation level is low. Good interlocking and adhesion may be expected.
- Corresponding deformability – particles and substrate deform during impact. The deposition begin after a delay time, necessary for roughening the substrate
- Particle material exhibiting higher deformability- in this case particles are not able to penetrate the substrate. Hardly or no substrate deformation occurs. The interlocking between particles and substrate is poor and adhesion is very low.

On the other hand Zhang at al [70] observed much more complex relationship between substrate properties and deposition process of aluminum powder. The initiation of deposition on soft metallic substrate was difficult due to lack of deformation of the aluminum particles. In case of tin substrate even melting of tin occurred. The deposition on harder substrate was much more favorable. Deposition on nonmetallic substrate (polymers and ceramics) was also not successful due to among other lack of ability to form metallic bond, low hardness of polymer etc. [70].

The importance of substrate/feedstock hardness ratio was also observed by Hussain et al [53]. He noticed the asymmetry in bonding formation for aluminum and copper depending on which material was the substrate and which a feedstock. For copper sprayed on aluminum much better bond quality was obtained than inversely.

4. Electrical conductivity of cold sprayed coatings

The main difference between cold spray and other thermal spraying methods which is emphasized is high conductivity of as sprayed coatings which can be additionally improved through heat treatment [38]. Cold sprayed coatings may reached even 90 % of conductivity of bulk copper [71]. Koivuluoto et al [72] reported the conductivity values to be 79 % IACS for HPCS, and 46 % IACS for LPCS sprayed coatings; they increased to 90 % IACS for HPCS and 69 % IACS after heat treatment (673 K, 2 h). The coatings were sprayed with spherical powders. In case of other method atmospheric plasma or HVOF heat treatment did not bring such spectaculars results [73]. The effect of heat treatment and process parameters on coatings conductivity was also evaluated by Sudharshan et al [74]. It was concluded that conductivity is significantly influenced by cold work and porosity of the coatings and may be improved through heat treatment. Porosity increase from 0.1 to 0.8 % caused conductivity decease from 19.1 to 4.1 MS/m (resistivity from 5.246 μΩcm to 24.39 μΩcm).

Venkatesh et al [75] investigated influence of spraying parameters on coatings deposited with dendritic powders. The lowest conductivity - 7.12 ms/m was recorded for gas temperature 673 K and pressure 1.4 MPa and highest - 20.53 ms/m for gas temperature 723 K and pressure 2.2 MPa which can be recalculated to resistivity 14.0 μΩcm and 4.87 μΩcm respectively. The conductivity was related to extent of recrystallization and porosity. Recrystallization depends on particles velocity and particles temperature. First factor is good known relation often correlated to critical velocity [39] and partially determined by gas preheating temperature, but gas preheating temperature and consequently particles temperature (independent on the velocity) additionally facilitates deformation and increases recrystallization. Porosity turned out to be only related to particles velocity and independent on particles temperature [75]. In other study copper coatings sprayed with granular powder at 673 K and 2 MPa reached resistivity at the level of 13 μΩcm [76]. Friction heat generation during impact of granular powder was higher than for spherical one and has beneficial effect on recrystallization and therefore resistivity [76] .

Dendritic copper sprayed on the polymers PVC reached resistivity of 11.39 μΩcm for spherical particles interlayer and 9.43 μΩcm for tin interlayer [77].

5. Gas thermodynamics in cold spray process

One of the major characteristics of cold spray process is using high-speed gas jet [4] as higher particles velocity results in better coatings properties i.e. bond strength [39]. The supersonic flows are usually obtained with convergent-divergent nozzle so called de Laval nozzle but the other type are also used including convergent-divergent-barrel [78, 79, 79] and convergent barrel [79, 80]. There are several methods to calculate the gas flow during cold spray. Computational fluid dynamics is used to simulate complex phenomena in two and three dimensions. For rough approximation usually one-dimensional approximation is sufficiently correct and usually used for calculation particles velocity at the nozzle exit [4]. For one dimensional flow it is assumed that all fluid properties are uniform over any cross section of the duct. More strictly it is taken that the rate of change of fluid properties normal to the streamline direction is very small compare to the rate of change along the streamline. The main advantage is great simplicity of this method and hence it is used for calculation of variety of engineering problems [81].

The gas flow in cold spray process is treated as [82]:

- isentropic (adiabatic and frictionless)
- ideal with constant specific heat
- compressible
- influence of powder flux on the gas flow is neglected.

The isentropic assumption is true apart from very thin layer near walls. In converging-diverging nozzle a large part of the thermal energy of the gas is converted into the kinetic energy. The gas pressure and temperature drop greatly and its velocity reaches supersonic values. In case of any obstruction or a wall protrusion the kinetic energy is locally converted back into thermal energy. Hence the nozzle inner walls should be smooth [83].
It is usually assumed that for flows with Mach number above M = 0.3, the compressibility effect may become noticeable [84] In cold spray process the flow is very fast (supersonic M>1) , the pressure ratio is large hence the kinetic energy the density changes may become dominant terms in the mechanical energy balance [85]

$$M = \frac{velocity\ of\ gas}{velocity\ of\ sound\ in\ the\ gas} = \frac{V}{c} \tag{3}$$

The fundamental assumption of compressible flow are following [82, 86]:

- The gas is continuous, what is valid for vacuum or very low pressure conditions
- No chemical changes occur in the flow
- Both specific heats at constant pressure C_p and constant volume C_v, are constant.

- Gravitational effects on the gas flow field are negligible
- Magnetic and electrical fields are negligible

When above assumption are satisfied then the flow field can be derived using following principles:

- Conservation of mass (continuity equation)
- Conservation of momentum (Newton's Law)
- Conservation of energy (first law of thermodynamics)
- Equation of state

The equations are solved simultaneously for four unknowns: temperature, pressure, density and flow velocity.

5.1. Isentropic flow through the nozzle

During isentropic flow of fluid through a passage of varying cross sections all possible states lie on a line of constant entropy. One of these states is state with zero velocity, at which the gas properties p, T are called stagnation properties and denoted with index *0* (Fig. 20) [81].

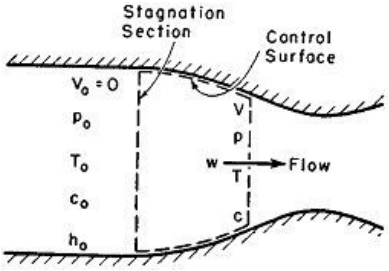

Fig. 20 Flow between stagnation region and other sections [81]

For one dimensional flow the mass equation is simplified. The mass per second is given with: ρAV , where ρ = mass density, A = area of cross-section, V = velocity and according to mass conservation law given by equation:

$$\rho AV = const \tag{4}$$

Hence in differential form the equation (4) takes form [87]:

$$\frac{d\rho}{\rho} + \frac{dA}{A} + \frac{dV}{V} = 0 \tag{5}$$

For one dimension when concerning flow from point 1 to point 2 the equation (5) can be reduced to:

$$p_1 + \rho_1 V_1^2 = p_2 + \rho_2 V_2^2 \tag{6}$$

The energy equation for one dimensional flow is given in simplified form:

$$h_1 + \frac{V_1^2}{2} = h_2 + \frac{V_2^2}{2} \tag{7}$$

where: h –enthalpy. This gives the expression in differential form

$$dp = -\rho V dV \tag{8}$$

Substituting equation (8) into (5) and using isentropic assumption:

$$dp / d\rho = \left(\partial p / \partial \rho\right)_s = c^2 \tag{9}$$

Following equation is obtained:

$$\frac{dA}{A} = \frac{dp}{\rho V^2}\left(1 - \frac{V^2}{c^2}\right) = \frac{1 - M^2}{\rho V^2} dp \tag{10}$$

This has following practical significance:

i) For subsonic speeds (M<1)

$$\frac{dA}{A} > 0; \frac{dA}{V} < 0 \tag{11}$$

ii) For supersonic speeds (M>1)

$$\frac{dA}{A} < 0; \frac{dA}{V} > 0 \tag{12}$$

iii) For sonic speeds (M=1)

$$\frac{dA}{A} = 0; \frac{dA}{V} = 0 \tag{13}$$

It means that for subsonic region M<1, when area decreases, velocity increases and pressure decreases. But for supersonic flow M>1, the velocity increases when the area increases (Fig. 21). In sonic point M=1 since infinite acceleration is impossible dA must be equal 0, it means a minimum area (throat) or maximum area (bulge). Combining the

section converging-diverging nozzle may be obtained which accelerates flow smoothly from subsonic through sonic to supersonic flow [88].

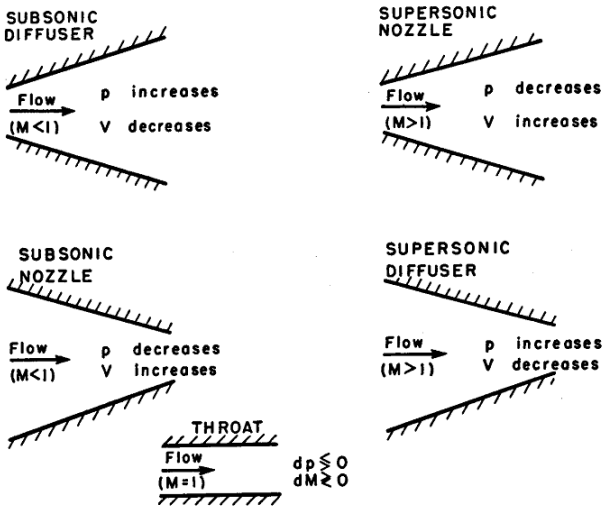

Fig. 21 Effect of area change on pressure and velocity in the nozzle [81]

Considering adiabatic flow following relations are valid

$$\Delta h = C_p \Delta T \tag{14}$$

$$C_p - C_v = R \tag{15}$$

$$C_p / C_v = \gamma \tag{16}$$

$$C_p = \frac{\gamma}{\gamma - 1} R \tag{17}$$

$$h_0 = h_1 + \frac{v_1^2}{2} \tag{18}$$

Using equations (14), (17) and (18) equation for velocity may be obtained

$$v = \sqrt{2C_p(T_0 - T)} = \sqrt{\frac{2\gamma}{\gamma - 1} \mathrm{R}(T_0 - T)} \tag{19}$$

which may be written in following form:

$$\frac{T_0}{T} = 1 + \frac{V^2}{2C_p T} = 1 + \frac{V^2}{\gamma R T} \frac{\gamma R}{2C_p} \tag{20}$$

Since $c_p = \gamma R/(\gamma-1)$ and the velocity of sound $c^2 = \gamma RT$

$$\frac{T_0}{T} = 1 + \frac{\gamma-1}{2}\frac{V^2}{c^2} = 1 + \frac{\gamma-1}{2}M^2 \tag{21}$$

For isentropic flow following relations are valid:

$$\frac{p}{p_0} = \left(\frac{\rho}{\rho_0}\right)^{\gamma}; \frac{T}{T_0} = \left(\frac{p}{p_0}\right)^{\frac{\gamma-1}{\gamma}}; \tag{22}$$

Using (21) and (22) perfect gas equation the temperature, pressure, and density ratios at the nozzle exit as function of Mach number may be obtained.

$$\frac{p_0}{p} = \left(1 + \frac{\gamma-1}{2}M^2\right)^{\frac{\gamma}{\gamma-1}} \tag{23}$$

$$\frac{\rho_0}{\rho} = \left(1 + \frac{\gamma-1}{2}M^2\right)^{\frac{1}{\gamma-1}} \tag{24}$$

The temperature, pressure, density ratios at the critical state i.e. at the minimum area may be calculated when substituting M=1 (the condition in the throat are sonic) in the above expressions [81].

$$\frac{T^*}{T_0} = \frac{2}{\gamma+1} \tag{25}$$

$$\frac{p^*}{p_0} = \left(\frac{2}{\gamma+1}\right)^{\frac{\gamma}{\gamma-1}} \tag{26}$$

$$\frac{\rho^*}{\rho_0} = \left(\frac{2}{\gamma+1}\right)^{\frac{1}{\gamma-1}} \tag{27}$$

5.2. Shock wave

Depending on the ratio of exit cross-section to the throat different shockwaves may appear (Fig. 22). If this ratio is too big the pressure will drop below the ambient pressure before the end of the nozzle and shock wave will occur inside it. In the other case (the ratio is too small) the gas will not have time to reach the value of ambient pressure in the nozzle and exit flow will match it in complex series of oblique shocks [89].

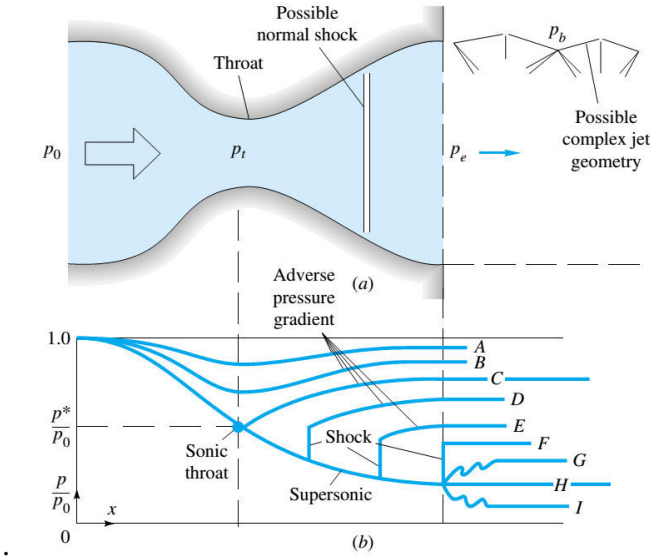

Fig. 22 Operation of a converging-diverging nozzle: (a) nozzle geometry with possible flow configurations; (b) pressure distribution caused by various back pressures [88]

Often calculated pressure at the nozzle exit is less than ambient and simple check is required to check if given solution is correct [20]. P_s represents shock pressure that would appear if a shock occurred at the nozzle exit and it is calculated from the equation(28).

$$\frac{p_s}{p_e} = \frac{2\gamma}{\gamma+1} M_e^2 - \frac{\gamma-1}{\gamma+1} \tag{28}$$

Following cases may take place [20]:

- p_s is equal to ambient pressure, then a shock occurs at a nozzle exit
- p_s is less than ambient pressure, a shock occurs somewhere inside the nozzle, and subsequent subsonic flow occurs past the shock location so the exit pressure is equal to the ambient pressure
- p_s is greater that ambient pressure and the exit pressure is less than ambient one. This is a normal operating conditions. For this case the flow is overexpanded and calculated solution represents real values. The flow slows down outside the nozzle as the pressure adjust to the atmospheric one [20].

5.3. Modelling of gas/particles interactions

Particle interaction with gas resulting in acceleration and heating of particle in gas stream can be calculated under following assumption [4]:

1. The spray particle is spherical with negligible internal temperature gradients.

2. The particle specific heat is independent of its temperature and constant.
3. The gravitational effect and the interaction between particles are ignored.
4. The influences of particles on gas flow are neglected. This is equivalent to stating that the gas energy decrease along the nozzle due to acceleration and heating of the particle is neglected.

Excluding the gravity force, the balanced force acting on a particle is as follows [90]:

$$\frac{dV_p}{dt} = F_D + F_x \tag{29}$$

where F_D - the drag force, F_x - acceleration term.

The drag force on unit mass of a particle can be expressed by the following relationship:

$$F_D = \frac{18\mu}{\rho_p d_p^2}\frac{C_D Re_p}{24}\left(V - V_p\right) \tag{30}$$

where μ – viscosity of the gas, ρ_p – density of the particle, d_p – diameter of the particle, C_D – drag coefficient, u_g – gas velocity, u_p – particle velocity, Re_p is the particle Reynolds number given in form:

$$Re_p = \frac{\rho d_p \left|V - V_p\right|}{\mu} \tag{31}$$

Equation (30) and (31) can be presented in form

$$\frac{dV_p}{dt} = \frac{3}{4}\frac{C_D}{d_p}\frac{\rho}{\rho_p}\left(V - V_p\right)\left|V - V_p\right| \tag{32}$$

In case of spherical particle the drag coefficient default for Fluent is taken from Morsi and Alexander [91]:

$$C_D = a_1 + \frac{a_2}{Re_p} + \frac{a_3}{Re_p^2} \tag{33}$$

Where a_1, a_2, a_3 are the coefficients applied over several ranges of Re (Tab. 2).

Tab. 2 Values of a_1, a_2, a_3 coefficients

Re	a_1	a_2	a_3
<0.1	0	24	0
0.1-1	3.69	22.73	0.0903
1-10	1.222	29.1667	-3.8889
10-100	0.6167	46.5	116.67
100-1000	0.3644	98.33	-2778
1000-5000	0.357	148.62	-4.75e4
5000-10000	0.46	-490.546	57.87e4
10000-50000	0.5191	-1662.5	5.4167e6

And M_p is the particle Mach number:

$$M_p = \frac{|V - V_p|}{\sqrt{kRT}} \tag{34}$$

Since it was assumed that the temperature of particle is below the vaporization temperature and the temperature gradient inside the particle was neglected, the particle temperature during process may be taken as follows [90, 92]:

$$\frac{dT_p}{dt} = \frac{h \cdot A_{pp} \cdot (T_e - T_{p0})}{m_p \cdot C_{pp}} \tag{35}$$

where: A_{pp} - outside surface area of a particle T_e – gas temperature at the nozzle exit, T_{p0} -temperature of powder before introduction to the nozzle, C_{pp} – specific heat of particle material at constant pressure, m_p – mass of a particle, k – heat transfer coefficient of gas related to the thermal conductivity of gas (λ) by Nusselt number (Nu) as follows:

$$k = \frac{\lambda Nu}{d_p} \tag{36}$$

Nusselt number is given by:

$$Nu = 2 + 0.6 Pr^{1/3} Re_p^{1/2} \tag{37}$$

Prandtl number (Pr) is described as:

$$Pr = \frac{\mu C_p}{\lambda} \tag{38}$$

Where, C_p is heat capacity of gas. It may be concluded from the equation (32) that particle velocity depends on particle size, particle density, gas velocity, and density of the gas and the ultimate particle velocity is equal to the gas velocity [20, 93].The most convenient way

to increase it is to increase gas velocity which is directly depended on nozzle shape, gas molecular weight and gas temperature. The stagnation pressure does not affect directly gas velocity after flow is choked [4]. However initial drag on the particle (dv_p/dt at $v_p = 0$) is linearly dependent only on the stagnation pressure and is independent of the total temperature [20]. Additionally increasing upstream pressure increases the density of the gas which influence the coupling between the gas velocity and the particle velocity [4]. Usually nitrogen, helium and air are used as process gas. The ratio of specific heat for He is 1.66 while for N_2 and O_2 is 1.4. Higher ratio of specific heat leads to higher velocity. Sonic velocity for helium is 989 m/s and for air only 343 m/s. However, helium is much more expensive which limits its applications [4]

6. Metallization of polymers – methods

Metallization of composite and polymers is widely used technique to improve i.e. their electrical properties. It seems especially interesting as it allows depositing directed conducting paths which could, in the future, replace traditional conductors. Nowadays it is commonly done with such methods as PVD, CVD, electroless deposition, electroplating and to a lesser extent with thermal spraying.

6.1. Electroplating, Electroless Deposition

Well established polymer metallization process consists of four stages: etching, activation, electroless deposition and building up deposition (Fig. 23).

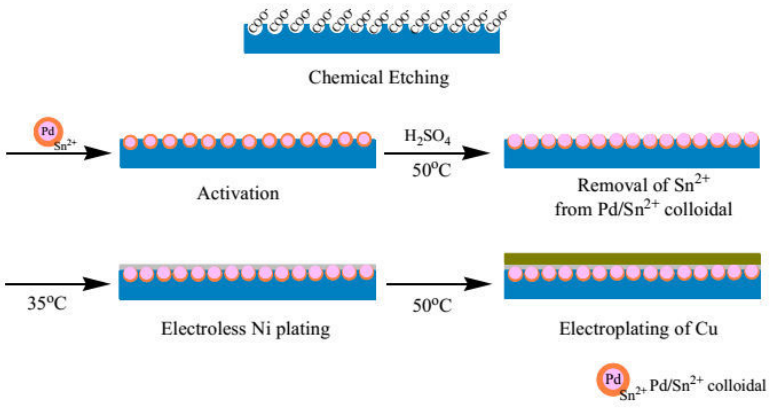

Fig. 23 Schematic diagram of traditional plastics metallization process [94]

First polymers have to undergo surface treatment to obtain pitting sites and functional groups that enhancing adhesion between substrate and deposited layer [95]. It may be done

using i.e. plasma, laser or UV treatment [96–98], however theses method are suitable only to a parts with limited size. The other industry used solution is modification by chemical reaction i.e. oxidation using chromium trioxide in concentrated sulphuric acid as etching bath for modifying ABS surface. The chemical composition of baths is still under investigation as traditional ones contain Cr^{6+} ions which cause serious pollution and are hazardous to human health [95, 99]. Etching may be also done by hydrolysis at the presence of sodium hydroxide [100, 101]. The next step is activation. Polymer with active sites are placed into activation bath containing palladium/tin (II), Pd/Sn^{2+} [95]. Sn^{2+} ions, surrounding Pd, form complex bond with carboxylate at active sites. When the bonding is formed the part of the Sn^{2+} ions is removed with H_2SO_4 solution to expose Pd which act as catalyst during following step electroless deposition. Metal ions are easily adsorbed by Pd surface and therefore obtaining continuous conductive layer, typically with electroless Cu and/or Ni plating is possible [95, 100, 102]. Ni plating is more stable and environmental friendly. The layers are characterized by excellent corrosion and wear resistance. On the other hand ductile Cu can act as buffer layer between substrate and the top metal layer and has better conductivity. Both solutions have some disadvantages. Cu baths contain EDTA and formaldehyde [103, 104] and Ni may cause allergy in contact with human skin [105]. As the end step electroplating is done. Series of metal layers may be applied depending on the product application i.e. Lee et al [106] tested electroless nickel-phosphorous coating deposited on carbon fiber reinforced plastics. The coatings decreased corrosion rate and exhibited strong passivity in 2.5 wt% NaCl solution.

6.2. PVD

The other commonly used method for coating polymers is PVD [95, 107–109]. It is a physical method of forming thin films in vacuum by evaporating bulk material (target) and transporting it to the substrate where it condenses [110]. The main criteria determining the possibility of coating polymer with PVD process are: outgassing rate per unit surface area, ability to withstand high temperature and homogeneity. The other factors are amount of plasticizers, additives fillers, and surface properties. Almost all polymers may be coated with this method including such as PS, PMMA, ABS, PC, PE, PP. However there are some problems with coating polyamides as they outgas in vacuums [111]. The layer might be deposited directly to the polymer surface but it must have extreme high quality. The other solution, required to hide imperfections, is applying UV-curable base coating. As the

vacuum deposited layer is approximately 100 nm thick, to protect it from abrasion and scratching, often the second UV topcoating is applied [112, 113].

6.3. Thermal spraying

Thermal spraying, due to its low costs, is the most commonly used technique of coating but in case of polymer substrates depositing by thermal spraying involves problem with thermal degradation of substrate. It was, among others, Voyer at al [114] who, with flame spraying, successfully applied an aluminum layer which despite high porosity had conducting properties. However, depositing without cooling system was possible only for large distance between flame and substrate therefore the process efficiency was low.

The other problem in metallizing polymers is large difference in coefficient of thermal expansion which causes delamination of the coatings and low adhesion strength. Knight et al [115] examined HVOF sprayed graded coatings consisting of polyamide matrix with varying volume of WC-Co. The obtained bond strength reached maximal 50 % of tensile strength of PMC substrate. Sutter at al [116] tested two types of erosion resistant coatings applied to the AE 3007 fan bypass made up of carbon-Kevlar TM in terms of adhesion, surface roughness and erosion resistance. The bond coat was sprayed with flame spray and top coat with plasma. It was reported that the erosion resistance was improved by a factor of two [116].

Liu et al [117] tested arc spraying with cored wire composed of steel skin and Ni-Cr-B–Si filler on a graphite fiber reinforced thermo-setting polyimide, which can work up to 644 K. The substrate was sandblasted and pure zinc was used as a bond coat due to low melting temperature and very good wettability. The bond strength amounted 9.4 MPa with optimum sandblasting conditions such as 28 mesh corundum powder and 0.2 MPa compressed air [117].

Ganesan et al [118] did research on adhesion behavior of plasma sprayed copper coating on CFRP plate in terms of different substrate pretreatment: mechanical, chemical and thermal. The highest adhesion strength reached about 2.5 MPa. Surface roughness was identified as decisive factor for achieving higher adhesion. Additionally XPS analysis confirmed chemical affinity of chemically treated polymeric substrate and copper coating [118].

The other studies including use of interlayer of epoxy mixed with sand [119], Al-12Si powder incorporated into polyurethane substrate in curing process [120], Cu

particles co-cured in PMC substrate [121]. The interlayers improved adhesion and protects substrate from thermal degradation.

6.4. Cold spray as coating method for polymers

Spraying coatings on polymers using cold spray seems very interesting way as there is no high temperature effect and the costs are relatively low. World-wide literature reports successful spraying of, to name some of them, tin on PC/ABS, polypropylene, polystyrene and polyamide-6 [122], aluminum on PEEK [123], copper on PA66 [124], and aluminum on polycarbonate Lexan [125]. These coatings were dense and of low porosity. In case when double aluminum-copper layers were made, a positive effect was observed when copper was deposited as the second layer. Due to its higher density, it caused compacting of aluminum, hence reduction of porosity [123].

The influence of technological parameters on the deposition of the metal powder on a plastic substrate was raised by Lupoi [122]. He noted that in case of copper deposition on ABS and composite reinforced with glass fibers, depositing was dependent on selected parameters. The most important was the gas pressure and hence the velocity of the powder particles. Favorable was low pressure spraying (0.5 MPa) without heat gas which allowed to deposit thin copper layer. When using a pressure 3 MPa without heating and thus increasing the velocity of particles mainly erosion of substrate was observed [122]. However, it was reported in [124], that in case of copper, when the first tight layer was successfully deposited, further deposition is scanty. This phenomena can be explained by a change of substrate surface to metallic one and hence a change of parameters necessary for depositing. It is probably caused by change in the substrate nature from polymeric one to the metal and thus the need to use the higher velocity. In the case of tin, the continuous coating was achieved using a nitrogen pressure of 3 MPa without heating and particle velocity calculated at 310 m/s. The resultant coating had a thickness in the range 45-100 μm and was characterized by good electrical conductivity [122] Basing on examined powders of copper, tin and aluminum, the authors forecasted behavior of other metallic powders as shown schematically in Fig. 24.

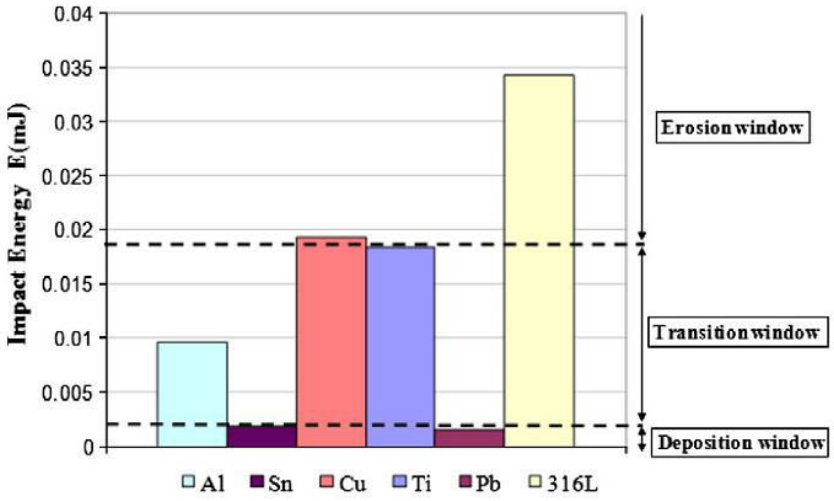

Fig. 24 Effect of impact energy of metal powder on the possibility of depositing onto the polymers [122]

Materials with a high density and high critical velocity generate a high impact energy *E* in accordance with the formula $E = 1/2mv^2$, where m is the mass, *v* – critical velocity, which can cause high stresses and damage the surface of polymer. For copper single impact energy particle is *E* = 0.2 mJ. However, for tin much lower critical velocity is needed, therefore, generated energy is 10.7 times less than for copper. Lightweight metals such as aluminum, are characterized by low density and required high velocity to generate energy sufficient for bonding [122]. But it is also worth pointing out that, since Lupoi et al used the gas at room temperature so the obtained velocity were relatively low in relation to the pressures, and the thermal softening of polymer substrates did not occur.

Most of the research done have concerned the coatings of transition metals – Al, Cu. Zhou at al [123] realized thick Al and Al/Cu on the high performance polymer PEEK450CA30. Affi at al [126] used plasma sprayed interlayer to obtain thick, cold sprayed Al coating on CFRP. The obtained coatings had higher electrical conductivity than plasma sprayed ones. Giraud et al [127] studied deposition parameters for cold sprayed Al onto PA66 polymer. They observed that coating started to be formed at the pressure of 1.5 MPa and the gas temperature of 473 K but the optimal process parameters were reached at 2.5 MPa and 523 K respectively. It was concluded that an increase in the number of spray passes increases the density of coating.

One of the few models describing the deposition process of ceramic powder on the polymer substrate has been proposed in [128]. Sprayed TiO_2 particles penetrate the plastic surfaces of PSU polymer and create characteristic jets, which then act as a binder (Fig. 25) [128].

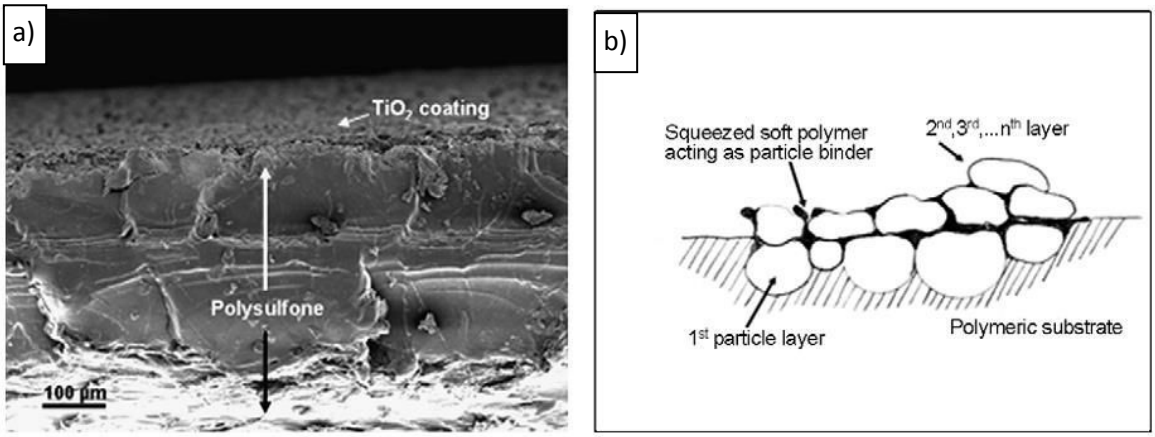

Fig. 25 Cross section of PSU polymer coated with TiO_2 (a) model of bonding mechanism (b) [128]

There are also works explaining the differences between the interaction of copper particles with thermosetting and thermoplastic polymers. Authors [129] observed, that metal deposition on thermoset is more difficult because of their greater brittleness. The impact of powder particles causes erosion of substrate instead of its plastic deformation. They achieved to obtain thick copper coating on i.a. PVC, epoxy polymer by using interlayers (Fig. 26). For PVC they sprayed first layer with spherical powder and after that use dendritic powder to form thick coating.

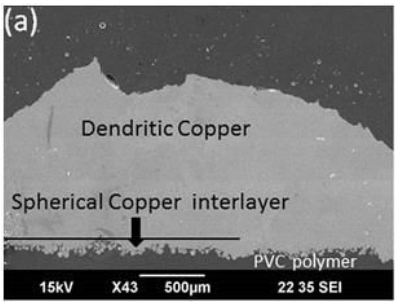

Fig. 26 Copper coating deposited on polymer substrate using interlayer [129].

7. Aim of the work and range of research

In this chapter the short introduction to the experimental part of this thesis is given. It contains the motivation of the work, its goals as well as the range of the conducted research.

7.1. Genesis of the work

Polymers consumption in industry is on the rise due to their numerous advantages compared to e.g. metals. Plastics are easier to process particularly in the manufacture of complex shapes, have a lower roughness after manufacture, provide lower density, and greater resistance to corrosion. Coating the surface of the plastic allows combining advantage of plastics with metal benefits. Obtained light components have surface with increased hardness, resistance to abrasion and temperature. The metal coatings provide additional electrical conductivity and prevent the accumulation of the electric charge. Literature review shows that cold spray might be used for deposition of coating with specific properties on the polymer surface. It is relatively new technology, with low cost of purchase and operating and acceptable coating quality. Using cold spray technology i.e. as a solution for direct printing is supposed to simplify the production process, reduce the production time and space occupied by the wires. The present technology is the use of cable harnesses. The problem occurs i.e. in case of parts tested in rotors. The sensor wires are glued to the polymer surface and tend to unstick due to centrifugal force and low surface energy of polymer matrix which reduces the adhesion of glue. It is supposed that sprayed coatings will have better adhesion and sufficient electrical conductivity.

The main requirements for the coatings are:

- Sufficient bond strength in conditions of use
- Good electrical conductivity
- Long-term stability
- Good repeatability of coatings process and low cost of production.

The other perspective areas of using metallized polymers are sensors [130], deicing [119] or antifouling solution [131, 132]. What is also significant with cold spray method it is possible to metallize of polymers difficult to coating with conventional methods without activation [125]. It appears also that even the polymers with embedded metal particles could be used as, e.g. a method of surface activation, or a surface characterized by a bactericidal or antifouling properties [133]. For example, arc spraying

have been used to produce the Cu-Ni-Zn alloy coating on the surface of the chairs from waiting room in the hospital to reduce the amount of Gram-negative bacteria Escherichia coli (DH5Į) [134]. It has been shown that the coatings have a bactericidal effect in contrast to sheets made of an alloy with similar composition [135, 136].

7.2. Aim of the work

Based on literature review following thesis for this work has been formulated:
"It is possible to use low pressure cold spray for directly deposition of metal coatings on polymers having properties similar to the coatings deposited with presently used methods".

The scientific goal of the work is the knowledge of the microstructure and properties of deposited coatings. Moreover deposition mechanism of metal powder on polymer substrate and influence of process parameters should be known.

The useful goal is selection of process parameters allowing to deposit: tin, aluminum and copper coating on polyamide 6 and polycarbonate.

The scope of research made within PhD is summarized in Fig. 27:

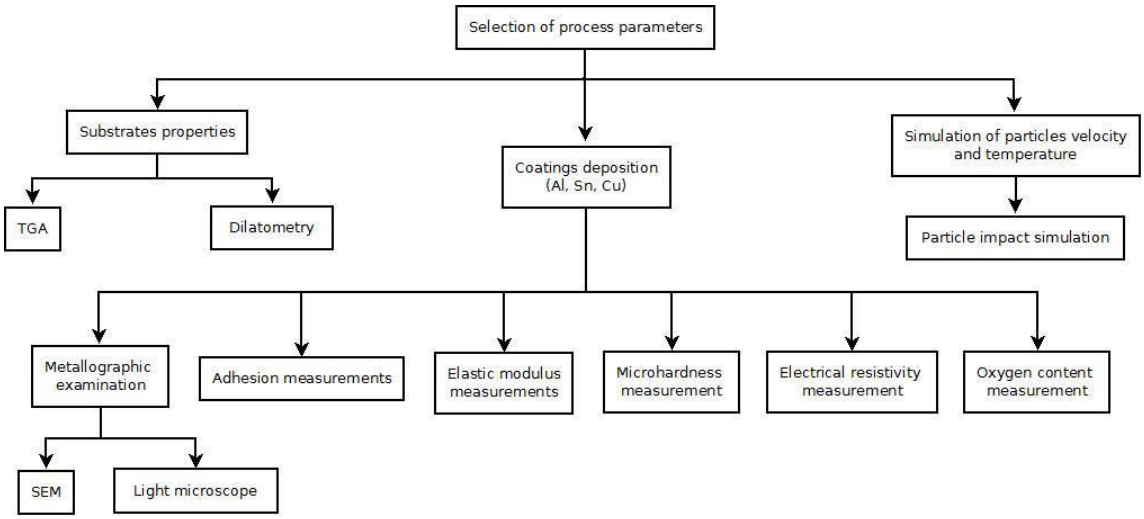

Fig. 27 Scheme of research made within the PhD thesis

8. Characterization of used materials

In this work two common polymer substrate materials (polyamide 6 and polycarbonate) and six powders (spherical copper, granular copper, dendritic copper, tin, mixture of alumide and tin, aluminium) have been studied and are briefly characterized in this chapter.

8.1. Substrates

Two widely used thermoplastic polymers were chosen for substrate material:

- Semicrystalline polyamide 6 - PA6 (Plastics Group, Poland) with glass transition temperature ~323 K and melting temperature ~ 493 K. It is high performance polymer commonly used as a matrix for carbon fibre-reinforced plastic (CFRP)
- Amorphous polycarbonate - PC (Plastics Group, Poland) with glass transition temperature ~ 423 K. It has excellent resistance to impact, abrasion, weathering and chemicals as well as high tensile strength, but it is stable against surface modification [125].

8.2. Powders

The coatings were produces using six commercial powders:

a) Gas atomized irregular aluminum (Pyrogarage, Poland) with purity grade 99.7% and mean particle diameter 29.0 μm (Fig. 28)

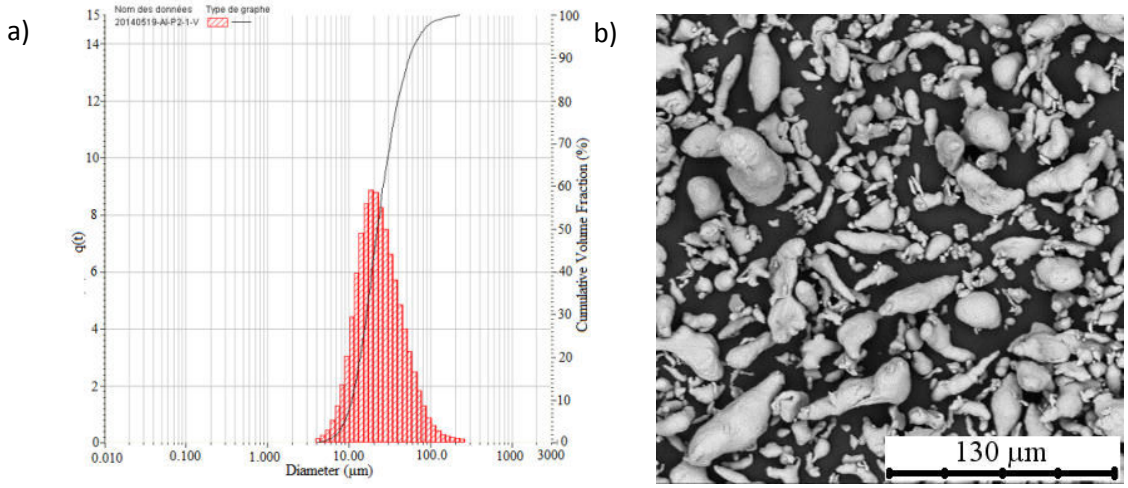

Fig. 28 Aluminium powder: particles size distribution (a) and morphology (b)

b) Gas atomized spherical copper (Libra, Poland) with purity grade 99.9%, mean particle diameter 22.8 µm (Fig. 29)

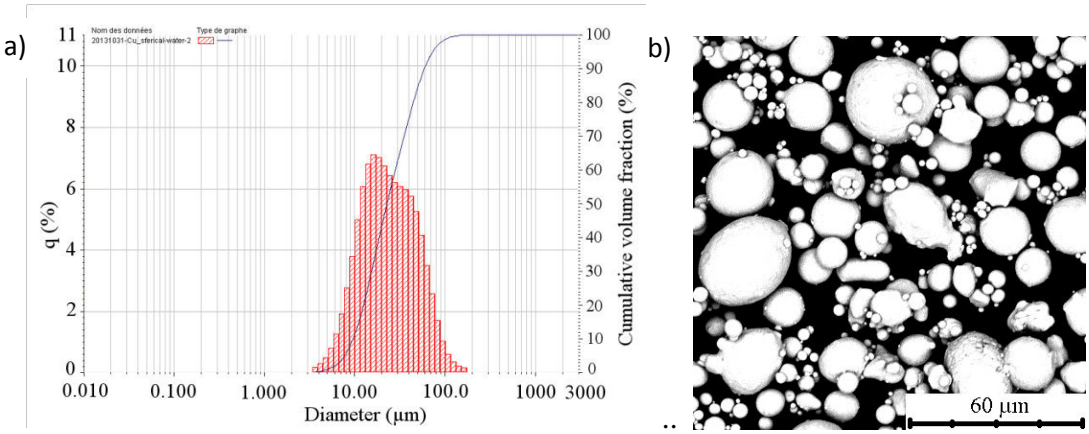

Fig. 29 Spherical copper powder: particles size distribution (a) and morphology (b)

c) Electrolytic granular copper (Libra, Poland) with purity grade 99.76%, mean particle diameter 23.5 µm (Fig. 30)

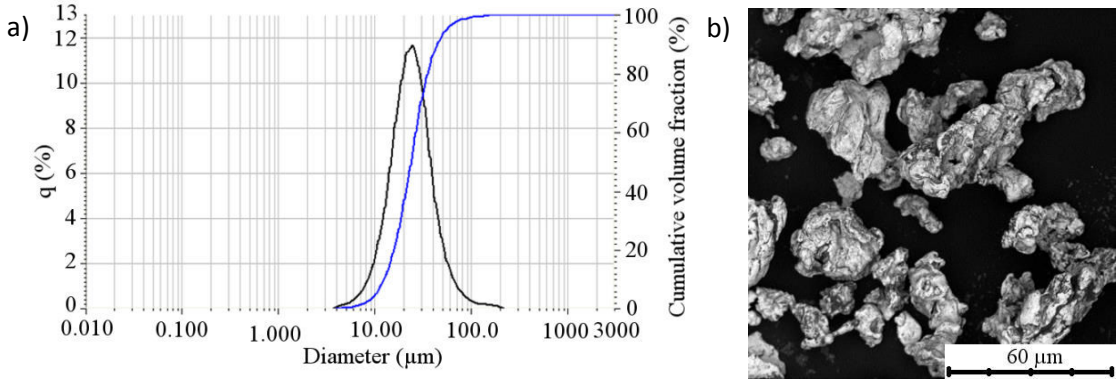

Fig. 30 Granular copper powder: particles size distribution (a) and morphology (b)

d) Electrolytic dendritic copper (Libra, Poland) with purity grade 99.7%, mean particle diameter 30.7 µm (Fig. 31)

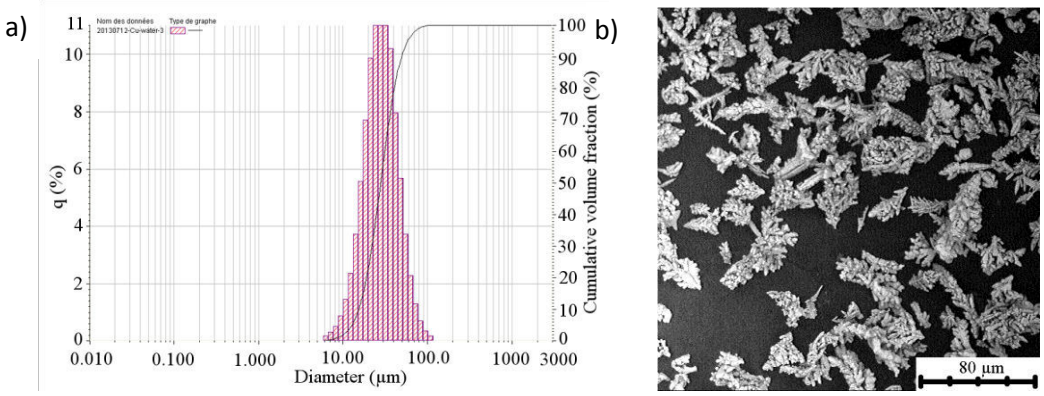

Fig. 31 Dendritic copper powder: particles size distribution (a) and morphology (b)

e) Gas atomized spherical tin (Libra, Poland) with purity grade 99.9%, mean particle diameter 8.6 µm (Fig. 32)

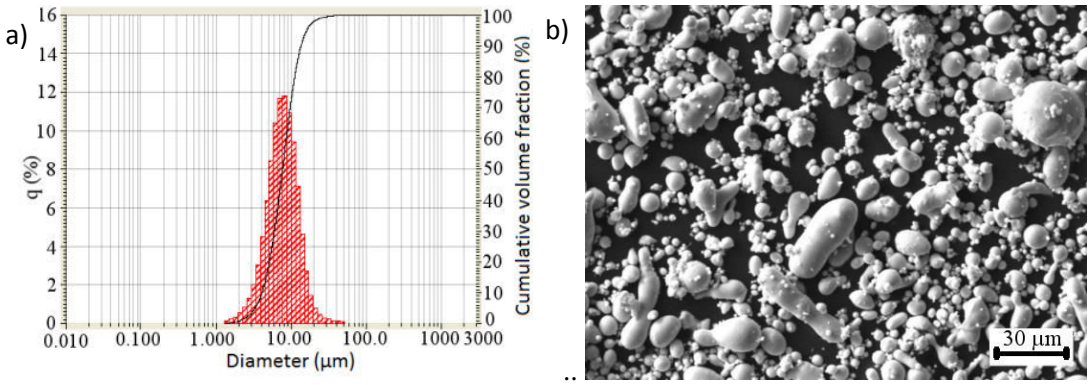

Fig. 32 Tin powder: particles size distribution (a) and morphology (b)

f) Mixture of spherical tin and alumina in the form of irregular polyhedral (Sn+50 wt. % Al_2O_3) (Obninsk Center for Powder Spraying, Russia) with mean particle diameter 24.3 µm. Purity grade was for tin 99% and for alumina 99.4% (Fig. 33).

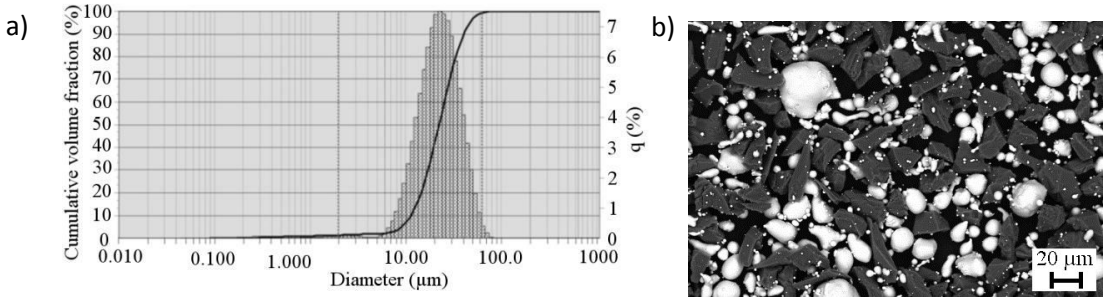

Fig. 33 Mixture of Sn + Al_2O_3: particles size distribution (a) and morphology (b)

9. Experimental methods

In this chapter experimental methods used in this thesis are briefly described.

9.1. Coating deposition process – low pressure cold spray stand

The coatings were sprayed with low pressure cold spray device, DYMET 413 (Obninsk Center for Powder Spraying, Russia) which is part of equipment of Faculty of Mechanical Engineering at Wroclaw University of Technology. The device is equipped with internal heater placed in the spraying gun and cylindrical de Laval nozzle. The spraying gun is mounted in the 3 axis (x,y,z) manipulator BZT PF 750C with maximal linear velocity 3000 mm/min. The spraying station consist of spray chamber, manipulator with computer control, compressor and exhaust fume system with filter to carry off the gases during spraying process. The temperature control unit operates stepwise. It is possible to spray with room temperature and in the range 473-873 K with an increment equal to 100 K. The gas pressure is regulated with a manometer from 0.1 to 0.9 MPa, but switching on the heater is possible from 0.5 MPa as it must be cooled with sufficient gas flow. The powder feeders are equipped with 10-step adjustment. The feed rate depends on feedstock material i.e. for Al amounts 1-6 g/min (manufacturer data). The feed rate is given as an average as it is irregular due to using of gravity feeder and suction of powder through underpressure created in the de Laval nozzle during gas flow.

Before deposition process all samples were cleaned with acetone or industrial methylated spirit and dried with compressed air. Part of the samples was sandblasted perpendicular to the substrate using low pressure cold spray device DYMET413 (Obninsk Center for Powder Spraying, Russia) and alumina powder type K-00-04-16 (Obnisk Center for Powder Spraying, Russia) with particle size below 350 μm. The initial tests were done on rectangular samples with 100 mm length, 50 mm width and 3 mm thickness. The parameters for coatings deposition are listed in further part of thesis.

9.2. Stereometric measurements

The roughness and waviness of the substrate were measured perpendicular to the spraying passes, both with stationary profilometer Form Talysurf 120L (Leicester, UK) equipped with a head with a diamond cone with an apex angle of 60° and fillet radius of r = 2 μm and confocal microscope OLYMPUS Lext OLS4000 (Olympus Inc., Tokyo, Japan). The cut-off length was 8 mm for both profilometer and confocal

microscope according to European standard (PN-EN ISO 4288:2011). The sterometric properties were characterized using waviness and three basis roughness parameters Ra, Rt, Rz (JIS) according to European standard (PN-EN ISO 4287:1999). The roughness was taken as a mean value of three measurements. The measurement distance for profilometer was 40 mm and for the confocal microscope the measurement area was rectangle 29x13 mm.

9.3. The adhesion measurements

The adhesion strength test was carried out according to European standard PN-EN 582. The samples with Ø 40 mm diameter were bonded to counter-sample using epoxy adhesive Distal (Fig. 34)

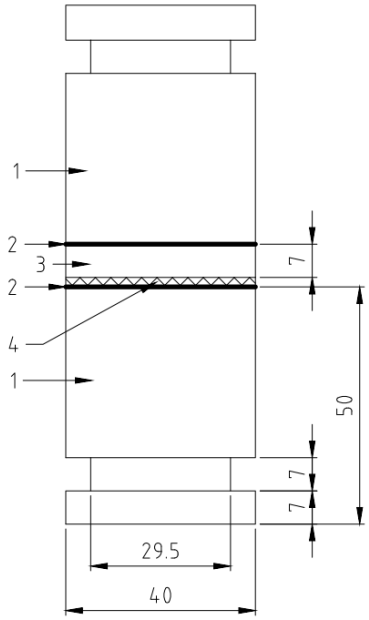

Fig. 34 Schematic representation of sample for adhesion measurements: 1 – counter sample, 2 –glue, 3 – sample, 4 – coating

Coatings bond strength was tested directly after spraying. The required thickness of the coatings is not given in the standard PN-EN 582 in contrast to USA standard ASTM C633 which recommends thickness above 380 µm to avoid glue penetration. The thickness of the coating was dependent on spraying conditions and it is given as reference together with bond strength value. The adhesion strength was taken as an average of three measurements.

Adhesion test were made using universal tensile testing machine Instron 1126 (Instron Corp., USA) with maximal load 250 kN. Bond strength was calculated as

$$R_H = \frac{F_H}{S} \tag{39}$$

where: R_H – bond strength [MPa], F_H – force at which the coating detached from the surface [N], S – surface area of sample [mm^2].

9.4. Microhardness measurements

Microhardness was measured with the use of a Digital micro Hardness Tester MMT-X7 MATSUZAWA CO., LTD (Akita, Japan) with Vickers indenter according to the standard PN-EN ISO 6507-3 of 2007. The load of 0,9807 N were chosen for each type of coating. The measurement was done on cross-sections in the middle of the coatings (Fig. 35). Microhardness was given as an average of five measurements.

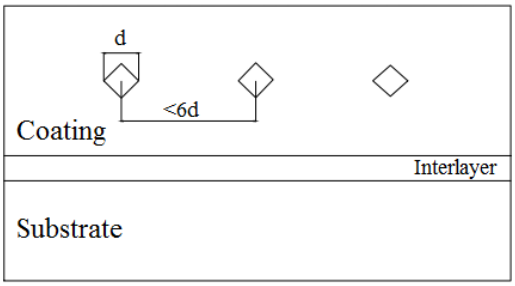

Fig. 35 Schematic representation of sample for hardness measurement.

9.5. Elastic modulus measurements

Elastic modulus of coatings was measured using a nanoindenter XP™ (MTS Nano Instruments, USA) with Berkovich diamond tip having three-sided pyramidal shape. Before measurements, the tip was calibrated on silica reference material. The properties were determined according to the Olivier and Pharr's methodology [137, 138]. The instrument was operated in the continuous stiffens mode (CSM) which allows to calculate mechanical properties at every acquired data point. Harmonic oscillation amplitude was set at 2 nm and oscillation frequency at 45 Hz. Indentations were performed on the polished sample at the cross-sectional view and at a constant 2000 nm depth. Presented data are an average value of 20 indents.

9.6. Electrical resistivity measurement

The resistance of the samples was measured using custom-built four-terminal sensing probe with spring-loaded pogo-pins. The distance between the voltage-sensing pins was

20 mm. The measurement system consisted of the Agilent E3632A power supply and Keithley 2000 and 2001 multimeters. The multimeters did not provide test current big enough (less than 10 mA) to measure the resistance of the samples with satisfying precision therefore the power supply and one multimeter were used to provide and measure the 100 mA test current while the second multimeter was used to measure the voltage. Low resistance of the samples (less than 100 mΩ) caused that the power dissipated in the sample was less than 1 mW.

The main contribution to the measurement error was the voltage measurement error and the precision of the sensing probe. The voltage sensing was affected by the thermoelectric potentials and the multimeter accuracy. The thermoelectric potentials observed during the tests were less than 4 μV which would cause the 40 μΩ resistance measurement error while the accuracy of the meter for the worst case (best conducting sample) was evaluated as 1.2 μV which would cause the 12 μΩ error. The sensing probe was precisely machined however the play at the pogo-pins was estimated at 0.2 mm at each of the pin which would give the resistance measurement error of 2% of the reading. The total error was therefore estimated as 60 μΩ + 2% of the measurement.

The electrical resistivity was calculated according to the formula:

$$r = \frac{S_r}{l} \cdot \frac{U}{I} \tag{40}$$

where: ρ - resistivity (Ωm), U – measured voltage (V), I – measured current (A), l - distance between measuring probe (m) S_r -the cross-section of the conductive layer = $a*g$, where a- width of the conductive layer (m), g – thickness of the conductive layer (m).

The samples for electrical resistivity measurements were in shape of rectangle with 5 mm width and 80 mm length. Before measurement were polished with 600 grit silicon carbide papers.

9.7. Temperature-programmed reduction measurement

The TPR measurements were done with 15 mg sample placed into a quartz microreactor. It was made with a mixture of 5 vol % H_2 in Ar, and the temperature was increased linearly to 1173±K at a rate of 10±K/min. The hydrogen consumption was monitored by TCD detector. The highest hydrogen consumption in case of dendritic

powder was ±573 K and in case of spherical powder ± 733 K (Fig. 36). It indicates that in case of dendritic powder the hydrogen is easier reducible.

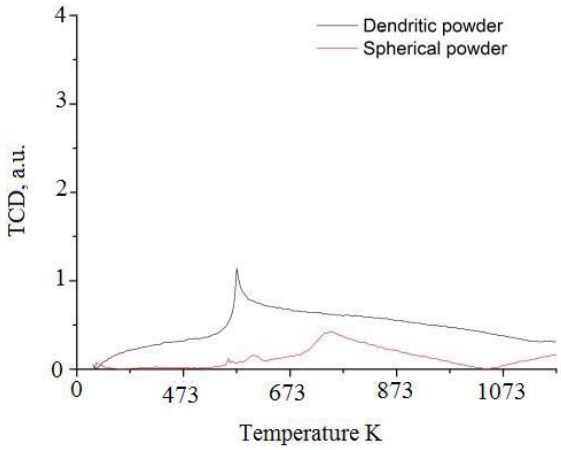

Fig. 36 TPR reduction of copper powder with hydrogen

9.8. Heat treatment of powder

Data obtained from TPR measurements were used to reduce the oxide present in powders. The reduction was made with hydrogen (commercial purity 99.995 %) using self-made set-up (Fig. 37) consisting of steel tube and furnace FCF7SM (Czylok, Poland), working in temperature range 293 – 1423 K with precision ±3 K. The powder was placed in the tube through with hydrogen was flowing, and then exit through the thin pipe. In the end the hydrogen was burned in the flame.

a) b)

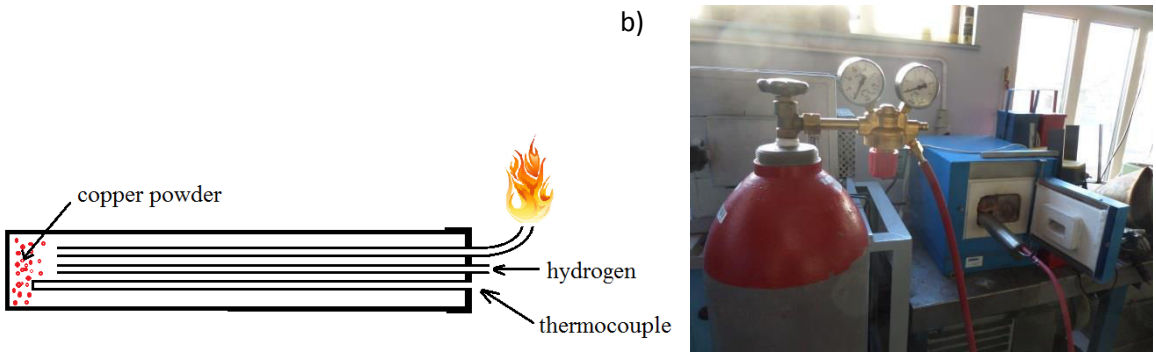

Fig. 37 Setup for deoxidizing copper powder: schematic of steel tube (a), research stand (b)

The temperature was measured using thermocouple placed in the tube. The dendritic and granular powder was reduced for 1 h in temperature ±573 K and the spherical one for 1 h in the temperature ±723 K. The powder after heat treatment was milled and sieved to get the fraction below 40 µm. The coatings were sprayed one day after preparing powder.

9.9. Oxygen content measurements

The oxygen content in the used powder and resulted coatings was analyzed using O_2 and N_2 analyzer - Leco TC436 (Leco, USA) with the inert gas fusion method. For this method the sample is placed in high purity graphite crucible and heated to high temperatures in an inert gas. Then the oxygen from the sample reacts with crucible and form CO or CO_2 which is measured by infrared detection.

9.10.Microstructure analysis

Powder and coatings morphology was characterized with light and electron scanning microscopes. The cross-sections were prepared from deposited coatings for metallographic examination. The samples were cut using cut-off machines, embedded in epoxy resin and grinded on SiC paper with grit from 120 to 1200. Final polishing was made with diamond suspension with 6 μm, 3 μm and 1 μm particles. The metallographic examinations were carried out using light microscopes: Nikon Eclipse MA 200 and electron scanning microscopes (SEM) HITACHI TM 3000 Table-top Microscope (Hitachi, Japan) and Phenom G2 pro (Phenom, Netherlands). The investigations were performed with secondary electrons, SE mode.

9.11.Granulometry

Particles size distribution was measured using laser scattering technique with granulometer Partica LA-950V2 (Horiba, Japan). In this method powder is transported through the cell and particles are detected through laser beam. On the basis of variation in intensity of scattered light particles size distribution is calculated.

9.12.Coating thickness

Coating thickness was evaluated on cross-sections with light microscope. The thickness was taken as an average from 10 to 15 measurements made in different region of coating. During spraying thickness of coating was controlled using dial thickness gauges. Because of the waviness of the coating, its thickness has been taken as an average from 10 measurements in lowest and highest point.

9.13.Coefficient of thermal expansion

Coefficient of thermal expansion of substrate and coatings were measured using dilatometer Netzsch DIL 402C (Netzsch, Germany) up to 353 K or 473 K (depending on the sample) both during heating and cooling. Air was used as shielding gas. The heating rate was 5 K/min. For every measurement conditions correction was done using alumina sample.

9.14.Thermogravimetric analysis

Thermogravimetric analysis was made using thermal analyzer Netzsch STA 449 F3 Jupiter (Netzsch, Germany). The measurements were done in air atmosphere with two heating rates 5 K/min and 10 K/min up to temperature of 1073 K. Before the analysis correction was made.

9.15.Temperature measurements

Temperature during deposition process was evaluated using thermocouples type J (sensitivity 55μV/K) with diameter 0.5 mm connected with thermocouple welder TP2 (Weldotherm, Germany) and data acquisition card DT9806 (Data Translation, USA). The spraying track has been extended to reach stable gun velocity (Fig. 38). Temperature was measured for two cases: with and without powder in the gas stream on the substrate surface.

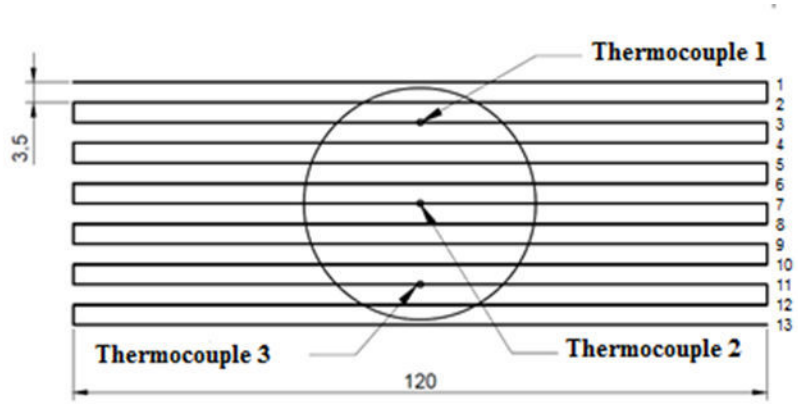

Fig. 38 Schematic of arrangement of spraying tracks and location of thermocouples for temperature measurements

10. Simulations

The main parameters in cold gas spraying are: velocity and temperature of particle (they influence coatings' quality i.e. adhesion, porosity and oxidation level). Velocity and temperature of particles can not be set directly but through the value of working gas inlet temperature and pressure. Two common ways exist to obtain the parameters for particles – one dimensional isentropic approximation or computational fluid dynamic for two or three dimensions. Initially the velocity was calculated using one dimensional isentropic gas flow model in Matlab software, and then refine simulation in Fluent has been made

10.1.Particles and gas velocity calculation 1D model

Equations for one dimensional isentropic gas flow model were calculated in Matlab software. The simplified contour of the Dymet nozzle geometry is presented in Fig. 39

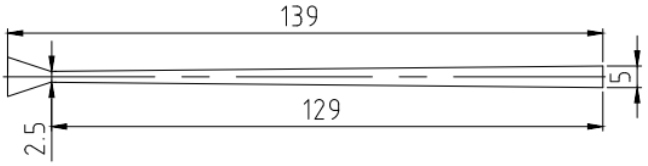

Fig. 39 Simplified contour of spraying nozzle used in Dymet 413

Air was treated as ideal gas. The gas state was calculated from equation given by Champagne et al [4]. The pressure P, temperature T_g, and gas velocity V_g can be calculated form the nozzle cross-sectional area A at a given point to the nozzle throat area A_t [4]:

$$\frac{\mathrm{A}}{\mathrm{A_t}} = \sqrt{\left(\frac{\gamma-1}{2}\right)\left(\frac{2}{\gamma+1}\right)^{(\gamma+1)/(\gamma-1)} \Big/ \left[\left(\frac{\mathrm{p}}{\mathrm{p_i}}\right)^{2/\gamma} - \left(\frac{p}{p_\mathrm{i}}\right)^{(\gamma+1)/\gamma}\right]} \tag{41}$$

The temperature is given as follow [4]

$$\mathrm{T} = \mathrm{T_i}\left(\frac{\mathrm{p}}{p_\mathrm{i}}\right)^{(\gamma-1)/\gamma} \tag{42}$$

The velocity might be calculated by following equation [4]:

$$\mathrm{V} = \sqrt{2\frac{\gamma}{\gamma-1}\mathrm{RT_i}\left[1-\left(\frac{\mathrm{p}}{\mathrm{p_i}}\right)^{(\gamma-1)/\gamma}\right] + \mathrm{V_i^2}} \tag{43}$$

The particles velocity and temperature were calculating using equation given it chapter [5.3] of this thesis. Initially gas properties were given with polynomial equations. The air viscosity was calculating using Sutherland's law [139]:

$$\mu = \mu_R \cdot \left(\frac{T}{T_R}\right)^{\frac{3}{2}} \cdot \frac{T_R + S}{T + S} \tag{44}$$

Where

μ_R =1.716e-5, S = *110.4,* T_R = 273.15

Thermal conductivity is given by equation [140]:

$$\lambda = (1.99e - 3) \cdot \frac{T^{\frac{3}{2}}}{T + 112} \tag{45}$$

And heat capacity of gas with equation [141]

$$C_p = \left(C_{pA3} + C_{pB3} \cdot T + C_{pC3} \cdot T^2 + C_{pD3} \cdot T^3\right)/M_m \tag{46}$$

where, C_{pA3} = 28.11, C_{pB3} = 0.1967e-2, C_{pC3} = 0.4802e-5 ,C_{pD3} =-1.966e-9;

M_m=28.960 ;

Then constant coefficients for air properties were applied (Tab. 3). The difference in powder particles velocity was on average ~10 m/s depending on the initial gas temperature and reaching maximum for initial 293 K. The particles temperature difference was correlated also with initial gas temperature. The difference reached i.e. ~20 K in case 20 µm Al particle for initial gas pressure 0.9 MPa and initial temperature 293 K for. The highest discrepancy was noted for tin particles due to low heat capacity. Eventually constant coefficient were applied as suggested in [92].

Tab. 3 Air properties

Gas viscosity [kg/m/s]	Thermal conductivity [W/m K]	Gas heat capacity [J/kgK]	R- Gas Constant [J kg^{-1} K^{-1}]	γ – ratio of specific heat [Ns/m2]
1.789410^{-5}	0.0242	1006.43	287	1.4

Powder material properties used in the simulation are specified in Tab. 4

Tab. 4 Powder material properties

	Cu	Al	Sn
Density [kg/m^3]	8960	2700	7365
Specific heat [J/(kg·K]	386	897	227

10.2.Particles and gas velocity calculation 2D model

The results obtained from the one isentropic approximation were compared with two dimensional model based on fluid dynamics made in Fluent. The coupled implicit method was used to simulated gas flow in low pressure cold spray. Particles were introduced to the stream after getting stable solution and tracked with discrete phase model (DMP). The nozzle dimensions were taken from spraying device and are presented in the Fig. 40. The effect of radial feeding was neglected to establish axisymmetric model [92].The atmosphere was modeled with cylinder with 30 mm diameter and 150 mm length from the nozzle end. Compressed air with constant viscosity, thermal conductivity and gas heat capacity (Tab. 3) was used in simulation and assumed to obey ideal gas law.

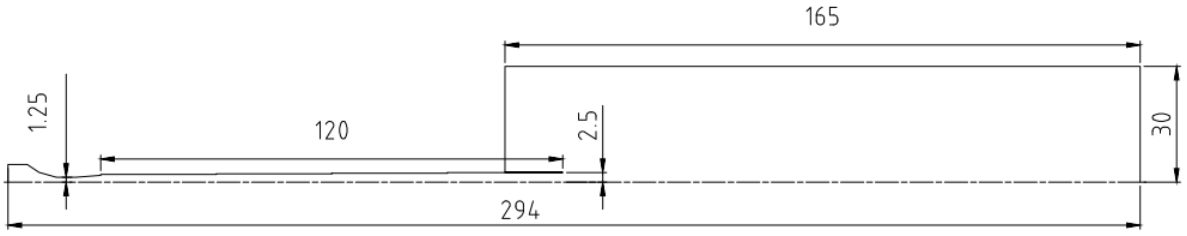

Fig. 40 Calculation domain in Fluent

The inlet was set as pressure boundary with inlet gas temperature 473 K. Simulation was made for three inlet pressures: 0.5, 0.7 and 0.9 MPa. The outlet conditions were set to pressure of 0.1 MPa and temperature of 298 K. The walls were treated as smooth, non-moving and adiabatic boundary. Turbulence of the gas was simulated RNG k-ε model which gives the improved accuracy for rapidly strained flows than standard k-ε [90, 92]. The velocity of powder in the inlet was set to - 5 m/s, the temperature of it to - 293K. The governing equation for powder particles/gas interactions are presented in chapter 5.3. The residuals were controlled to go down below 10^{-6}.

10.3.Simulations results

The results of 1 D calculation are presented in Fig. 41. It can be noticed that that both pressure and temperature of gas affect particles velocity. The temperature increase accelerates the gas stream, and gas pressure enlarges the density of the gas. In case of smaller and lighter powder particles which behave like gas stream [4] the gas temperature is decisive factor. For 20 μm aluminium particles, with the increase in inlet temperature from 293 K to 573K the velocity increased from 428 m/s to 525 m/s at constant pressure of 0.9 MPa. In case of 50 μm aluminium particles the increase was only from 320 m/s to

369 m/s (Fig. 41). The gas pressure contributed more in case of bigger particles for the 50 µm aluminium particle the increment in pressure from 0.5 MPa to 0.9 MPa accelerated them by about 52 m/s in compare to 45 m/s for 20 µm aluminium particles at constant temperature of 473 K (Fig. 42). The inlet gas temperature influences as well the final particles and gas' temperature.

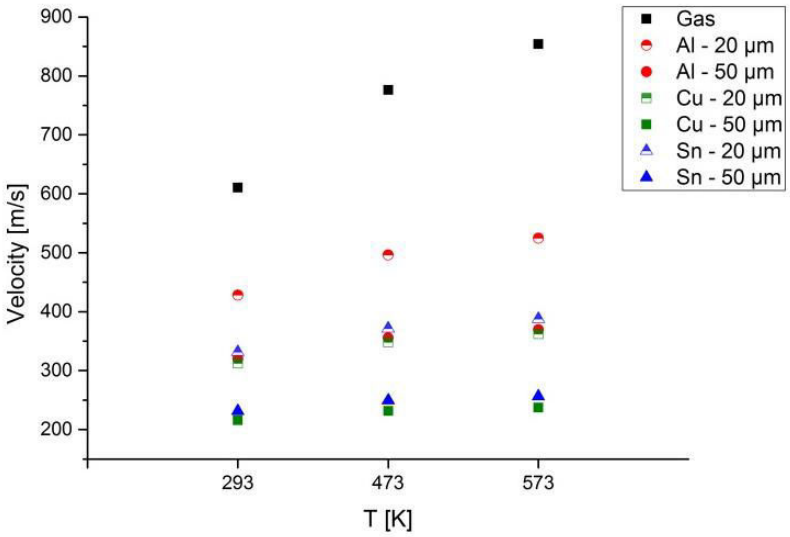

Fig. 41 Particles velocity calculated in Matlab for constant gas initial pressure 0.9 MPa

The obtained results of velocity of particles at the nozzle exit overlaps with the simplified 1D model (when the powder injection is axial), but the particles temperature varies (Fig. 42). The higher gradient of gas temperature in case of one dimensional model causes that particle temperatures are underrated in compare to two dimensional one. It is especially visible in case of particle with low heat capacity - tin. The final value of temperature differ by about 12 K .

a)

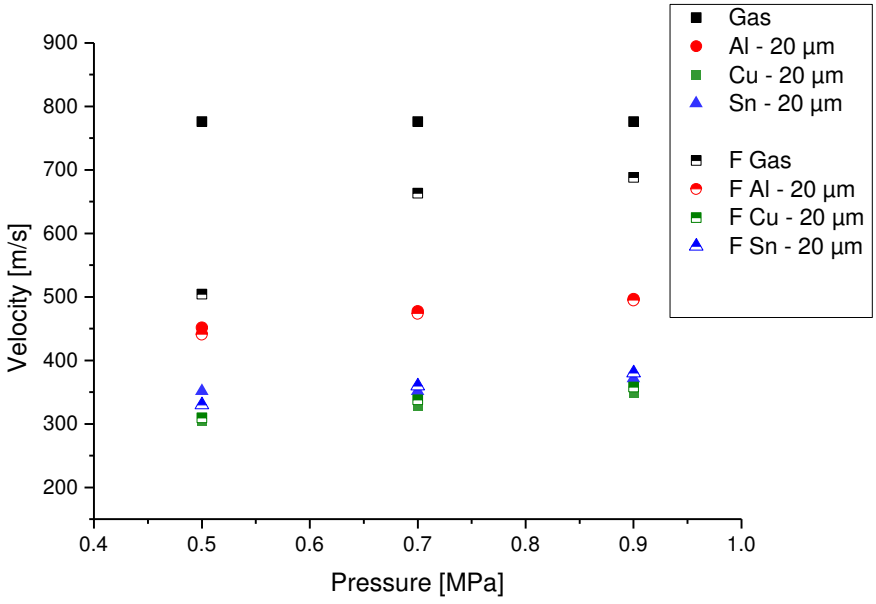

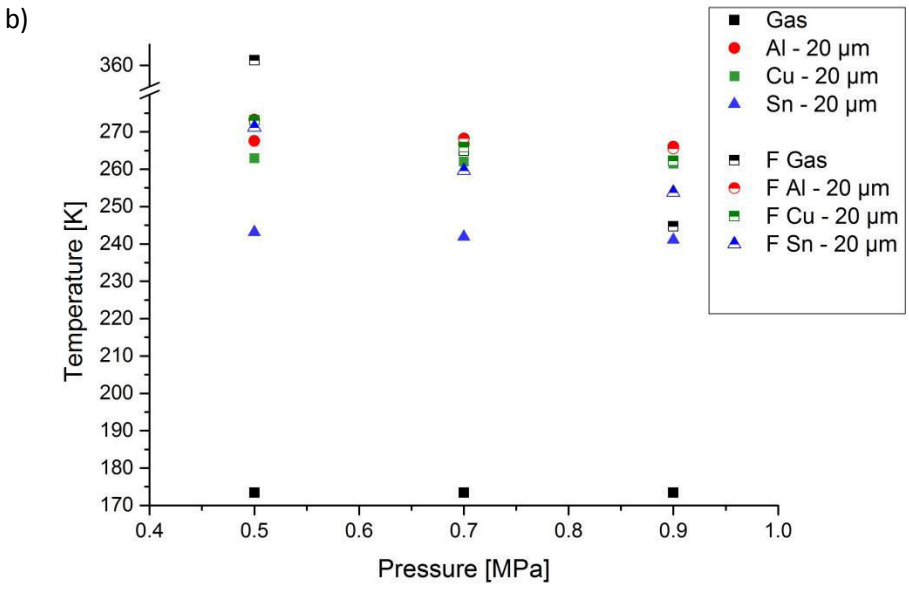

Fig. 42 Comparison of velocity (a) and temperaturę (b) of particles obtained from 1 D and 2 D model

One and two dimensional model differs in gas velocity and temperature (Fig. 43). Below the 0.7 MPa pressure the nozzle works as under expanded one with is not incorporated into the 1D model as well as the shock wave caused by adjustment to ambient conditions. A shock wave zone appears inside the nozzle for pressure 0.5 MPa, moves towards nozzle exit, reaches it for pressure 0.7 MPa and then is gradually reduced. In obtained diagram it may be seen that the velocity of gas oscillates because the nozzle diameter in DYMET 413 changes in steps along its whole length.

The particles are accelerated and heated up beyond the nozzle exit as the gas temperature and velocity are still higher than particles ones. It might be concluded that gas temperature will be decisive for substrate temperature during deposition process and particles will contribute to it mostly through heat generation during impact.

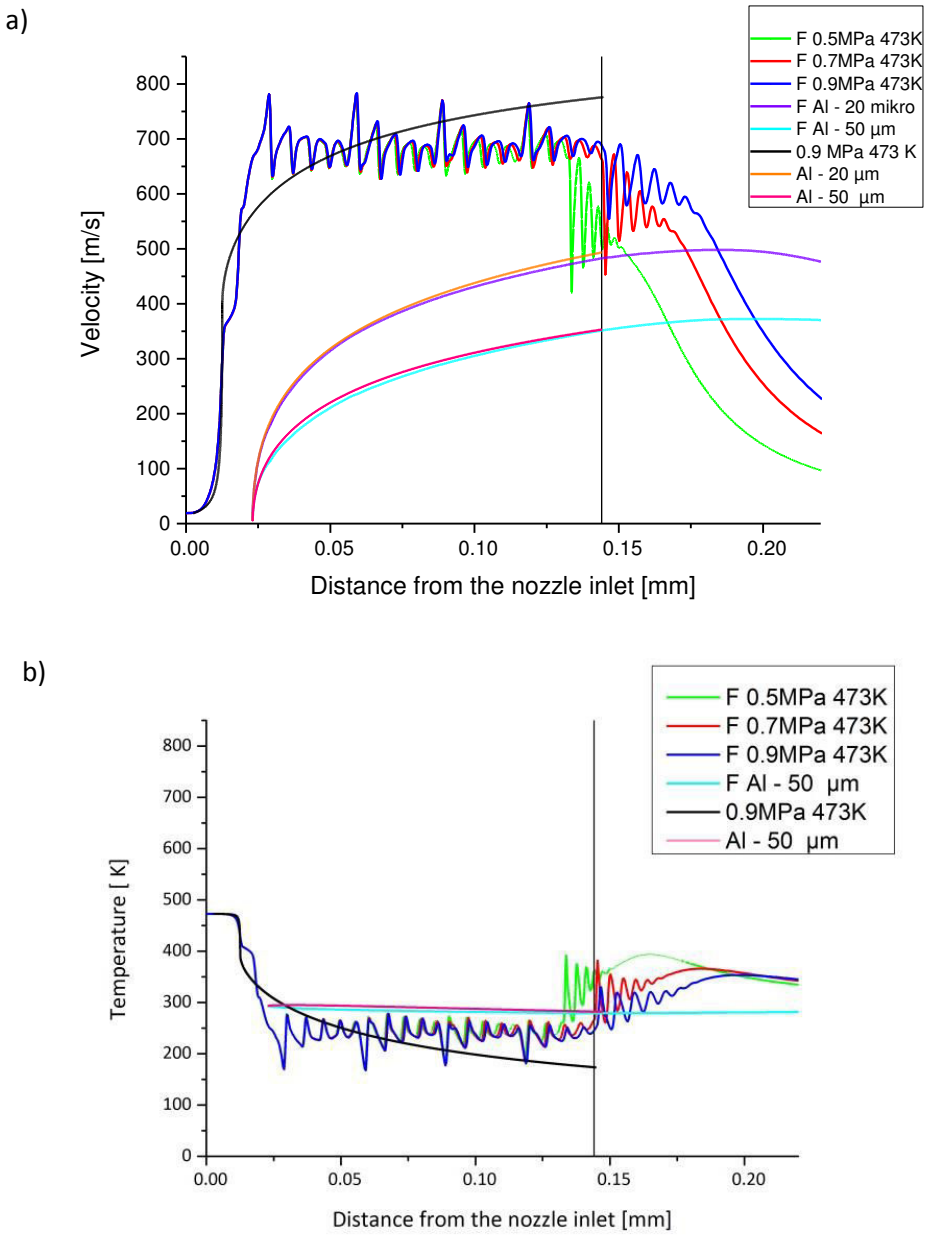

Fig. 43 Comparison of gas velocity (a) and temperature (b)

Presented values are recorded for nozzle axis. The profile of gas and temperature will vary depends on the location in the nozzle (Fig. 44). This phenomenon will affect particles temperature and velocity.

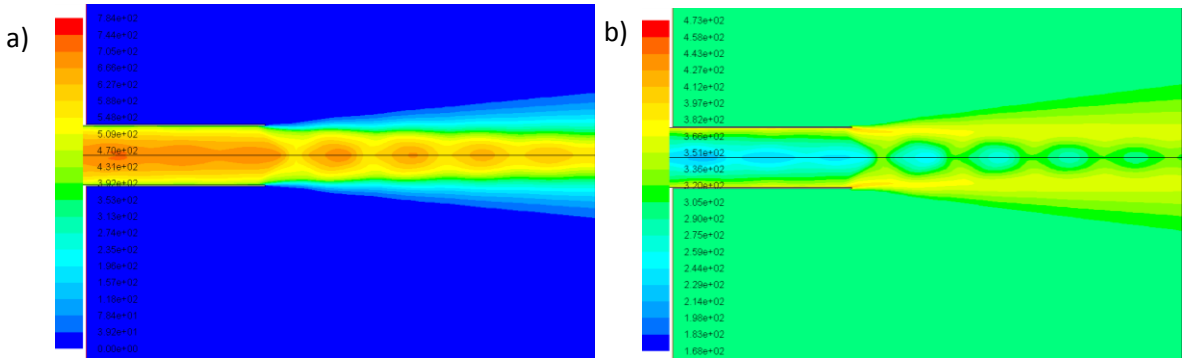

Fig. 44 Velocity (a) and temperature (b) profile at the nozzle exit

Another important factor include i.e. radially powder feeding or feed rate. The increasing value of powder feed rate will result in lower gas and particle velocity. However detailed 3D study of particle and gas flow method is beyond the scope of this thesis.

11. Temperature measurements

Temperature measurements were done for pure gas stream and for gas stream with injected aluminum powder particles (Tab. 5). The mean gas temperature on the substrate surface was 338 K. For deposition process with aluminum powder the temperature raised to about 345 K. Slightly higher temperature recorded when supplying powder was caused by heat generation during particles impact (up to 90% of impact energy is converted to heat as estimated by Grujicic et al [44]). The temperatures inside the substrate will be lower due to low heat conductivity. Measured temperatures are in agreement with ones obtained from simulation. However surprisingly highest temperatures were recorded for highest pressure. It might be caused by instability of heating control unit due to high gas flow rates. The temperature during spraying process varied which resulted in high standard deviation

Tab. 5 Temperature measured for different spraying conditions.

No.	Gas pressure [MPa]	Gas temperature [K]	Nozzle distance from substrate [mm]	Traverse gun velocity [mm/min]	Measurement without powder in the gas stream		Measurement with aluminum powder in the gas stream	
					Mean temperature on the substrate surface [K]	Standard deviation	Mean temperature on the substrate surface [K]	Standard deviation
1	0.5	473	10	2000	334	26	338	26
2	0.7	473		2000	338	26	349	27
3	0.9	473		2000	342	25	347	30
Mean value					338	25.7	334.7	27.7

12. Preliminary deposition tests

The critical velocity calculated for chosen feedstock materials may be approximated using equation proposed by Schmidt et al [1]. The equation takes into account thermal softening, tensile strength and density of material. The influence of o particle diameter may be also incorporated. The values calculated for room impact temperature for particles with diameter 20 μm are [16]:

- Al 620-660 m/s
- Cu 460-500 m/s
- Sn 160-180m/s

From these values it may be seen that apart from Sn particles the critical velocity is not reached when spraying with low pressure device with temperature 473 K. The η coefficient (v_p/v_{cr}) for highest used parameter (0.9 MPa and 473 K) amounts to :

- for Al ~ 0.8
- for Cu ~ 0.78

It means that spraying conditions are not optimal. Two ways may be taken to get value of η coefficient close to 1 which assures us creating of shear instabilities – increasing of particles velocity or decreasing critical velocity of the feedstock. In order to increase particles velocity we can: increase spraying parameters (gas pressure and temperature), use gas with higher ratio of specific heat, change the size of feedstock particles or its morphology (to get higher drag coefficient). The second way is to decrease the critical velocity. Critical velocity of a particle is fundamentally influenced by its oxidation level, temperature, morphology and size and the substrate material. The value of 310 m/s was recorded in [55, 62] for concentration of oxides 0.02 %. With increasing level of surface oxide 0.38 %, critical velocity can reach about 610 m/s [62]. Similar high value of critical velocity - 640 m/s was found by Gilmore et al [36]. Size dependence was noted by Schmidt et al [1]. Critical velocity decreases with increasing size of particle which was attributed to effect of heat conduction and strain hardening. Morphology of powder influences both drag coefficient and impact behavior. Koivuluoto et al [142] noted that coatings sprayed with dendritic powder, in compare to spherical one, have higher porosity and lower bond strength. It was attributed to higher oxide content in case of dendritic powder. On the other hand Kumar et al [76] observed more dense coatings in case of granular in compare to spherical one. Dendritic particles are more suitable for spraying

onto polymer. Ganesan et al [77] noted that dendritic powder have higher velocity in the gas stream but the overall impact energy is minimized through several contact points with substrate material. The lower critical impact velocity of dendritic powder was also indicated by Winnicki et al [143].

Increasing spraying parameters was rejected. The preliminary tests demonstrated that for temperature above 473 K no coating will be formed, the coating will be delaminated or the surface of the polymer will be damaged. The gas temperature of 473 K when spraying on polymers, was also indicated as optimal one by Ganesan et al [129]. The higher gas pressure is outside the limit of the device, the gas type was also not changed. In the end playing parameters were: morphology (spherical or dendritic) and oxidation level.

12.1.Aluminium coatings

Aluminium powder was deposited with various parameters (Tab. 6) on extruded PA6 (Plastics Group, Poland) in order to select initially appropriate parameters. Influence of pressure, temperature and gun traverse velocity was tested.

Tab. 6 Spraying parameters for initial trials of spraying aluminum powder

Sample number	Pressure [MPa]	Temperature [K]	Gun traverse velocity [mm/min]	Spraying distance [mm]
P1	0.5	273	1000	10
P2	0.7			
P3	0.9			
P4	0.5	473		
P5	0.7			
P6	0.9			
P7	0.5	573		
P8	0.7			
P9	0.9			
P10	0.5	0	2000	
P11	0.7			
P12	0.9			
P13	0.5	473		
P14	0.7			
P15	0.9			
P16	0.5	573		
P17	0.7			
P18	0.9			

For gas temperature equal to 273 K no coating was formed for any gas pressure and gun traverse velocity, and for 573 K coatings detached immediately after spraying (Fig. 45). Substrate material - PA6 has melting temperature at the level of 493 K , but its glass transition temperature is 323 K. Above T_g mechanical properties of polymers decreases gradually. Additionally thermal expansion coefficient of aluminum is four times lower than of PA6 which causes thermal stresses during cooling and in consequence delaminating of coating. In cold spray process quality of the coating is influenced mostly by velocity of the

particles (controlled by gas preheating temperature and pressure). Hence impossibility of use higher temperature will result in lower particle velocity and lower coating quality.

The other observed phenomenon was related to the feedrate; the aluminum coating was not formed below feedrate equals to 30 g/min. But this effect was not further studied as it might have been caused by very unstable behavior of commercial powder feeder being integral part of DYMET system. Similar phenomena was observed in [125]. Aluminum coating started to deposit on Lexan from 20 g/min. Below this value only scanty, local deposition was observed.

For further deposition trial gas preheating temperature 473 K and gas pressure 0.9 MPa was chosen.

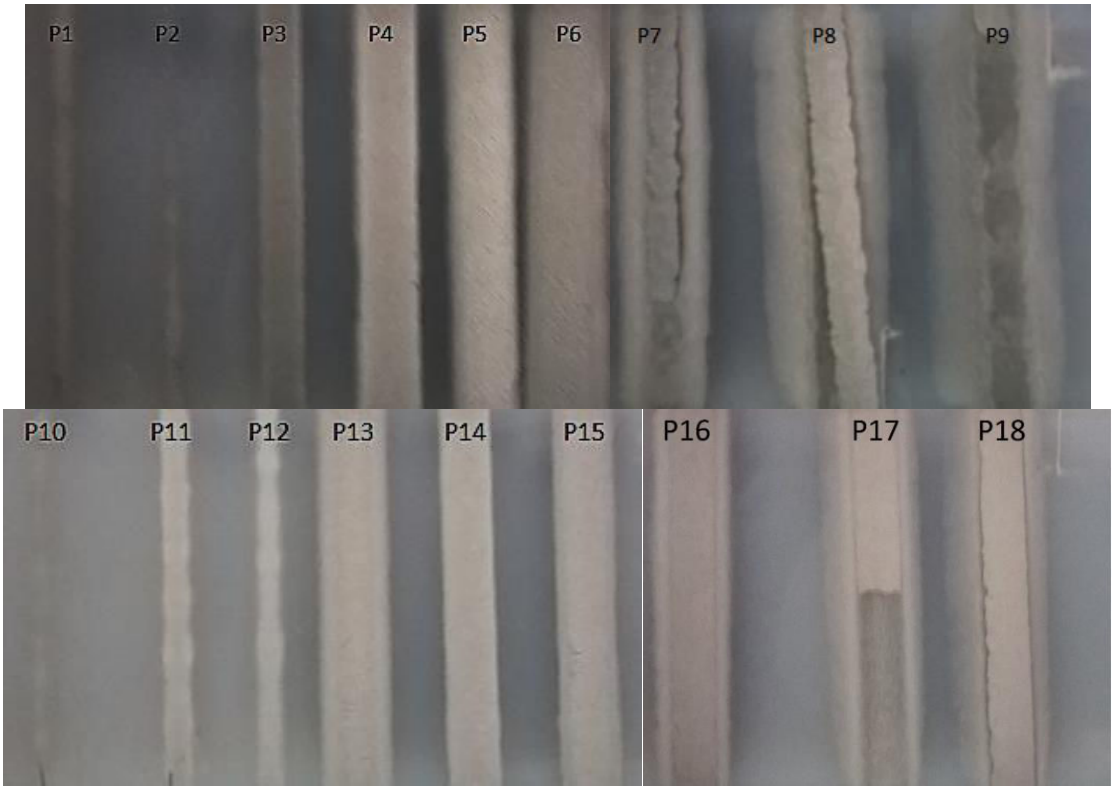

Fig. 45 Aluminium tracks deposited for parameter given in Tab. 6

12.1.1.Aluminum deposition on sandblasted substrate

Aluminum deposited directly on the substrate have very low adhesion strength and tends to delaminate spontaneously even for optimal chosen parameters - gas preheating temperature 473 K and gas pressure 0.9 MPa. Due to limitation of the spraying setup further increasing of gas pressure was not possible therefore substrate surface was modified to increase bond strength. The substrate material was extruded PA6 (Plastics Group, Poland) in form of cylinder with Ø 40 mm diameter and 10 mm of thickness.

The same samples were used for tensile pull test of coatings, stereometric measurements and microstructure analysis. The samples were grit-blasted before coating with commercial alumina type K-00-04-16 (Obninsk Center for Powder Spraying, Russia) with particle sizes lower than 350 μm. Tab. 7 shows the operational parameters used at blasting. The geometry of surface was investigated by profilometer and confocal microscope and its influence on the adhesion strength of coatings was analyzed.

Tab. 7 Parameters of sand blasting

Run no.	Grit feed rate [g/min]	Traverse speed υ_l [mm/s]	Gas pressure p_g [MPa]	Gas temperature T_g [K]	Stand-off distance [mm]
1	12	1000	0.7	473	15
2				573	
3				673	
4				773	
5			0.8	473	
6				573	
7				673	
8				773	
9			0.9	473	
10				573	
11				673	
12				773	

The coatings were produced with air at pressure 0.9 MPa (maximal operating pressure for the device) and temperature 473 K (maximal possible for polymers as estimating previously). The powder feed rate was 30 g/min and stand-off distance was of 10 mm. The arrangement of individual spraying gun passes is shown in Fig. 46. Spraying was started in the middle of the substrate and continued alternately on the both sides to enable a uniform heat distribution. The distance between the spraying tracks was 3.5 mm so the neighbouring spraying tracks were overlapped. The same spraying design was used both for grit-blasting and spraying coatings.

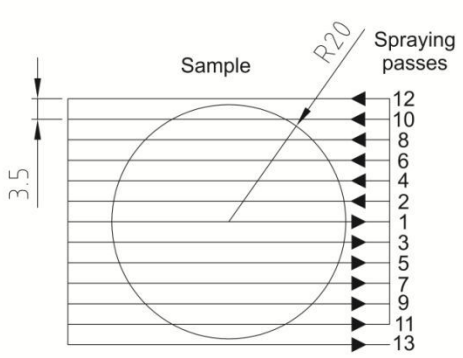

Fig. 46 Arrangement of individual spraying gun passes on the sample

12.1.2.Results of aluminum deposition on sandblasted substrate

Substrate geometry

The roughness of PA6 substrate sand-blasted with different parameter is given in Fig. 50. The roughness showed to be dependent from the air temperature and independent from the air pressure. The dependence from the temperature was roughly linear. The highest value of roughness were obtained for highest temperature 773 K and amounted to R_a =~90 μm. The lowest value was R_a =~30 μm. For comparison the roughness of substrate after turning was R_a =~4 μm.

The stereometry of selected coatings was studied also using confocal microscope (Tab. 8). As can be seen from comparison the roughness and waviness value obtained from measurement with confocal microscope are similar with values obtained while using profilometer. The difference is noted for R_t and R_z roughness parameters.

Tab. 8 The roughness and waviness of PA6 substrate after sand-blasting

Trial No.	Output parameter							
	Profilometer (cut off length 8 mm)				Confocal microscope (cut off length 8 mm)			
	Roughness [μm]			Waviness [μm]	Roughness [μm]			Waviness [μm]
	R_a [μm]	R_t [μm]	R_z (DIN) [μm]	Wa [μm]	R_a [μm]	R_t [μm]	R_z [μm]	Wa [μm]
1	31.3	206.4	195.2	12.1	34.6	311.3	226.9	44.3
4	90.6	450.5	408.5	37.7	83.9	621.5	512.8	30.9
9	33.0	210.3	197.8	21.1	44.3	433.8	341.2	21.5
12	86.8	473.7	412.3	34.988	77.5	612.5	472.7	40.7

The profile of the surface after sandblasting for selected samples can be seen in Fig. 47 and Fig. 48

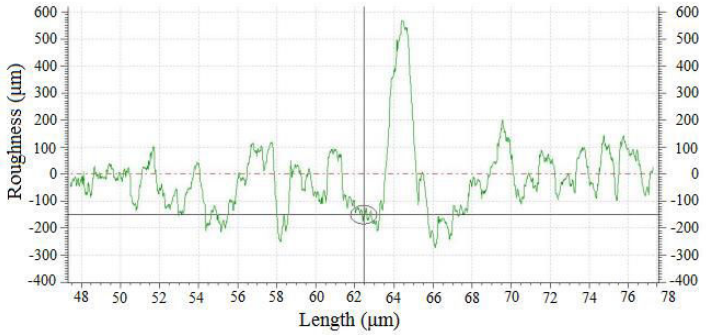

Fig. 47 Profile of sand-blasted substrate PA6 measured by profilometer.

The profiles obtained using profilometer and confocal microscope are similar. In Fig. 48 might be seen that surface is much more developed for higher temperature of sand-blasting what will facilitate deposition of coating and increase bond strength while the effect of pressure on surface stereometry is negligible. The sharp peak in the middle of sample for temperature 773 K is caused by shape of spraying gun track.

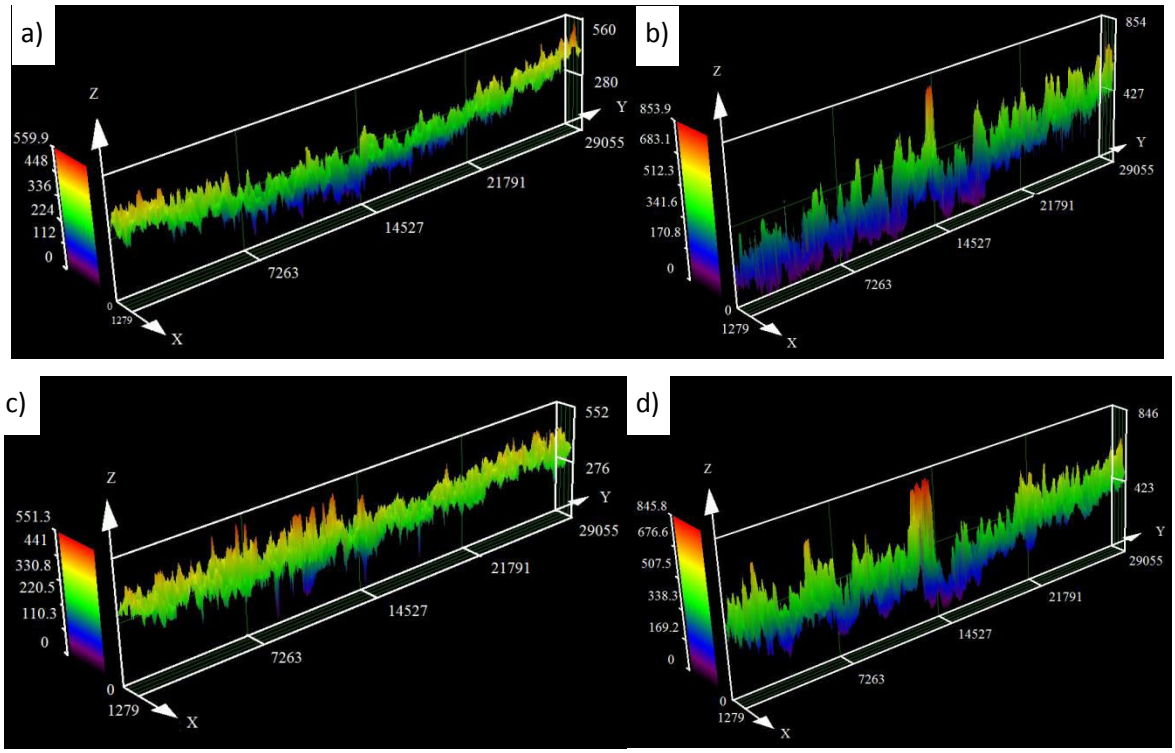

Fig. 48 The profile of sand-blasted substrate PA6 measured by confocal microscope for a) 0.7 MPa and 473 K, b) 0.7 MPa and 773 K, c) 0.9MPa and 473 K d) 0.9 MPa and 773 K.

The adhesion measurements

The thicknesses of the coatings were measured with the dial thickness gauge and were equal to 600±100 μm in all cases. The high standard deviation is caused by corrugated surface of coating. The thickness was measured in ten points including lowest and highest ones and then the average was taken.

The sample after adhesion test is shown in Fig. 49. The cohesive type of fracture is clearly seen. The adhesion strength was directly related to the temperature of sandblasting the substrate. It increases with the temperature up to 673 K after with no change was observed. The highest value was approximately 4 MPa. In case of sand-blasting pressure 7 MPa the biggest rise was noticed between the temperature 573 K and 673 K. For higher pressures the increase with sandblasting temperature was significant for both temperature rise from 473 K to 573 K and from 573 K to 673 K.

Fig. 49 View of cohesive type of fracture after adhesion test.

The correlation between the substrate roughens and the temperature of sandblasting can be seen (Fig. 50). The adhesion strength of sample not prepared by sand blasting was very small and equal to about 0.5 MPa. The coatings delaminate easily after process and detached. Although the part of the Al particles remains embedded in the surface (Fig. 51).

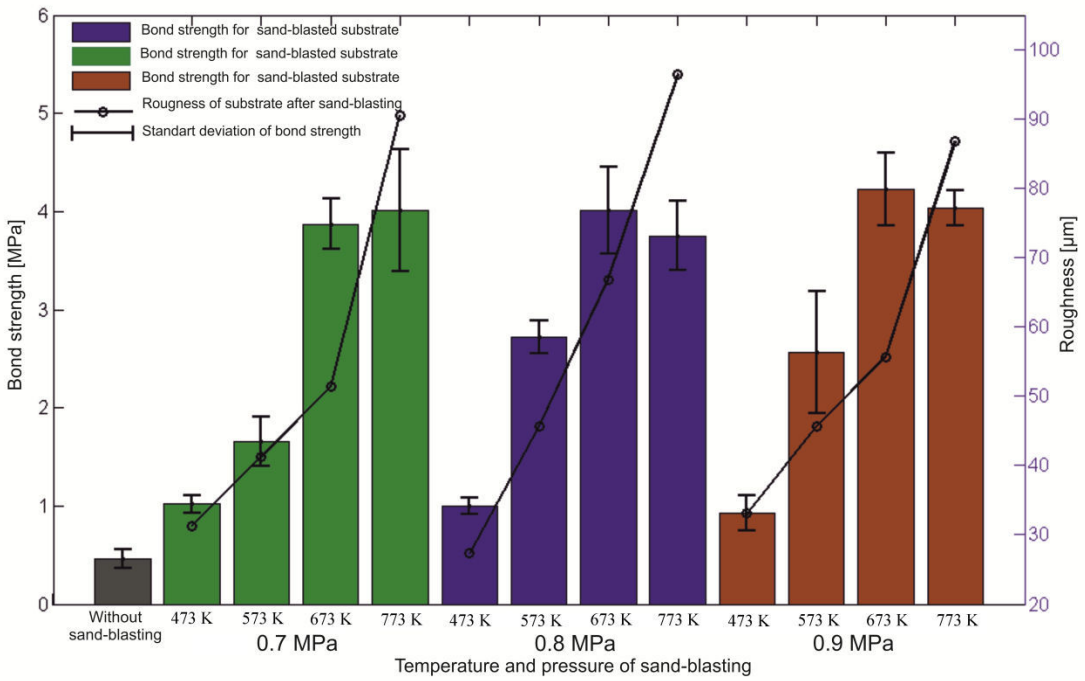

Fig. 50 Bond strength of coatings on the substrates sand-blasted with different parameters

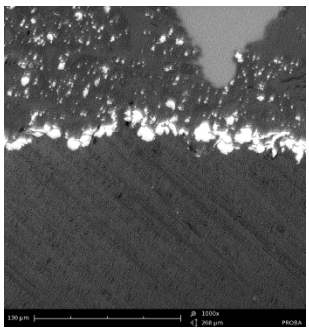

Fig. 51 SEM of substrate after detaching off the Al coating.

The metallographic examinations

The cross-sections of selected coatings are shown in Fig. 52 and Fig. 53. The thickness is in all cases comparable and high porosity is visible. The main difference is in the porosity distributions. In case of coatings deposited on substrates sandblasted with temperature 773 K regardless the pressure the dense layer can be seen right next to substrate. For coatings deposited on substrate sandblasted with lower temperature this layer is shifted to the middle of the coatings. The amount of embedment alumina particles in the substrate after sandblasting on rise with the pressure and temperature and reach peak for the samples sandblasted with pressure 0.9 MPa and temperature 773 K. Its presence favours densification of the coating although the thickest dense layer was obtained for sample sandblasted with pressure 0.7 MPa and temperature 773 K. Only in some parts of the coating the deformation of aluminium was sufficient to eliminate the visibility of grain

boundaries. It had been shown in [144] that sandblasting has slightly positive effect on resistance to stress corrosion cracking in case of E-glass/polymer. However loading polymer surface with alumina particles can cause internal stress leading to the failure under the coating/surface interface. Also the influence of temperature on the polymer structure is important factor. Slight delamination's areas and cracks can be seen for coating with low adhesion strength. For all coatings in its upper layer the particles remains very weak bounded to each other (Fig. 53). This is related with densification phenomena. Particles previously deposited on the surface are compacting by successive incoming particles. Hence the material layers situated in the lower part of coating supposed to be more dense [32, 123, 145]. However in case of soft substrate i.e. polymer the shifting of the dense layer to the middle of the coating can be observed (Fig. 52). The firstly arrived particles are subjected to only slight deformation as the substrate is too soft. I may be assumed that new incoming particles instead of tamping them just hammering them deeper into the substrate. At the moment when the layer is thick enough and hence the substrate is harder the tamping effect may be observed.

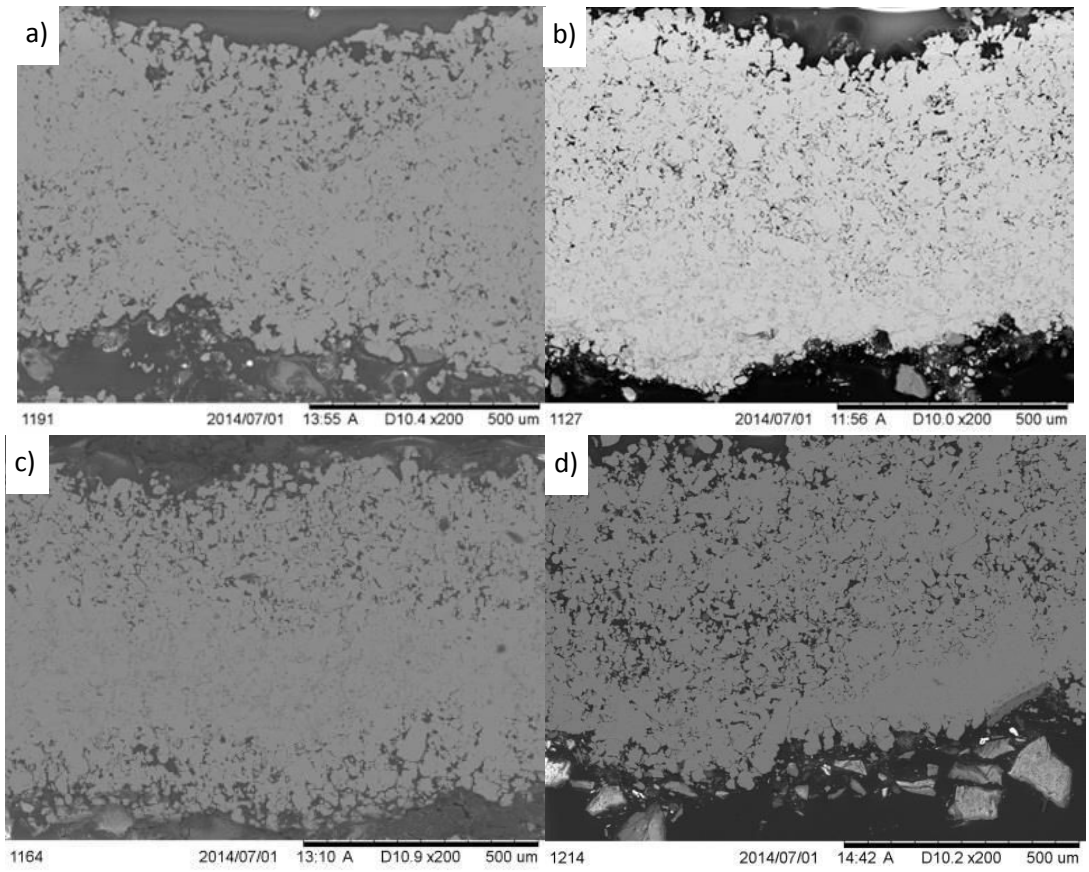

Fig. 52 SEM of Al coating on PA6 substrate sandblasted with various pressures and temperatures: a) 0.7 MPa 473 K, b) 0.7 MPa 773 K c) 0.9 MPa 473 K, d) 0.9 MPa 773 K.

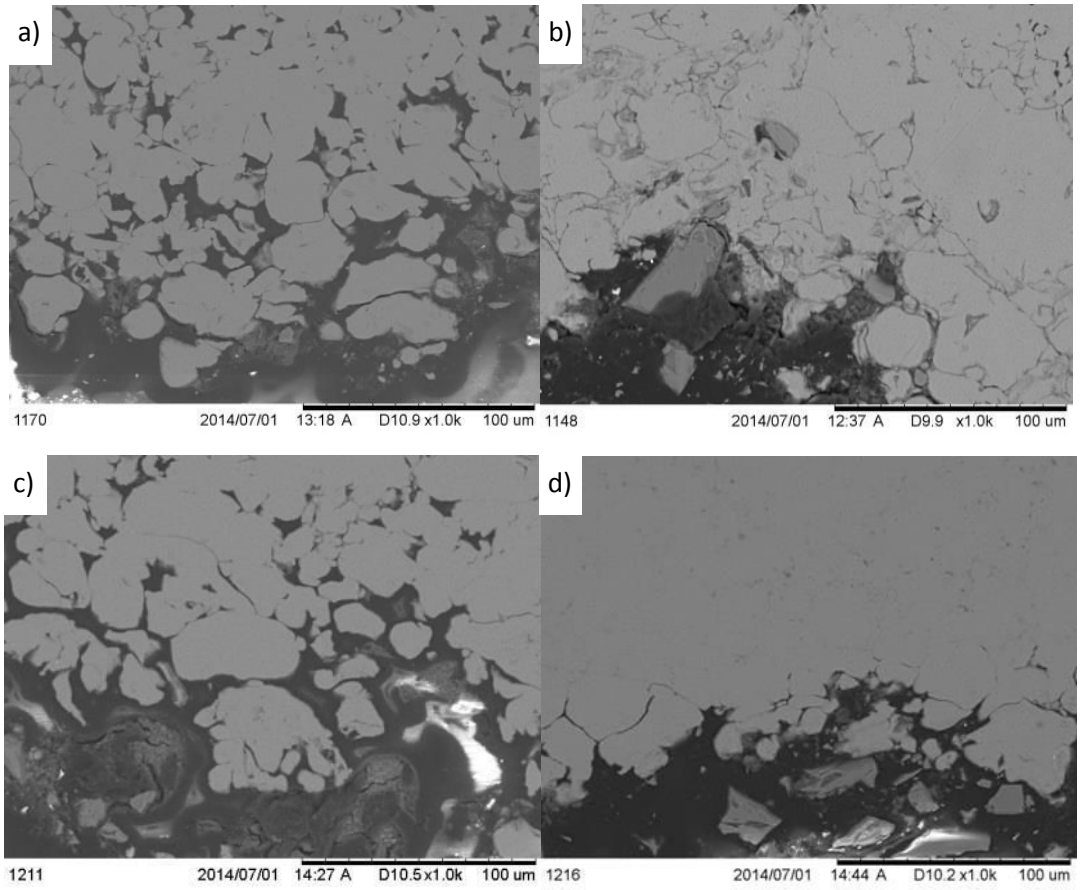

Fig. 53 SEM of interface between Al coating and PA6 substrate sandblasted with various pressures and temperature: a) 0.7 MPa 473 K, b) 0.7 MPa 773 K, c) 0.9 MPa 473 K d) 0.9 MPa 773 K.

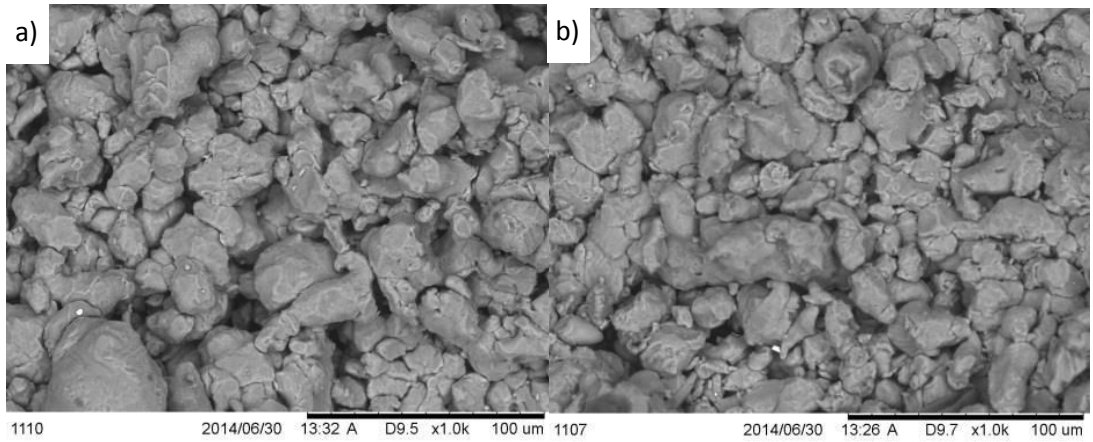

Fig. 54 SEM of surface of Al coating on PA6 substrate sandblasted with various pressures and temperature: a) 0.9 MPa 473 K, b) 0.9 MPa 773 K.

The stereometry of the substrate influences significantly adhesion strength of coating. The adhesion increases with roughness. Additionally, the substrate preparation changes pores distribution in the coating. It may be caused both by increasing the amount of alumina (Al_2O_3) in the substrate. Substrate hardness is an important factor. In places where alumina particles were present the coatings were denser. It must be noted however that

alumina presence may cause additional stresses and be the origin of the cracks. In case of higher temperature of sandblasting i.e. 773 K the dense layer was right to the coating and was equalled about one third of its thickness (Fig. 52b, d). The sandblasting pressure was also important factor. For lower pressure the dense layer was bigger but with more visible grain boundaries compared to samples sandblasted with pressure 0.7 MPa. In case of lower sandblasting temperature and therefore lower amount of alumina particles in substrate firstly some layer of aluminium must be built on the substrate to enable, due to its higher hardness, forming dense layer (Fig. 52a, c). The upper parts of the coatings, in all samples, were bonded weak. This is the result of the hammering effect of incoming particle which compact the layer underneath. The observed increase in adhesion strength of aluminium on PA6 was from 0.5 to about 4 MPa. This increase was caused by changing properties of surface stereometry as well as amount of alumina in substrate which formed quasi interlayer. The spraying parameters were constant. Using higher spraying parameters and additional layer of cooper in order to compact aluminium coating Zhou et al [123] obtained adhesion strength on PEEK450CA30 amounted 2.26 MPa. This is about 50 % less than in present study. The bonding mechanism of metal particles with substrate was describe in i.e. in [128, 145]. It is believed that firstly the metal particles are embedded in the polymer squeezing it. Next the coating is built based on this first layer. It means that the conditions for depositions changes while spraying. One of proposed solution is producing interlayer from material with low critical velocity i.e. tin and then deposition the target coating.

12.2.Tin coatings

Tin coatings were deposited on PC substrate with parameters given in Tab. 9. Tin has low melting temperature ~ 503 K therefore gas preaching temperature 573 K was not tested.

Tab. 9 Spraying parameters for initial trials of spraying tin powder

Sample number	Pressure [MPa]	Temperature [K]	Gun traverse velocity [mm/min]	Stand-off distance [mm]
S1	0.5	273	1000	15
S2	0.7			
S3	0.9			
S4	0.5	473		
S5	0.7			
S6	0.9			

Similarly to aluminum powder no deposition was observed for gas preheating temperature equal to 273 K for any pressure. Gas pressure influences notable deposition at gas preheating temperature equal to 473 K. For 0.5 MPa smooth tin coating was formed but for 0.7 MPa coatings waviness starting to appears reaching maximum at pressure 0.9 MPa. Gas and particles velocity in the axis of nozzle was to high pushing already deposited particles sideward and causing high waviness of the coatings (Fig. 55). Optimal coatings conditions were taken as: gas preheating temperature 473 K and gas pressure 0.5 MPa.

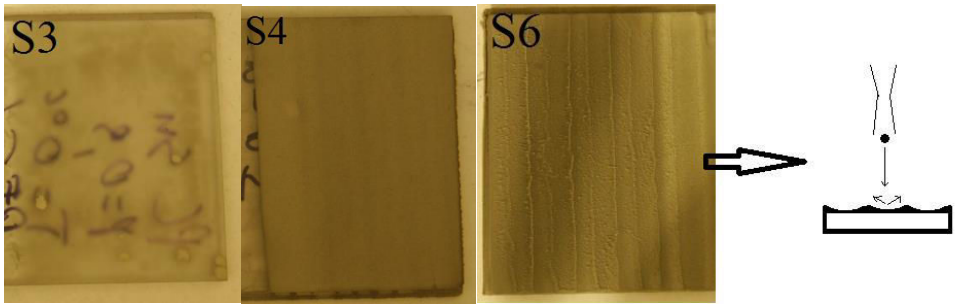

Fig. 55 Deposited tin tracks for parameter given in Tab. 9

12.3.Copper coatings

In this chapter results of preliminary deposition trials of copper powder with different morphology with and without heat treatment are given.

12.3.1.Deposition trials with untreated powders

Copper powders in delivery state was sprayed directly on PA6 substrate with parameter listed in Tab. 10.

Tab. 10 Spraying parameters for initial trials of spraying copper powder in delivery state

No	Powder	Gas temperature [K]	Gas pressure [MPa]	Standoff distance [mm]	Gun traverse speed [mm/min]	No. of spraying gun passages	Powder feeding rate [g/min]
CS1	Cu spherical	473	0.9	10	1000	1	30
CS2	Cu spherical	473	0.9	10	1000	3	30
CN1	Cu spherical	573	0.9	10	1000	1	30
CN2	Cu spherical	573	0.9	10	1000	3	30
CN3	Cu spherical	473	0.9	10	1000	1	30
	Cu granular	473	0.9	10	1000	1	30
CN4	Cu spherical	473	0.9	10	1000	2	30
	Cu granular	473	0.9	10	1000	1	30

The preliminary test indicates that it is impossible to get thick Cu coating using low pressure cold spray equipment. In case of spherical powder the particles were just stuck to the substrate independent on the number of passes (Fig. 56 and Fig. 57). Increased number of passes changed only slightly thickness of layer (accumulation of particles). No deformation of spheres took places after contact with substrate. This indicates that the hardness and stiffness of the substrate was too low to cause deformation or the velocity of sprayed particles was well below critical one (calculated η~0.78 for particles with diameter 20 μm). It the literature may be found that bigger particles have lower critical velocity [1] but in the case of soft substrate it seems that only very small ones can deform. Additionally, although there is a high difference in tensile strength and young modulus between the polyamide 6 and the copper, the copper particles are not driven deep into the substrate and rather remain on the surface.

a) b)

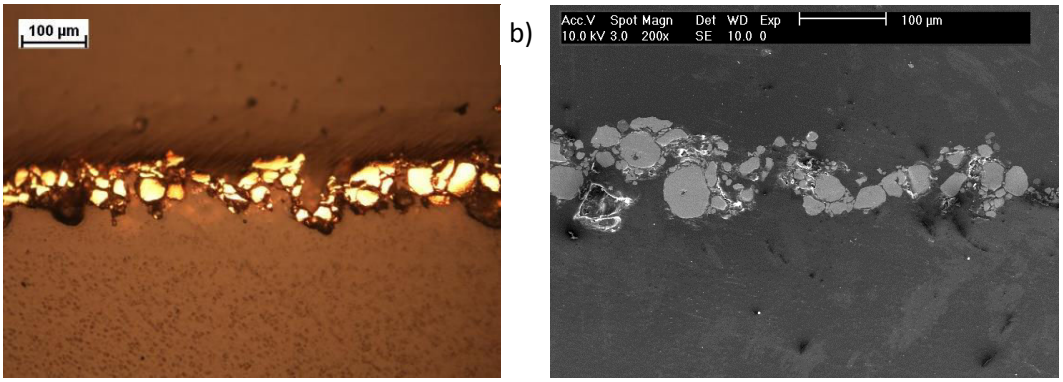

Fig. 56 Copper tracks deposited for parameters CS1 given in Tab. 10 (light microscope (a), SEM (b))

a) b)

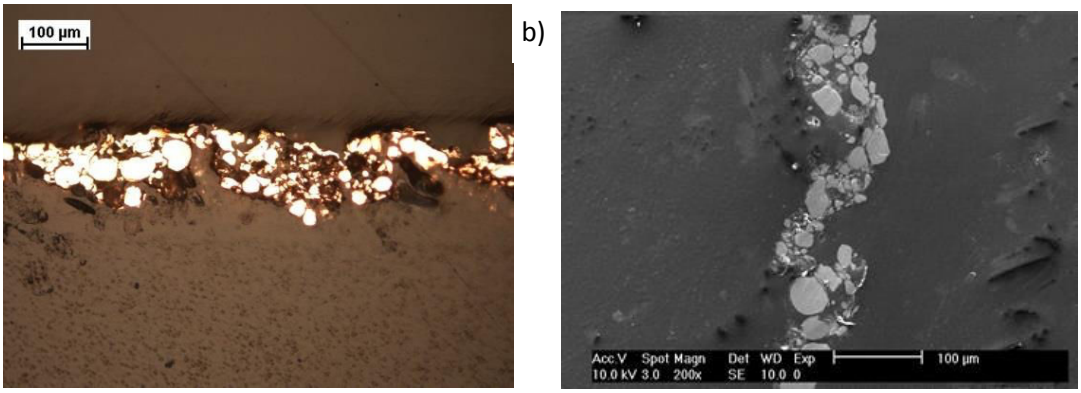

Fig. 57 Copper tracks deposited for parameters CS2 given in Tab. 10 (light microscope (a), SEM (b))

Similar phenomena may by observe in case when spraying with higher gas inlet temperature. The continuous layer has not been formed independent on the number of layer but with increased number of passes the layer seems to be more packed and wavier since the particles are driven deeper into the substrate (Fig. 58 and Fig. 59). The uncontinuous layers are thicker than in case of spraying with lower temperature.

a) b)

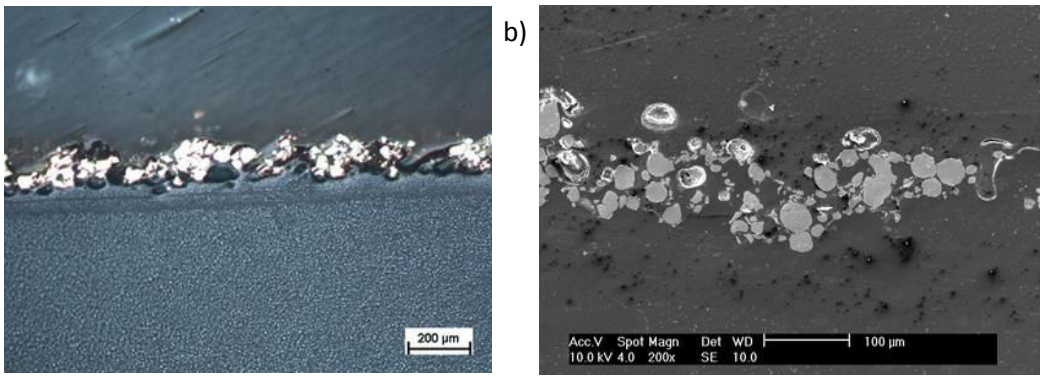

Fig. 58 Copper tracks deposited for parameters CN1 given in Tab. 10 (light microscope (a), SEM (b))

a) b)

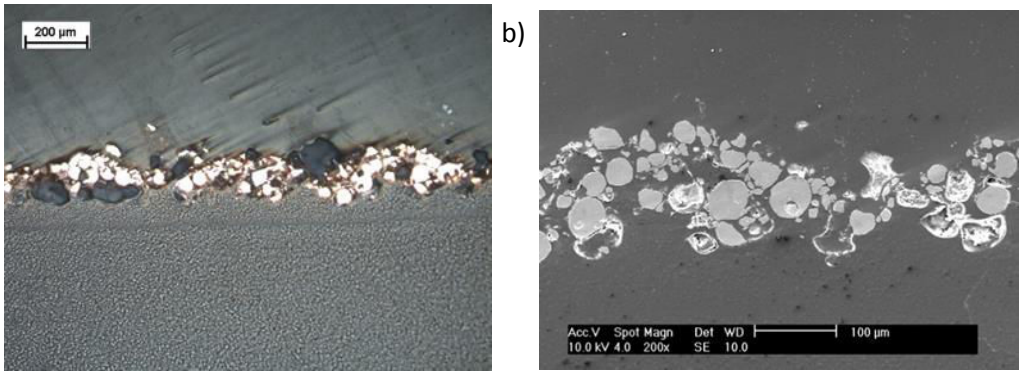

Fig. 59 Copper tracks deposited for parameters CN2 given in Tab. 10 (light microscope (a), SEM (b))

The solution proposed by Ganesan et al [129] to use spherical particles as interlayers was tested. The globular particles were sprayed on the previous deposited spherical ones but without success. It can be seen that globular particles fragmented and partially deformed but no bonding may be found (Fig. 60 and Fig. 61). The interlayer was probably too loose and the velocity of the granular particles to low. The spherical particles were displaced by upcoming granular particles. There are only several places in which the spherical particles remained. The second pass with globular particles hammered already deposited ones and the small fragments of particles seem to be closer to each other.

a) b)

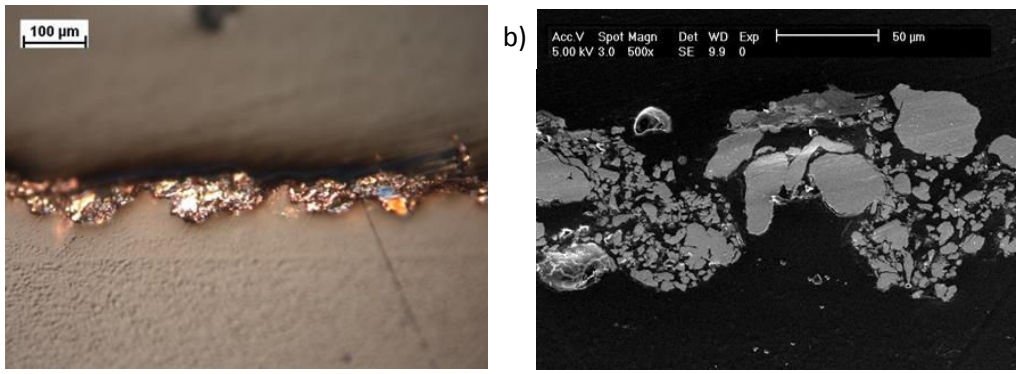

Fig. 60 Copper tracks deposited for parameters CN3 given in Tab. 10 (light microscope (a), SEM (b))

a) b)

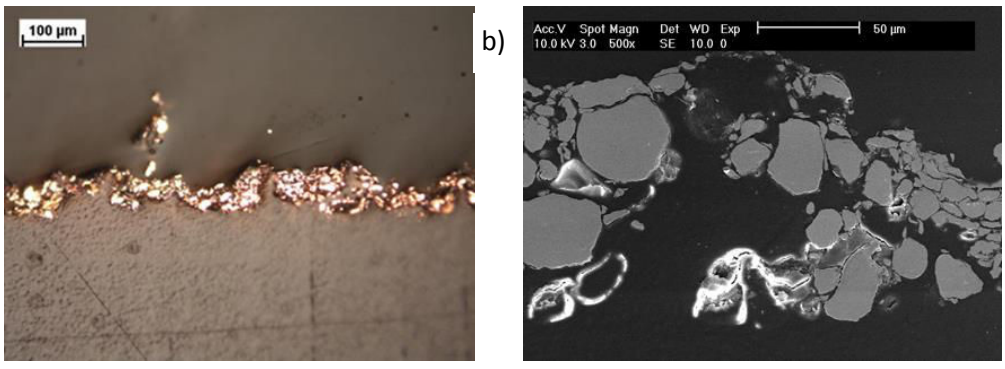

Fig. 61 Copper tracks deposited for parameters CN4 given in Tab. 10 (light microscope (a), SEM (b))

The copper was also sprayed onto tin interlayers but without success.

12.3.2.Deposition trials with powder after heat treatment

Copper powders after heat treatment were sprayed on PA6 substrate with parameter listed in Tab. 11 as single tracks.

Tab. 11 Spraying parameters for initial trials of spraying copper powder after heat treatment

No	Powder	Gas temperature [K]	Gas pressure [MPa]	Standoff distance [mm]	Gun traverse speed [mm/min]	No. of spraying gun passages	Powder feeding rate [g/min]
CC1	Cu spherical	473	0.9	10	3000	3	30
	Cu granular	473	0.9	10	3000	1	30
CC2	Cu spherical	473	0.9	10	2000	3	30
	Cu granular	473	0.9	10	2000	1	30
CC3	Cu spherical	473	0.9	10	1000	3	30
	Cu granular	473	0.9	10	1000	1	30
CX1	Sn+Al_2O_3	473	0.9	10	1000	1	30
	Cu granular	473	0.9	10	3000	2	30
CX2	Sn+Al_2O_3	473	0.9	10	2000	1	30
	Cu granular	473	0.9	10	3000	2	30
CX3	Sn+Al_2O_3	473	0.9	10	3000	1	30
	Cu granular	473	0.9	10	3000	2	30
CX4	Sn	473	0.9	10	3000	1	30
	Cu granular	473	0.9	10	3000	2	30
CX5	Sandblasting with Al_2O_3 <63 µm	673	0.9	15	2500	1	30
	Al	473	0.9	10	3000	1	30
	Cu granular	473	0.9	10	3000	2	30

Spherical particles interlayer

Firstly the trials with interlayers from spherical powder particles were made with varying gun scan velocity. The first trial was done with velocity *v*=1000 mm/min (Fig. 62). In this case the globular particles replaced spherical ones, even in places where spherical particles remained no deformation may be observed. It seems that the loading of particles impacting in one place was too high causing detaching already deposited ones.

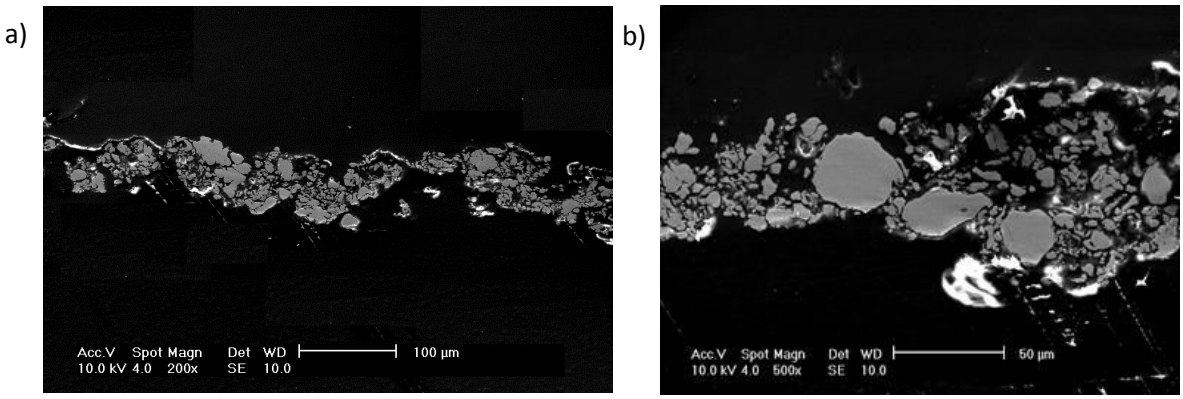

Fig. 62 Copper tracks deposited for parameters CC3 given in Tab. 11 (200x (a), 500x (b), SEM)

For higher scan velocity v=2000 m/s deformation of the dendritic particles was observed especially in places with already deposited spherical ones (Fig. 63).

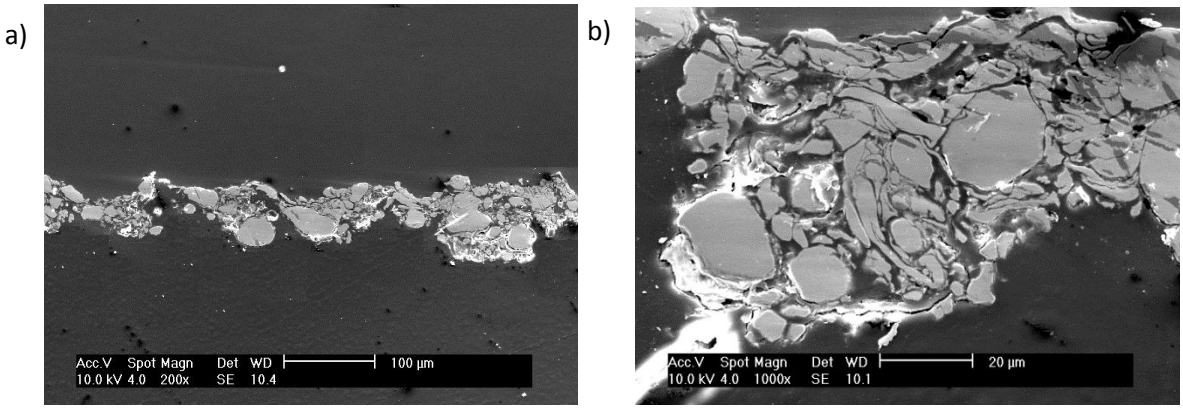

Fig. 63 Copper tracks deposited for parameters CC2 given in Tab. 11 (200x (a), 1000x (b), SEM)

This observation suggest that loading effect and resulting impact energy concentration in defined region plays a role in deposition mechanism. The bonding of first layer is decisive for possibility of obtaining thick coatings.

Sn interlayer

Sn was tested as the interlayer because it poses lowest critical velocity among usual cold spray feedstock material. As a variation also Sn+A_2O_3 was applied. Addition of Sn+A_2O_3 is commonly added in low pressure cold spray method: it hammers additionally

already deposited metal particles, sandblasts the substrate and prevents nozzle clogging [142]. However tin is easy metal to deposit and for the used temperature 473 K no clogging occurs. So, why ceramic addition was used? In low pressure Dymet 413 device the powder feeders are gravitational type and the amount of feeding powder is not constant in time especially for powder with low flow ability. Flow ability is affected by particle size, its morphology, electrostatic forces, temperature and humidity [146]. The flow ability of tin was not measured but it was difficult to set stable very low feed rate, especially, for higher pressure 0.9 MPa because underpressure in the nozzle tends to vanish. On the other hand higher federates result in very uneven coatings. The velocity of tin particles when using parameters pressure 0.9 MPa and temperature 473 K was too high causes that only part of them were driven into the substrate the rest bounced off and shifted sideward. Additionally the particles on the outskirts of stream had smaller velocity and were deposited in form of straps with higher thickness (Fig. 64). This behavior was especially visible for higher number of spraying passes. During subsequent deposition of Cu particles, newly formed coating partially detached in these places. When using lower gas pressure to get uniform tin coating the bonding was to week and subsequent deposition of Cu particles caused erosion only.

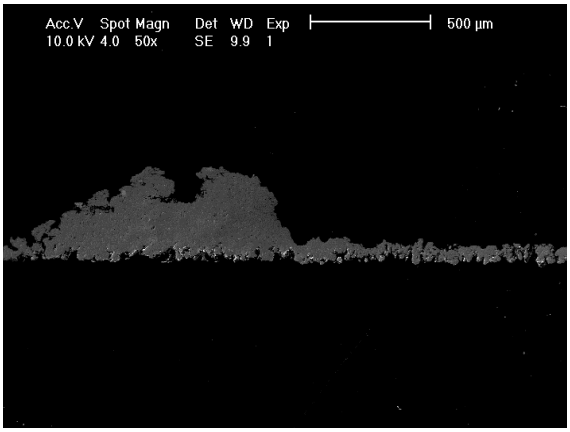

Fig. 64 Tin interlayer sprayed with gas pressure 0.9 MPa and gas preheating temperature 473 K

The feeding rate of $Sn+A_2O_3$ powder was much more stable and it was easier to obtain uniform thin layer. It might be seen that thick $Sn+A_2O_3$ is disadvantages; lots of cracks appeared in it, they may be partially caused by cutting samples for metallographic preparation (Fig. 65 and Fig. 66).

The granular copper was sprayed on the interlayers. In case of $Sn+A_2O_3$ the obtained coatings were thin and relatively dense however depending on the use parameters some cracks appeared in the interlayer and coatings (Fig. 65 and Fig. 66)

a) b)

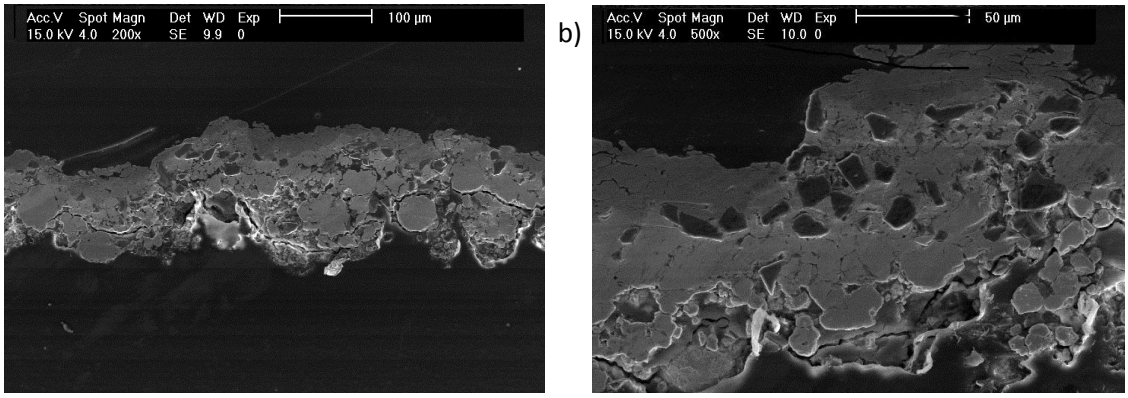

Fig. 65 Copper tracks deposited for parameters CX1 given in Tab. 11 (200x (a), 500x (b), SEM)

a) b)

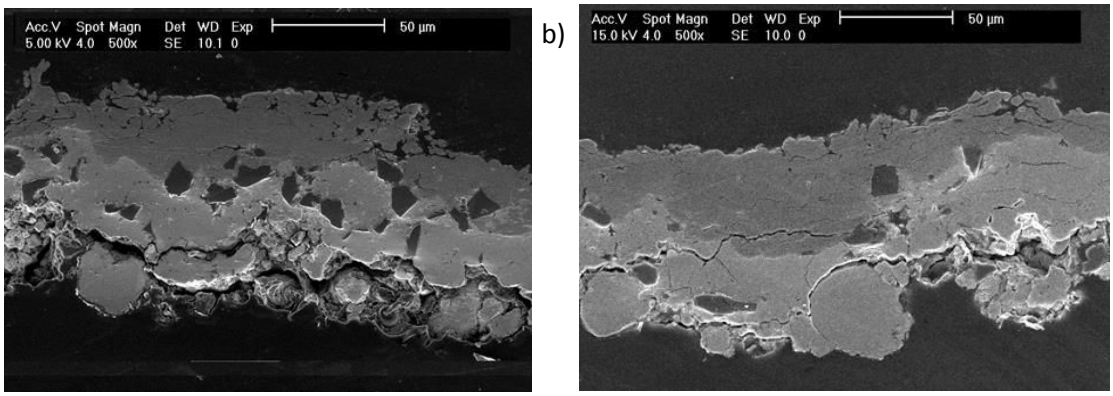

Fig. 66 Copper tracks deposited for parameters CX2 (a) and CX3 (b) given in Tab. 11 (SEM)

Copper coating deposited on the tin was cracked heavely (Fig. 67). It might be seen that cooper particls did not deform sufficiently to form bonding. As consequence coating has layer structure, where succeeding particles are separeted with cracks. The velocity of powder did not exceed crtical one.

a) b)

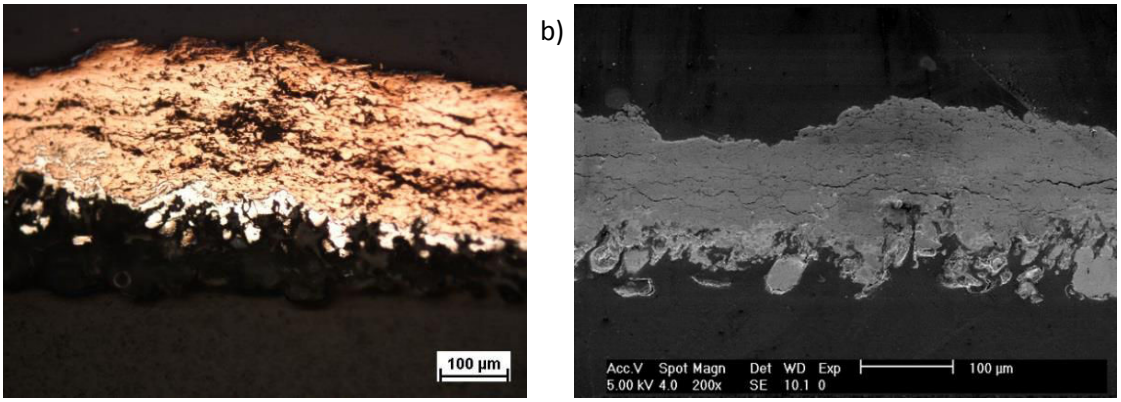

Fig. 67 Copper track deposited for parameters CX4 given in Tab. 11 (light microscope (a), SEM (b))

In all cases of deposited tin coatings bonding of first Sn or Sn+ A_2O_3 layer was insufficient to outlast subsequent deposition; already deposited tracks often delaminate

partially or completely due to interaction with pressurized gas and impacting particles (Fig. 68).

Fig. 68 Trial of deposition additional tracks to form a coating

The coating from granular copper powder particle was also deposited on PA6 with aluminium interlayer with similar parameters (Fig. 69). It might be seen that due to higher mechanical strength of the substrate copper coating is relatively dense and no cracks appears. The influence of the substrate was highlighted by Zhang [70]

a) b)

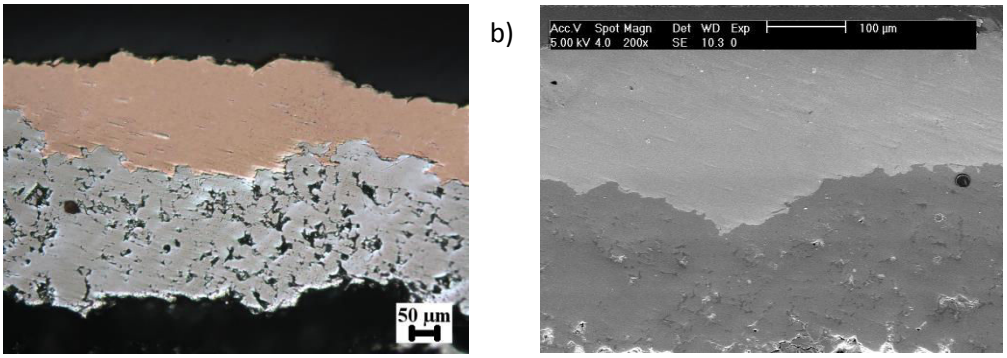

Fig. 69 Copper tracks deposited for parameters CX5 given in Tab. 11 (light microscope (a), SEM (b))

Deposition trials with Dendritic powder after heat treatment

Third trials were made with dendritic copper powder after heat treatment. Copper was successfully deposited on PA6 and PC with $Sn+A_2O_3$ interlayer. Exemplary spraying parameter are given in the Tab. 12

Tab. 12 Spraying parameters for initial trials of spraying dendritic copper powder after heat treatment

No	Powder	Gas temperature [K]	Gas pressure [MPa]	Standoff distance [mm]	Gun traverse speed [mm/min]	No. of spraying gun passages	Powder feeding rate [g/min]
Cu1	$Sn+A_2O_3$	473	0.9	10	3000	1	30
	Cu dendritic	473	0.9	10	3000	1	30
Cu2	$Sn+A_2O_3$	473	0.9	10	3000	1	30
	Cu dendritic	473	0.9	10	3000	2	30
Cu3	$Sn+A_2O_3$	473	0.9	10	3000	1	30
	Cu dendritic	473	0.9	10	3000	3	30
Cu4	$Sn+A_2O_3$	473	0.9	10	3000	1	30
	Cu dendritic directly after heat treatmen	473	0.9	10	3000	3	30

Deposited coatings were well bonded with the substrate. Their morphology depended mostly on number of spraying; coatings deposited in several passes were densified by hammering effect. It is especially noticeable in coating deposited in three passes, in which main porosity area is situated in the top region, which was not impacted by upcoming particles (Fig. 70). Despite the hammering effect porosity may be observed in whole coating. Particles velocity was too low to eliminate it. Probably also morphology of the powder contributed to porosity as impact energy was not cumulated in one contact point.

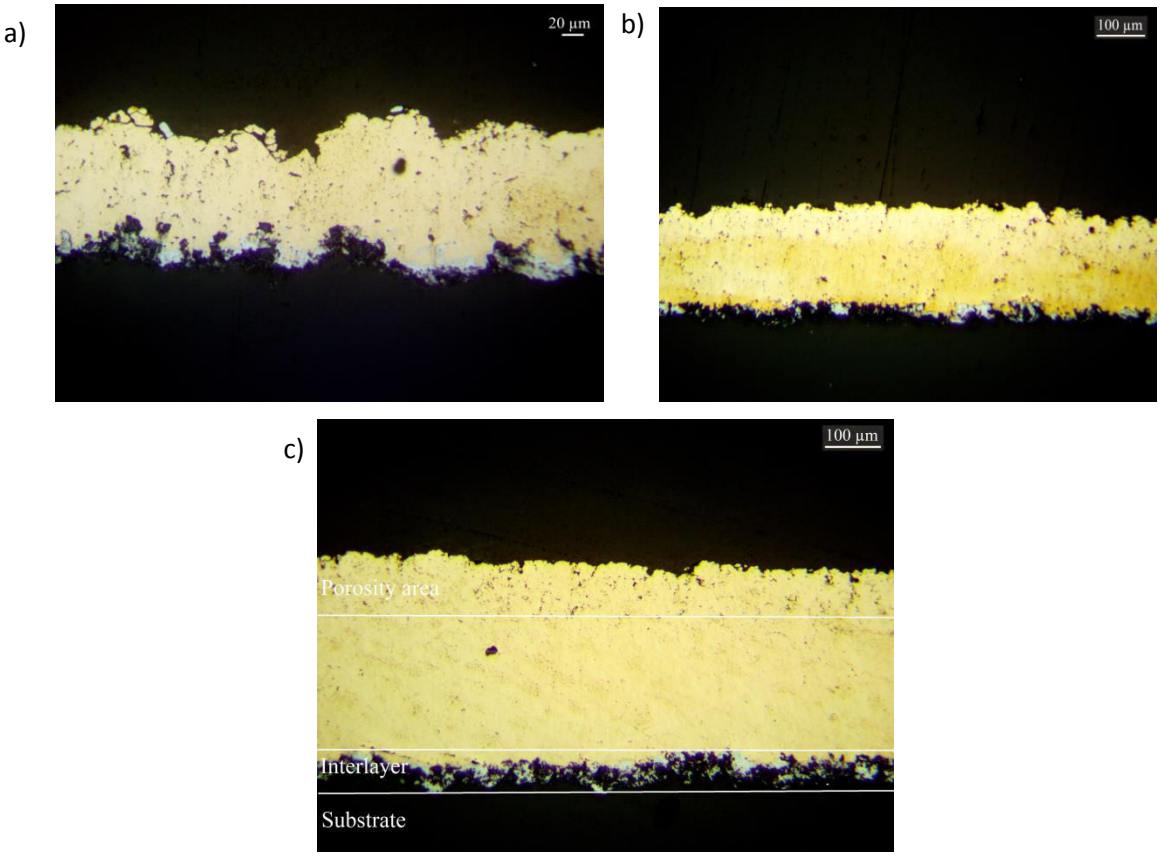

Fig. 70 Copper coating deposited for parameters Cu1 (a), Cu2 (b) and Cu3 (c) given in Tab. 12 (light microscope)

For comparison reason powder directly after deoxidizing was sprayed on PA6 with $Sn+A_2O_3$, with low velocity 1000 mm/min in three passes (Fig. 71). Coating is dense only small porosity area are present: one on the top of coating and one close to substrate on the verge of spraying track. Porosity on the top of the coating is typical for cold sprayed method and was already described [32, 145]. The second one is resulted through combined effect of low mechanical strength of substrate with uneven velocity distribution in the nozzle. Particles move slower close to the nozzle walls which obstruct deformation especially on soft substrate. Porosity near substrate is usually not observed in typical cold spray process [32].

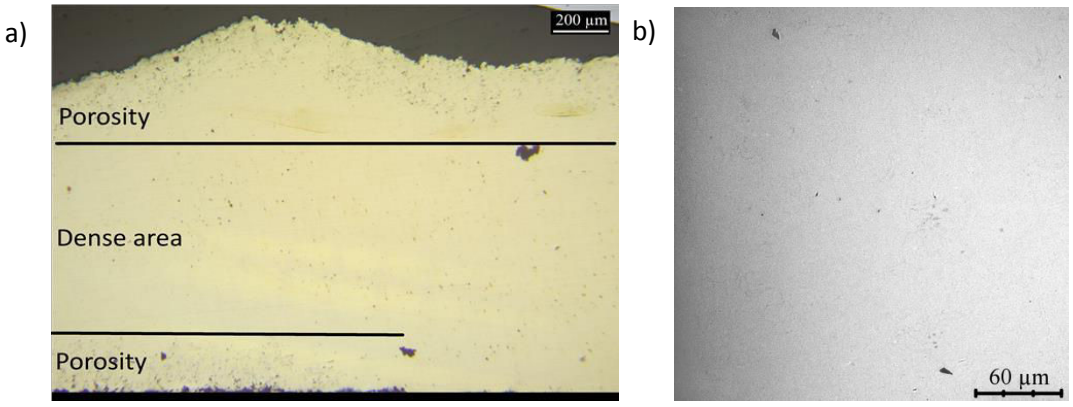

Fig. 71 Copper coating deposited for parameters Cu4 given in Tab. 12 (light microscope (a), SEM (b))

12.3.3.Initial trials of deposition with high-pressure cold spray method

Initial trails with high pressure cold spray method were made by courtesy of Chemnitz University of Technology (Technische Universität Chemnitz). Aluminum, copper and tin was sprayed on PA6 and PC with parameters listed in Tab. 13.

Tab. 13 Spraying parameters for initial trials with high pressure cold spray method

No	Powder	Gas temperature [K]	Gas pressure [MPa]	Standoff distance [mm]	Gun traverse speed [m/s]	No. of spraying gun passages	Powder feeding rate [RPM]
SnH	Sn	473	28	30	0.3	3	1
AlH	Al	643	28	30	0.2	3	1
CuH	Cu spherical	643	28	30	0.3	3	1
	Cu dendritic	643	28	30	0.3	3	1

All deposited coatings were not continuous 0.02 ÷ 0.03 mm, apart from tin coatings (Fig. 72). Even aluminum coating has not been formed though it deposited with less advanced low pressure cold spray. Particles remained mostly on the substrate surface and were weak bonded to the substrate. In consequence incoming particles replaced already deposited ones as observed by Lupoi et al [122]. It might be conclude that increased pressure and hence higher velocity of particles is not sufficient solution to get coatings on

soft. Additional modification substrate surface with appropriate interlayer, selection of suitable powder morphology and spraying parameters is required.

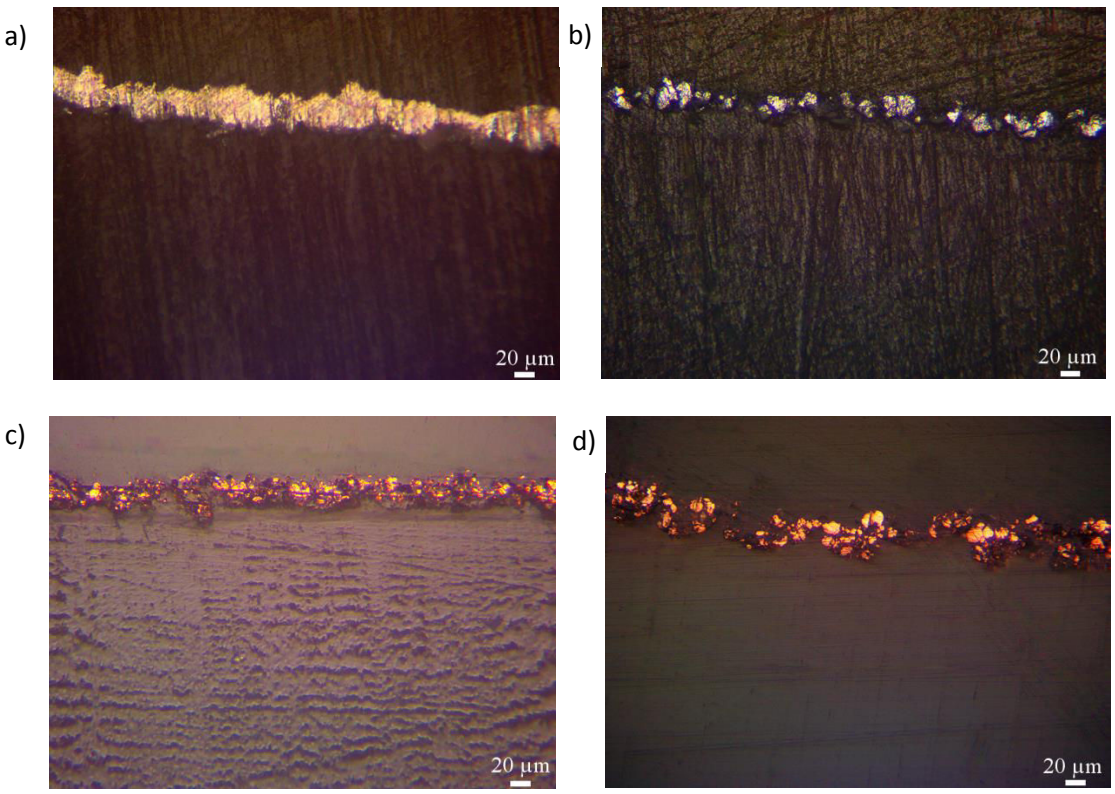

Fig. 72 Coatings deposited with high pressure method: Sn on PA6 (a) Al on PA6 (b), Cu on PA6 (c), Cu on PC (d). Spraying parameters listed in Tab. 13

13. Coating characterization

Based on preliminary tested optimal conditions for coatings deposition was chosen (Tab. 14) for characterization.

Tab. 14 Coatings deposition parameters

Label	Type	Powder	Powder feed rate [g/min]	Traverse speed υ_l [mm/s]	Gas pressure p_g [MPa]	Gas temperature T_g [K]	Stand-off [mm]	Number of spray passes
Al on Sn	Interlayer	Sn	15	2000	0.9	473	10	1
	Coating	Al	30	3000	0.9	473	10	1 or 2
Al on Sn_2O_3	Interlayer	Sn_2O_3	15	2000	0.9	473	10	1
	Coating	Al	30	3000	0.9	473	10	1 or 2
Al-400	Sandblasting	Al_2O_3	12	2500	0.9	673	15	1
	Coating	Al	30	3000	0.9	473	10	1 or 2
Al-200	Sandblasting	Al_2O_3	12	2500	0.9	473	15	1
	Coating	Al	30	3000	0.9	473	10	1 or 2
Al without treatment	Coating	Al	30	3000	0.9	473	10	2
Sn3 vel=3000	Coating	Sn	15	3000	0.5	473	15	3
Sn1 vel=1000	Coating	Sn	15	1000	0.5	473	15	3
Cu3 on Sn_2O_3	Interlayer	Sn_2O_3	15	2000	0.9	473	10	1
	Coating	Cu dendritic after heat treatment	30	3000	0.9	473	10	3

The distance between successive spraying passes was 3.5 mm so they overlapped. The same spraying design was used both for grit-blasting and spraying coatings

13.1.Adhesion measurements

The adhesion strength of three metals – aluminium, copper, tin was tested on two substrates – polyamide 6 (PA6) and polycarbonate (PC). The values of bond strength of coatings independent on the substrate material were at similar level, however small difference in favor of polycarbonate may be seen (Fig. 73 and Fig. 74). The bond strength of all coatings was below 8 MPa which is about 17% of tensile strength of polyamide 6 (amounts 45 MPa). The highest value of bond strength was recorded for thin tin coating – 6 MPa for PA6 and 7.3 MPa for PC. This result was expected as tin is the easiest deformable feedstock material from the chosen. The η coefficient for 20 μm spraying

parameter (0.5 MPa, 473 K) was in the range 1.5- 1.7. This should ensure appearing of adiabatic shear instabilities and in consequence good bonding [39] but the value of bond strength is much lower than in case of tin coating on metal. Additionally the coatings were thin ~ 100 μm. In case of thicker tin coatings sprayed with traverse gun velocity v=1000 mm/min sprayed in 1 pass the bond strength was reduced to 4.3 MPa for PA6.

Aluminium coating was sprayed on: untreated substrate, substrate after sand blasting in elevated temperature – 673 K, and two interlayers: tin interlayer, tin with addition of alumina interlayer and all of them had similar thickness. Aluminium coating sprayed on to untreated substrate tends to delaminate intrinsically and the bond strength was below 1 MPa for PA6. For PC it was impossible to measure bond strength on untreated sample because the coatings delaminated soon after deposition. The coatings were applied on sandblasted substrate and the value was ~0.2 MPa so actually there was no bonding. Additional treatment (tin interlayer or sandblasting in temperature 400° C) before spraying increased it up to ~4.5 MPa for PA6 and ~5.3 MPa for PC. Although using of pure tin brought the best results in view of adhesion it was a complicated task to spray uniform tin interlayer and aluminium coating. Zhang et al [70] observed scanty deposition of aluminium particles on tin substrate. It was attributed to low melting temperature; during impact tin melted, loose its strength and therefore – aluminium particles easily rebounded. Only small amount of small aluminium particles was deposited on the substrate, but if they formed bonding or were just embedded in soft tin remains unclear [70].

The third coatings material was copper. It was sprayed on $Sn+Al_2O_3$ interlayer due to previously described difficulties with obtaining uniform thin tin coating (chapter 12.3.2). The bond strength of copper coatings amounted 3.5 MPa for PA6 and 3.4 MPa for PC which was on the level of aluminium ones. Koivuluoto et al [142] reported bond strength of dendritic copper sprayed with low pressure cold spray (pressure 0.6 MPa and temperature 813 K) to be ~ 7.5 MPa. It increased significantly up to ~17.5 MPa with addition of 50% Al_2O_3. Obtained value amounts ~ 50% of it.

The small difference in bond strength on PA6 and PC substrate might be attributed to different physical and mechanical properties [147, 148]

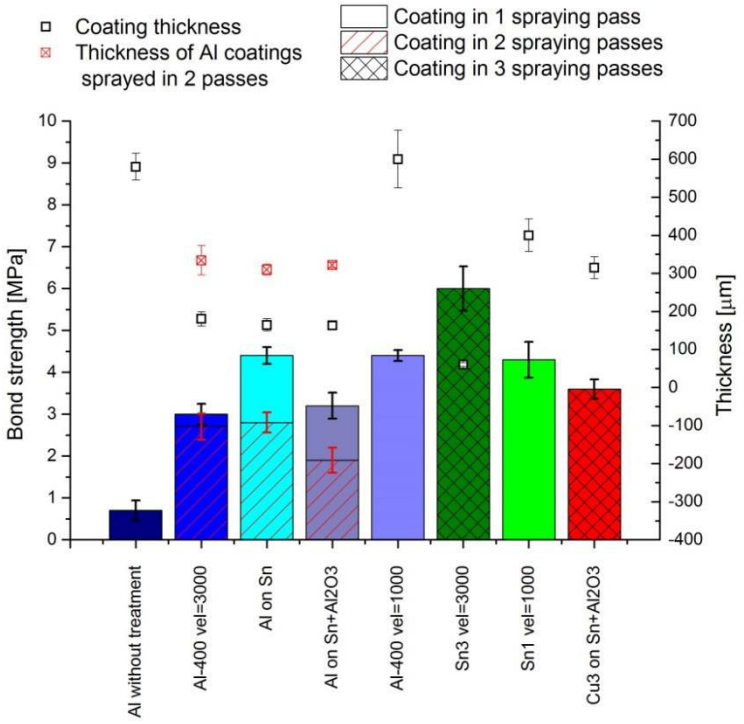

Fig. 73 Bond strength for coatings deposited on PA6. Spraying parameter listed in Tab. 14

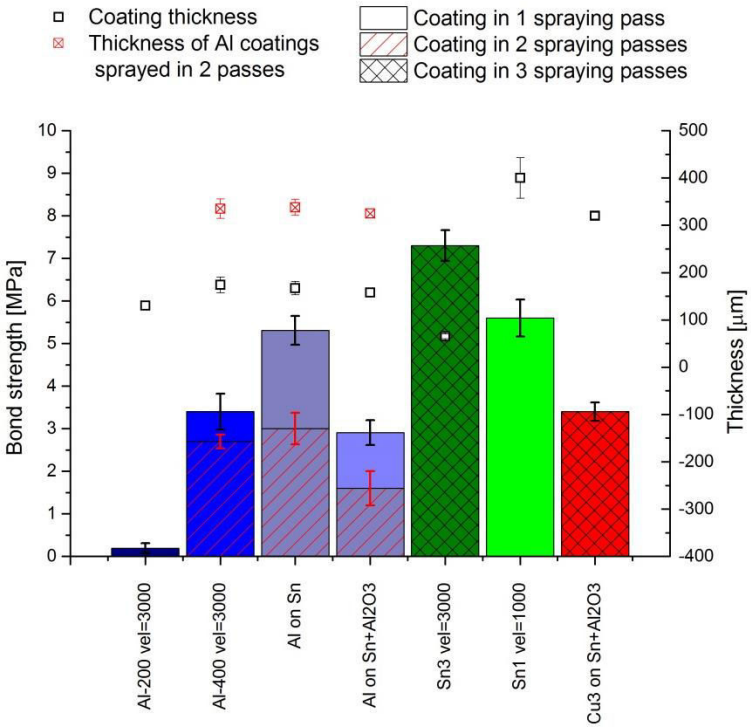

Fig. 74 Bond strength for coatings deposited on PA6. Spraying parameter listed in Tab. 14

The fractures of samples are shown in Fig. 75. It might be seen that for pure aluminum coating with no interlayer the surface after coating delaminating is smooth with no irregularities. For aluminum coating sprayed on sandblasted substrate surface after sandblasting might be recognized with no change caused by spraying process. Tin coating detaches also close to the substrate surface. In case of aluminum and copper coatings sprayed on Sn and Sn+Al_2O_3 fracture occurred partially in the interlayer and partially in the coatings.

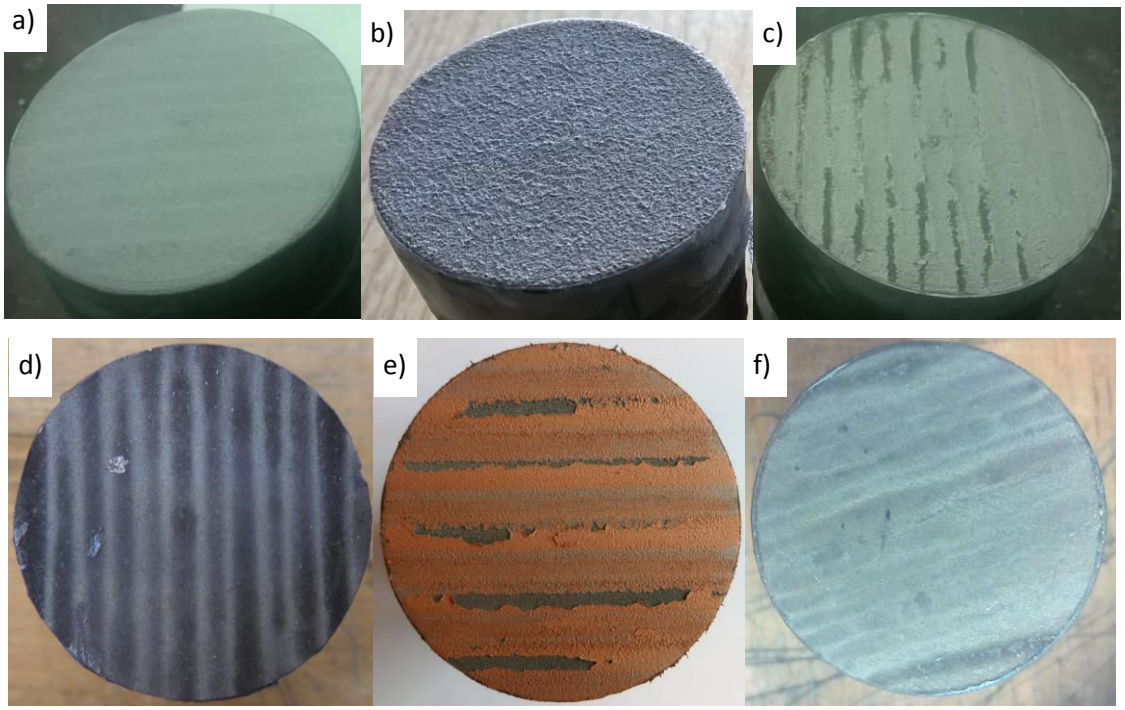

Fig. 75 Fractures after bond strength test of: Al coating with no interlayer (a), Al coating on sandblasted substrate (b), Al coating on Sn interlayer (c), Al coating on Sn+ Al_2O_3 interlayer (d), Cu coating on Sn+ Al_2O_3 interlayer (e), Sn coating with no interlayer (f)

In all cases cohesion of the coatings was decisive factor for its detachment (Fig. 76). When cutting the sample the crack appears between first interlayer and the coating. In the same place porosity unusual for cold spray process was observed. The sudden change in material properties causes formation on stresses which increase with additional spray passes due to heat input and blocking of thermal expansion. To minimalize this effect graded coating might be used [115, 149]

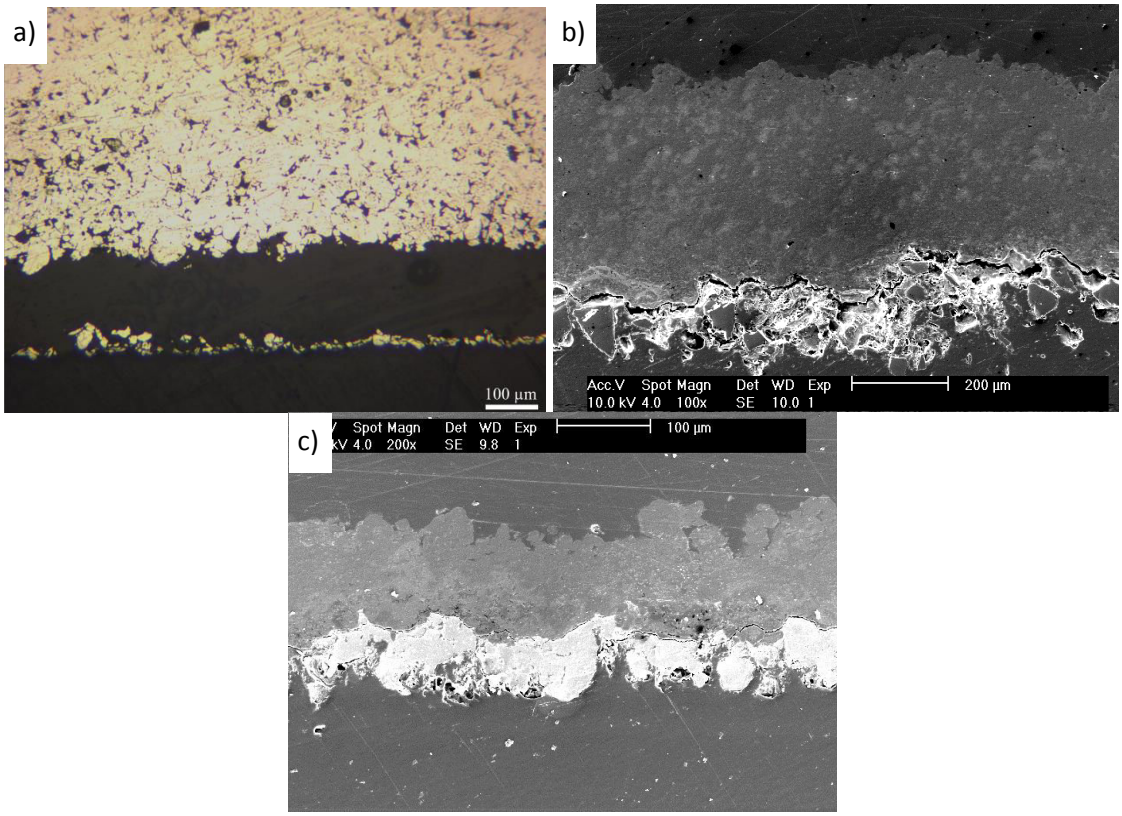

Fig. 76 Fracture in aluminium coatings after sample cutting process: with no interlayer (a), sprayed on sandblasted substrate (b), tin interlayer (c)

Bonding mechanism and its strength is usually attributed to two main mechanisms: formation of shear instabilities in particle/substrate and particle/particles interface caused by extensive plastic deformation during impact [21, 22] and mechanical interlocking [51]. However in case of polymer/metal bonding only the second one may appear due to different nature of coating and substrate material. Additionally "interlocking might not be as strong as the one observed on the metals substrate due to the soft nature of the polymer" [77] . The other problem [77, 128] when creating bonding was attributed to squeezed out polymer during particles impact which might partially enclose the metal particles and act as barrier against bonding formation. This was claimed to happen when using spherical copper as interlayer [77]. Tin turned out to have more beneficial influence on adhesion strength [77, 129]. Ganesan et al attributed it to low mechanical properties of tin particles which were able to undergo the deformation instead of damage the surface. This initial interlayer enabled then bonding or interlocking for subsequent layer having higher mechanical properties i.e. copper [77, 129]. In case of spherical copper particles the shear strength of copper coating was 1.93±0.7 MPa in compare to 5.4±0.9 MPa for tin interlayer [77]. This behavior was not observed in case of aluminum coatings in this work. Using of tin interlayer brought similar results to Al_2O_3 interlayer and no effect of squeezed

polymer was observed. The efficiency of the interlayer seemed to be correlated to the depth of particles embedment and hence the force of mechanical interlocking. In case of sandblasted samples the crack appeared between the aluminum coating and the substrate, but for sample with tin interlayer the fracture appeared inside the tin interlayer.

Apart from interlayer adhesion was influenced by thickness of the coating. Coating sprayed in two passes revealed lower adhesion; the drop was more significant in case of using tin interlayer than sandblasted samples. But it might be noted that bond strength values recorded in chapter 12.1.1 for aluminum coatings were higher although thickness of the coatings was much higher 600 μm. The main difference was spraying velocity. It seems that low spraying velocity enables deeper embedment of the powder particles on which may then coating be created. Additionally, during coating spraying lower velocity facilities hammering of deposited particles and prevents rebounding of particles. But in case when incoming particles have to high mechanical properties to deform lower velocity increase erosion due to cumulative higher energy impact. High particle loading in the gas stream results in destruction of polymer surface and exposing the embedded particles which are then easily detached form the substrate during subsequent impacts of upcoming particles. Using concept proposed by Lupoi et al [122] and calculating impact energy of copper and aluminum particles with known equation for kinetic energy $E=mv^2$ and substituting v with calculated velocity for used spraying parameters we get E=1.41E-06 J for aluminum and E=2.28E-06 J for copper; the impact energy of copper is almost two times higher although the spraying velocity. This results in higher degradation of substrate and explains why it is possible to obtain aluminum without using any interlayer and for copper it is not.

13.2.Young modulus measurements

The elastic modulus was determined using indentation method developed by Marshal et al [150] which commonly used for thermally sprayed coatings despite measurement's difficulties: splat-like microstructure, porosity and surface preparation which may noticeable influence the results [151]. Five coatings were measured: two aluminum coatings on sandblasted substrate sprayed in one and two passes, one aluminum coating sprayed on tin interlayer, copper coating sprayed on $Sn+Al_2O_3$ sprayed on PA6 substrate (Fig. 77).

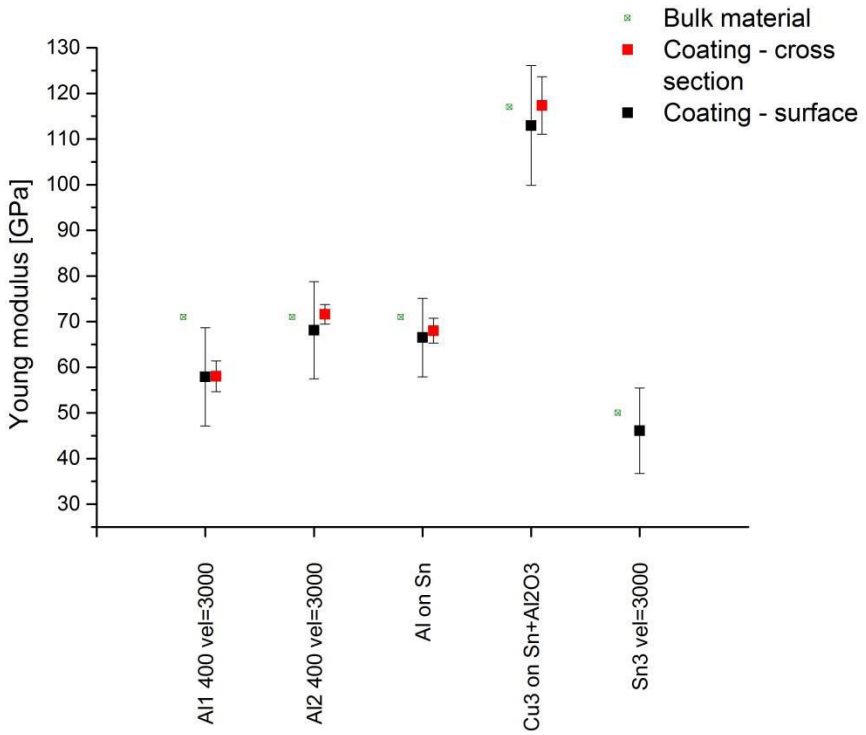

Fig. 77 Young modulus values for coatings deposited on PA6. Spraying parameters listed in Tab. 14

Al coating sprayed in one pass reached ~ 80% of bulk material data taken from literature) which is in coincidence with [152]. The values obtained for Al2 coating and Al coating with tin interlayer are at the level of bulk material, on average ~70 and ~67 GPa respectively. For copper and tin coatings elastic modulus values were on average ~115GPa and ~46 GPa, respectively. Thermally sprayed coatings usually have lower elastic modulus than bulk materials therefore these results are quite unexpected. It might be caused by measuring in the dense coating area and omitting the influence of porosity. Similar behavior was observed in [151]. Elastic modulus value of aluminium coating measured with indentation method was 74±20 GPa, however impulse excitation technique indicated

only 49.4 ± 0.2 GPa. It may be concluded that the indentation method in case of porosity may not give correct values for whole coating only for local areas, which is confirmed by high value of standard deviation but still the values are high in compare to coatings obtained with high pressure cold spray method. The measurement on cross-section in compare to measurement on the surface brought similar results. This is also quite unexpected behavior. Cold sprayed particles undergo plastic deformation and elastic modulus should differ in the direction perpendicular to the surface but no anisotropy was observed. Probably, deformation grade of the particles was low which is also indicated by high porosity value. Roca et al [153] noticed that young's modulus decreases with increasing plastic deformation of metallic alloys up to 10-15% in compare to annealed materials. In case of iron these changes were assigned to the dislocation density changes; it increased from 3.5 10^{-9} cm^{-2} at 0% deformation to 14 $\cdot 10^{-9}$ cm^{-2} at 6% deformation with simultaneous Elastic modulus drop [154]. This behavior is consistent with Mott model [155]:

$$\frac{\Delta E}{E} = -\rho \left| \frac{l^2}{6\alpha} \right|$$

Where ρ – dislocation density, l – average length of dislocations between pinning points α – function of l.

Model was confirmed for iron and pure aluminum; for aluminum alloys elastic modulus change is very low, due to interaction between precipitates and dislocations resulting in very low l parameter [156].

The hardness and elastic modulus curves obtained in case of tin drops quickly without distinct plateau (Fig. 78); therefore determination of correct values is difficult. The course curve reveals impact of the low hardness substrate material; thin coating (with low mechanical properties) can not balance low mechanical substrate properties and stiffen it which will notable influence spraying behavior of subsequent layer.

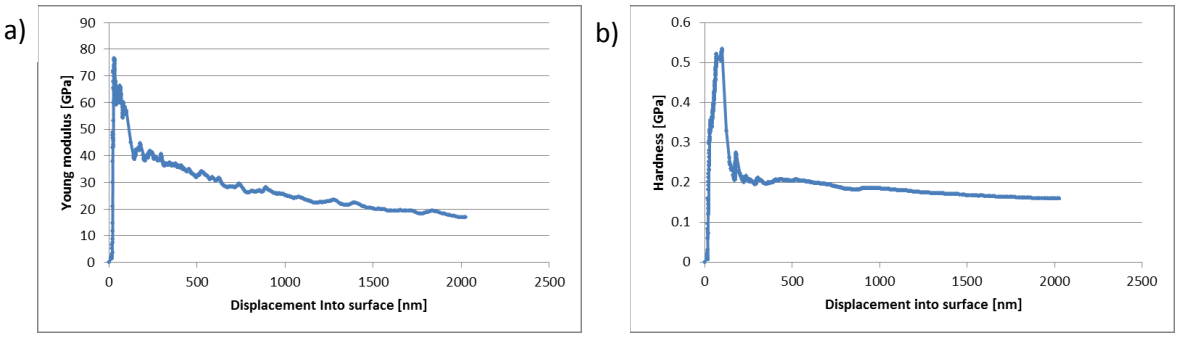

Fig. 78 Young modulus and hardness curve for Sn coating on PA6

13.3.Electrical resistivity

Resistivity of coatings deposited on PA6 and PC was measured using four probe method. The results are presented in Fig. 79 and Fig. 80.

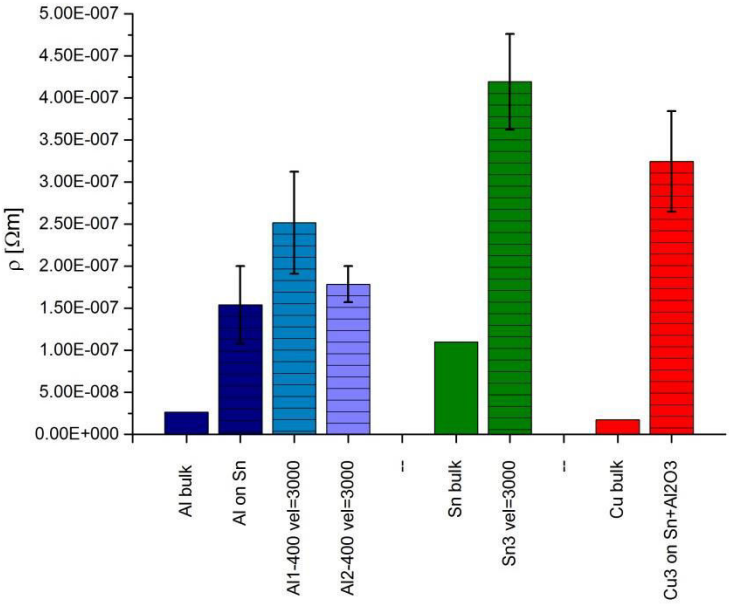

Fig. 79 Resitivity values calculated for coating deposited on PA6. Spraying parameteris listed in Tab. 14

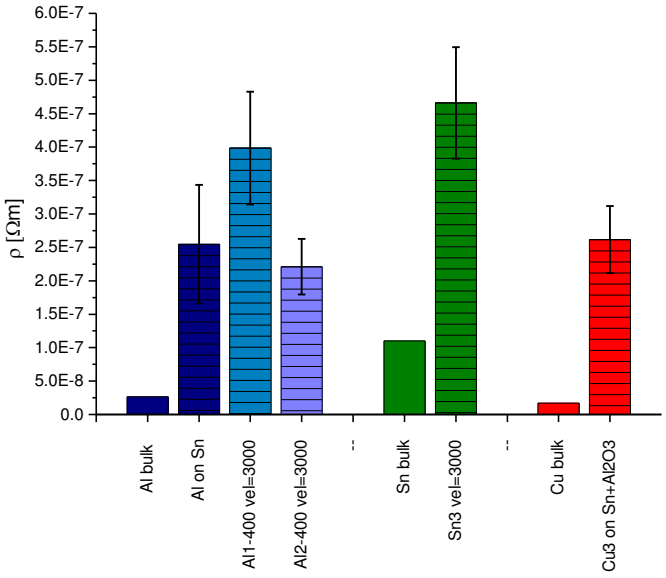

Fig. 80 Resitivity values calculated for coating deposited on PC. Spraying parameters listed in Tab. 14

The resistivity of all coatings was approximately one order magnitude higher than bulk material. The lowest difference was obtained for tin coatings on PA6, about 25% of bulk material, but lowest absolute value was noted for Al coating on PA6 - 15 μΩcm which gives 11% IASC. In case of aluminum may be seen resistivity drop when increasing

number of spraying passes. Resistivity values for copper were close to aluminum values or even higher, which is quite unexpected. King et al [157] characterized aluminum coatings sprayed on lead zirconate titanate. The in-plane resistivity of the 42±8 μm thick coating was 9.9 μΩcm and was taken as indicative of high density and good contact between particles. Similar value for in plane resistivity value (~10 μΩcm) for aluminum coatings was given by Choi et al [158]. The coating was sprayed with helium at 250 psi and 598 K, the mean particle size was ~25 μm. Affi et al [126] sprayed aluminum onto CFRP substrate with plasma sprayed interlayer. The coatings sprayed with gas temperature at 573 K were characterized by resistivity equal to 17.1 μΩcm. It increased to 26 μΩcm for gas temperature at 673 K. Values obtained in this thesis are in coincidence with ones obtained by Affi, although spraying parameters were much lower and huge porosity reaching 5% may be seen in the coatings independent on substrate material (Fig. 81, Fig. 82 and Fig. 83).

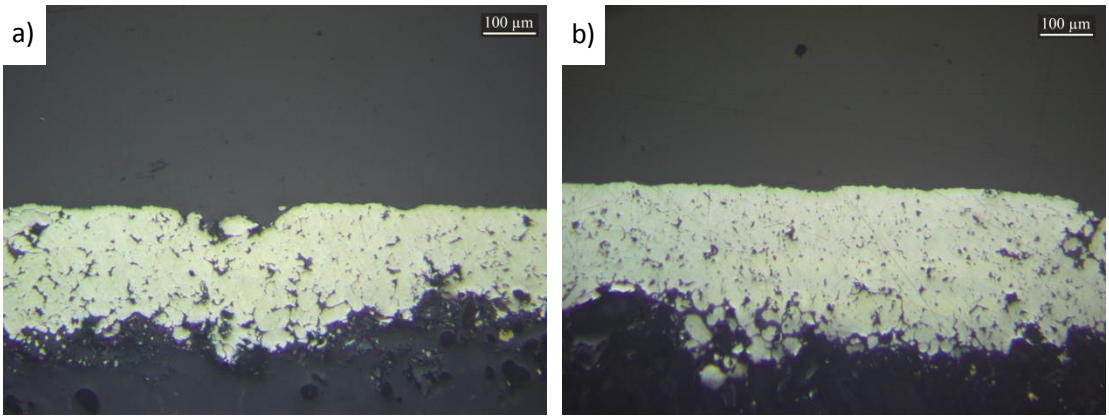

Fig. 81 Aluminum coating sprayed in two passes(Al2-400 vel=3000) on: PC (a) PA6 (b), (light microscope)

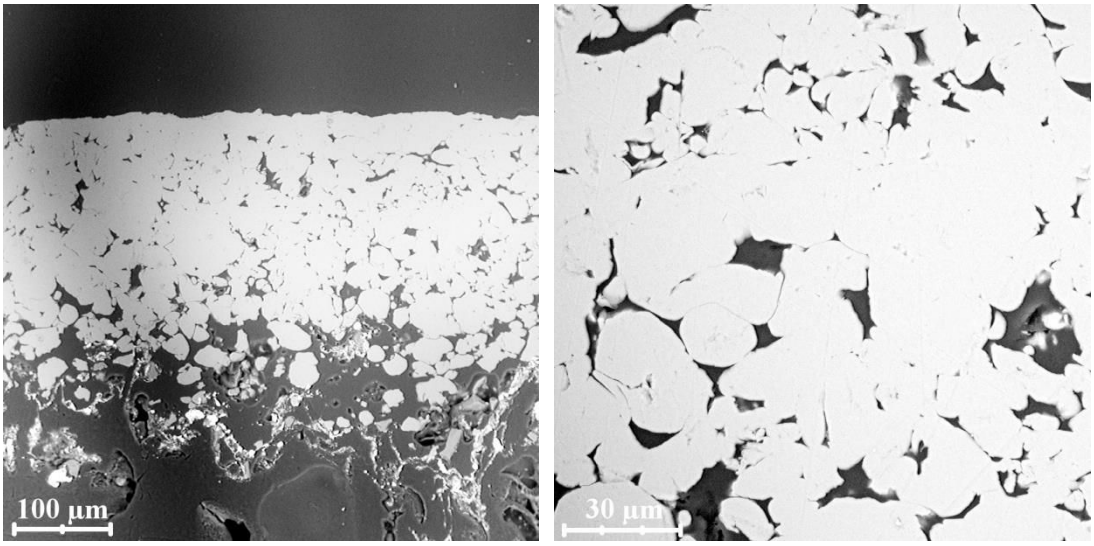

Fig. 82 Aluminum coating sprayed in two passes (Al2-400 vel=3000) on PA6 (SEM)

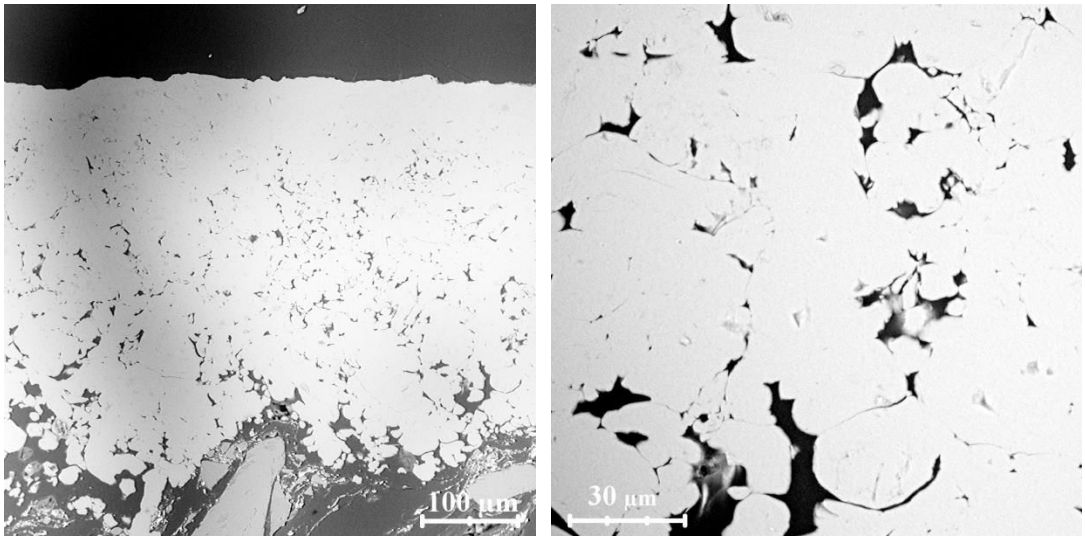

Fig. 83 Aluminum coating sprayed in two passes(Al2-400 vel=3000) on PC (SEM)

Resistivity values for copper coatings amounted to 22.3 ± 0.24 µΩcm on PC and 31.6 ± 0.19 µΩcm on PA6.

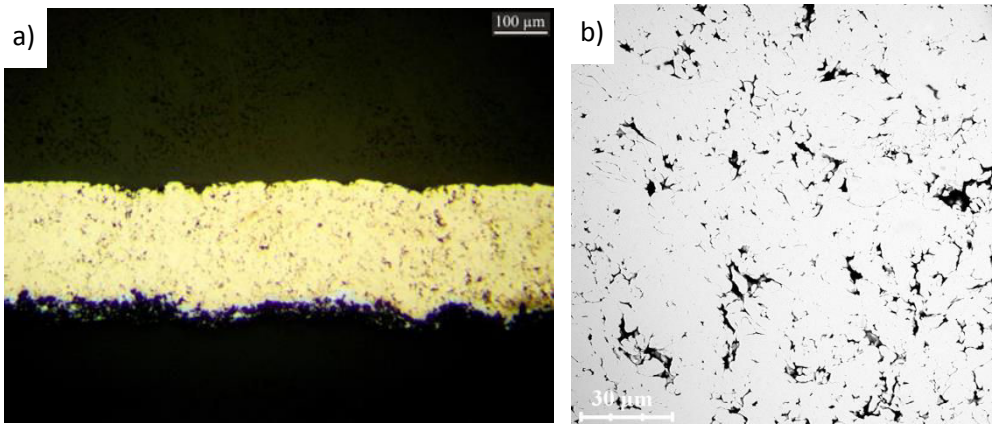

Fig. 84 Cu3 coating on PC6 with Sn+Al2O3 interlayer (light microscope (a), SEM (b))

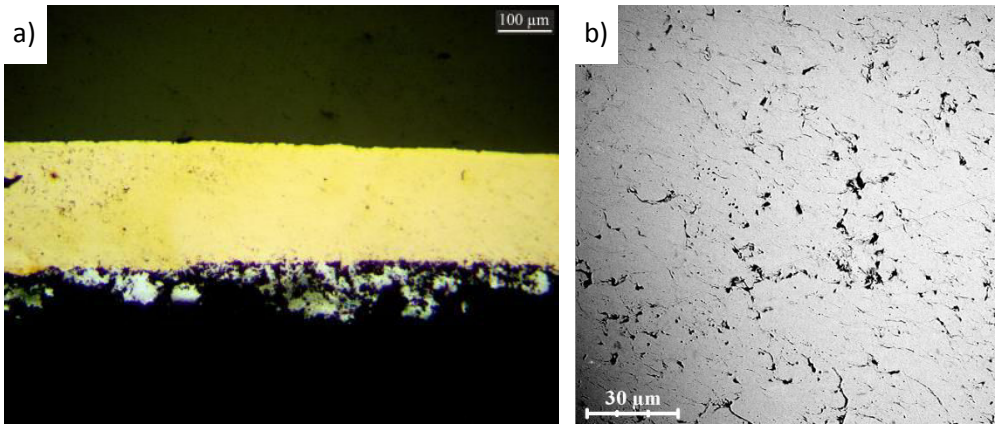

Fig. 85 Cu3 coating on PA6 with Sn+Al_2O_3 interlayer (light microscope (a), SEM (b))

Coating deposited on PA6 was characterized by lower porosity (Fig. 84 and Fig. 85) than one deposited on PC. The main area of porosity was situated at the verges of spray beads (Fig. 86). This porosity might be eliminated through reducing distance between adjacent spray beads.

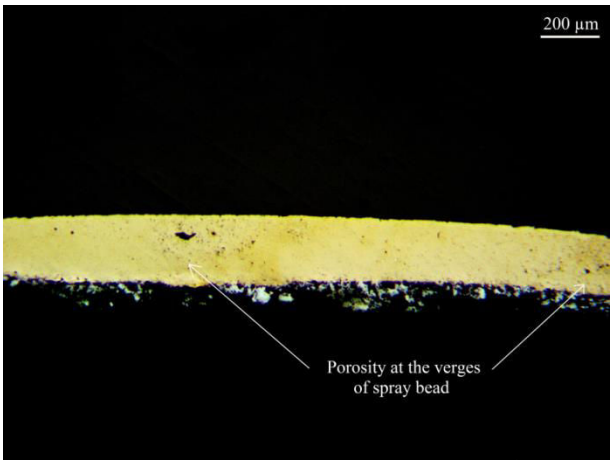

Fig. 86 Cu3 coating on PA6 with Sn+Al_2O_3 interlayer (light microscope)

In Fig. 87 Copper coating sprayed with 2.5 mm distance between adjacent spraying beads instead of 3.5 mm might be seen. Lower distance resulted in higher thickness of deposited coating and reduction of porosity.

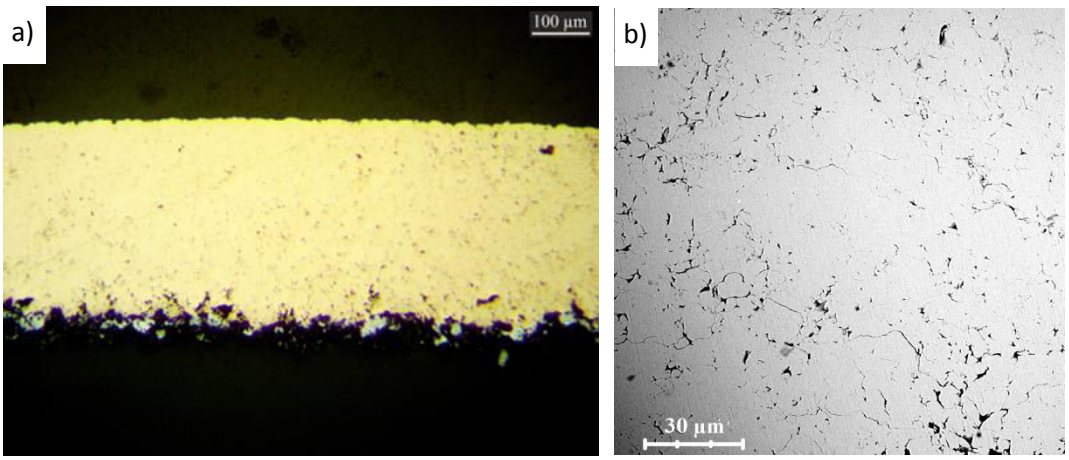

Fig. 87 Cu3 coating on PC6 with Sn+Al2O3 interlayer with 2.5 mm distance between adjacent spraying beads instead of 3.5 mm (light microscope (a), SEM (b))

Suprisingly, the porosity amount and ditribution affect only slighty resitivity. Coating with modified distance between adjacent spraying beads has resitivity 25.2 ± 0.31 µΩcm which is almost same value with unmodified one - 22.3 ± 0.24 µΩcm. Values or resistivity were random correlated with porosity in the coating and the effect of densification by subsequent spraying passes had little effect on resistivity. It seems that for given spraying parameter and powder small variation in coating structure influences slightly coatings

resistivity. Probably the creation of metallic boding due to shear instabilities was restricted to small local areas due to insufficient velocity. It contradicts the study of Sudharshan et al [74] who claimed that porosity increase from 0.1 to 0.8 % caused conductivity decease from 19.1 to 4.1 MS/m (resistivity from to 24.39 μΩcm to 5.25 μΩcm). Not only the value but also the source of the porosity seems to be important factor.

Venkatesh et al [75] correlated resistivity value with extent of recrystallization and with porosity. Recrystallization depends on particles velocity and particles temperature. First factory is good known relation often correlated to critical velocity [39] and partially determined by gas preheating temperature, but gas preheating temperature and consequently particles temperature (independent on the velocity) additionally facilitates deformation and increases recrystallization. Porosity turned out to be only related to particles velocity and independent on particles temperature [75].

The resistivity values for all copper coatings are in the range given by Sudharshan [74] (24.39 μΩcm) for following spraying parameters gas pressure: 1.4 MPa and temperature 573 K, but two times higher than this given by Ganesan [77] for copper coating on PVC at 473 K and the pressure 2 MPa [77, 129]. The difference could be only partially explained through pressure difference because almost no effect of gas pressure on deposition efficiency was observed [129]. The main factor is probably much lower spraying velocity – only 500 or even 100 mm/min resulting in thickness 800 or 1000 μm depending on the used interlayer [77, 129]. It causes hammering during deposition, local temperature rise due to impact of subsequent particles; in consequence porosity is reduced and metallic bonding might occur easier.

In the literature it is claimed that cold sprayed coatings may reach even 90 % of conductivity of bulk copper [71]. On this background obtained results are small. One on the way to improve the conductivity is heat treatment of coatings after spraying. Koivuluoto et al [72] reported the conductivity values to be 79 % IACS for HPCS, and 46 % IACS for LPCS sprayed coatings; they increased to 90 % IACS for HPCS and 69 % IACS after heat treatment (673 K, 2 h). The coatings were sprayed with spherical powders. However, heat treatment was not applied due to nature of the substrate.

The resistivity of tin coating was 42 μΩcm on Pa6 and 46 μΩcm on PC respectively, which is ~25 % of bulk material. No porosity might be observed in the coatings structure, only small cracks near the substrate surface (Fig. 88). Probably, the drop in the restively is caused by cold work and oxidation. Winnicki [159] observed notably increase in conductivity of tin coatings after heat treatment from ~10 % IASC to 60% IASC.

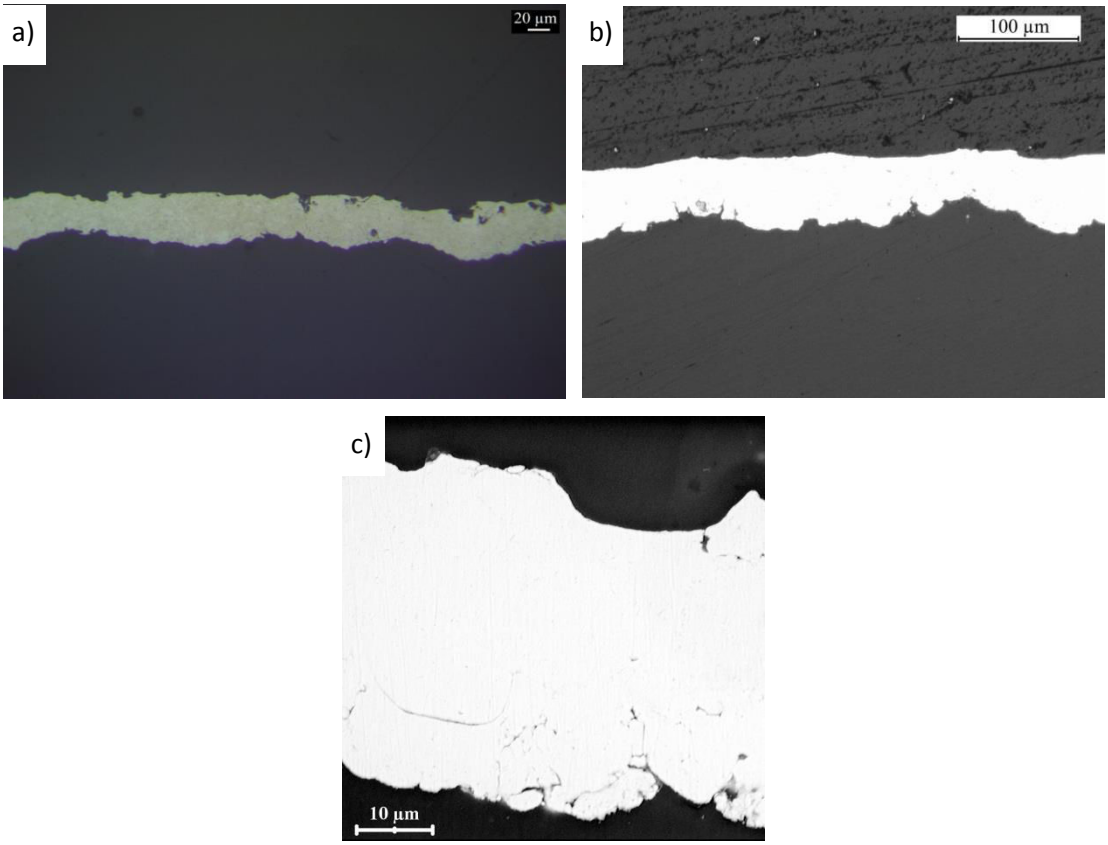

Fig. 88 Sn coatings on: Pa6 (a) PC (b)(light microsope), PC (c) (SEM)

Finally, for comparison mixture of Sn and Cu (1:4 weight ratio) was also deposited (Fig. 89) on PC with same conditions as copper coating (pressure 0.9 MPa, temperature 473 K, traverse velocity 3000 mm/min). The conductivity amounted to 32.5 ± 0.74 µΩcm and was similar to values obtained for pure tin coatings and slightly higher than for pure copper coatings. Almost non porosity can be distinguished in the coating and the disposition conditions were sufficient for tin to create shear instabilities, therefore high resistivity is probably caused by cold work Sudharshan et al [74]. The resistivity of tin determines the resistivity of whole coating.

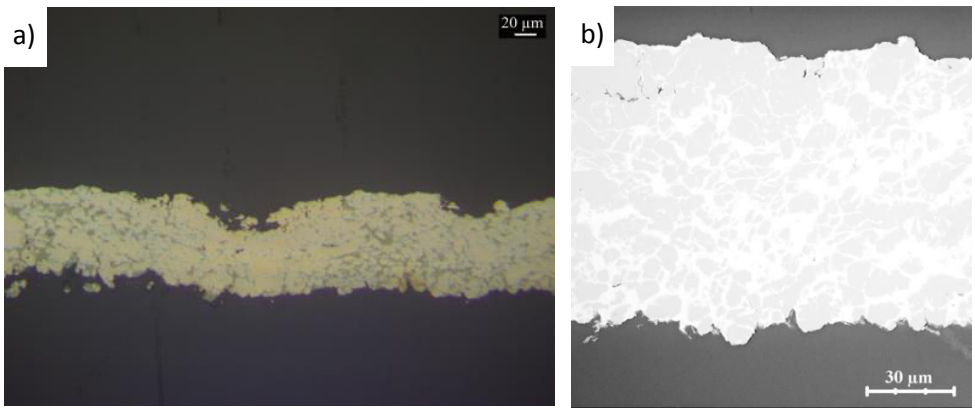

Fig. 89 Sn – Cu coating on PC (light microscope (a), SEM (b))

13.4. Microhardness measurements

The measured values of microhardness are similar for coatings on PA6 and PC (Fig. 90). They indicate low deformation and lack of strain hardening

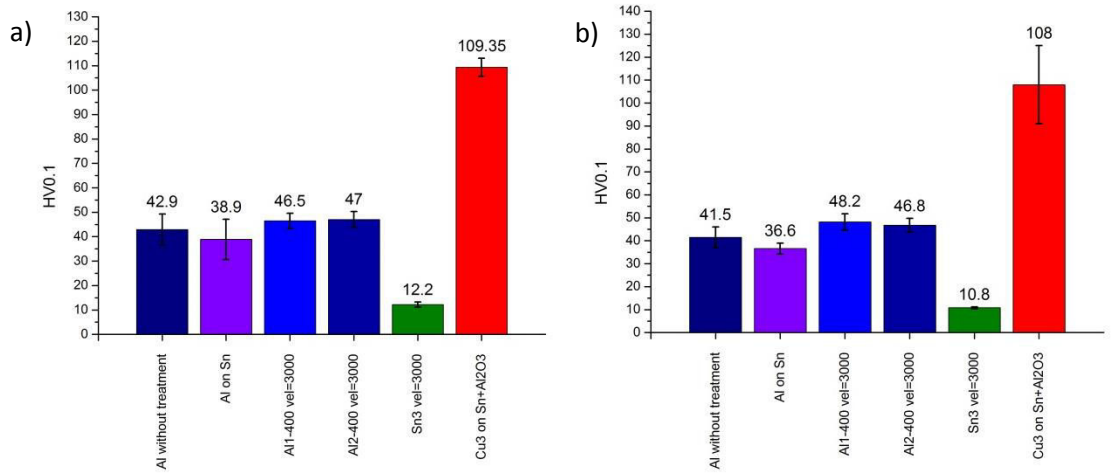

Fig. 90 Microhardness values for coatings deposited on PA6 (a), PC(b)

The aluminum coatings on Al_2O_3 interlayer reached on average 47 HV0.1 for PA6 and 48.2HV0.1 for PC, the values on Sn interlayers was slightly less 38.9HV0.1 for PA6 and for PC. These values are in coincidence with values given by Zhou for pure Al coating on PEEK450CA30 – 42HV0.1 [123]. In case of using Al coating as interlayer for Cu coating on PEEK450CA30, aluminum was additionally compacted by the top layer and obtained value was higher 42HV0.1 [123]. Much higher values were recorded for Al coatings on magnesium alloys ~180HV0.1 [160]. This confirms low deformation of aluminum caused by soft substrate and insufficient velocity. Tin coating on PA6 has microhardness equal to 12.2HV0.1 and 10.8HV0.1 on PC. Deposited copper coatings reached 125HV0.1 on PA6. This value is much lower than given by Sudharshan - 300 or even 450HV0.1 for copper coatings on aluminum [74] but similar to values given by [77, 142] though due to different load used for measurement the values can be not directly compared. The low values of copper microhardness might be prescribed apart from low deformation grate to heat pretreatment of feedstock material. Lower microhardness of feedstock after heat treatment results in lower value of coatings microhardness [161]

13.5.Measurement of coefficient of thermal expansion

Thermal expansion of polymers is anisotropic and structure-dependent. It varies with filler type and reinforcement. Above T_g temperature polymers expand isotropically and hysteresis appears after cooling to room temperature [162]. Additionally thermal expansion curves exhibit a sudden change in a slope in T_g point, before and after which there is usually linear dependence between temperature and expansion [162]. This effect is used to determine T_g from thermal expansion curves. When the change is not well visible derivatives are applied [163]. Glass transition temperature is a threshold point, below it polymers are brittle, hard, and glassy while above behave rubbery [162]. For semicrystalline polymers like polyamides exact value depends on structure (isotropic or anisotropic) of amorphous region and degree of crystallinity [164]. High crystallity grade causes that semicrystalline polymer might be used above T_g. The glass transition temperature measured for Pa6 and PC amounted to 322.7 K and 412 K respectively (Fig. 91). These values are in coincidence with given by literature [164].

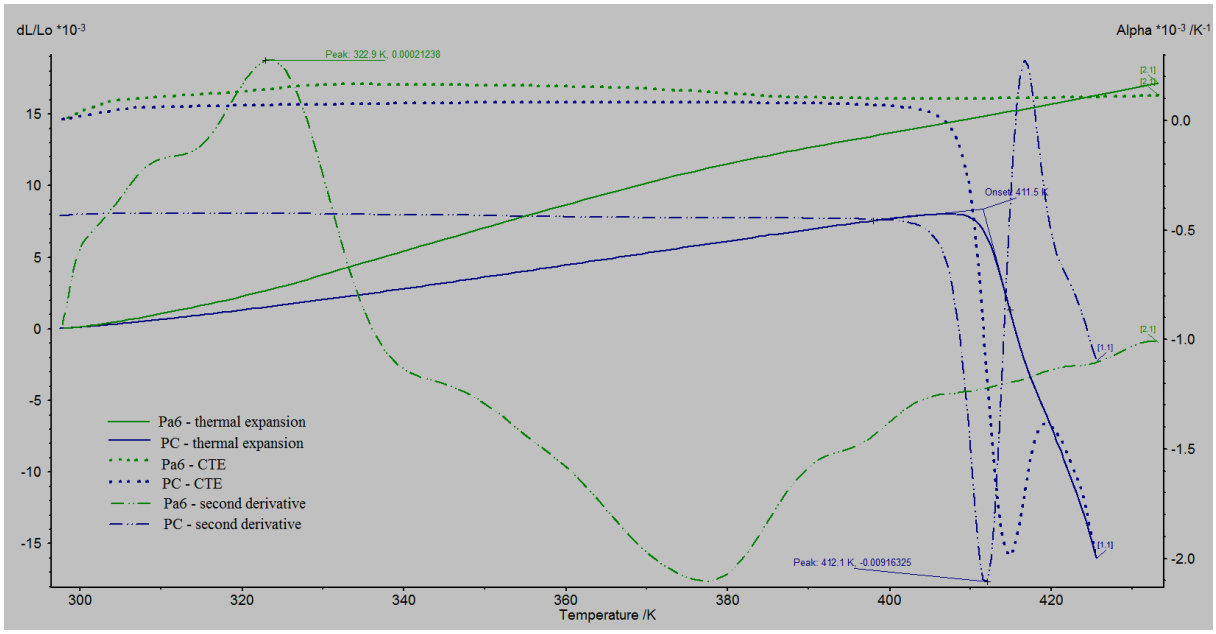

Fig. 91 CTE Measurement for Pa6 and PC

During deposition process the substrate and coating achieves in average temperature of 353 K; which gives following CTE values for polymers, PC ~ 84e-6 K^{-1} and double of this value for Pa6 ~161e-6 K^{-1}. Aluminum deposited in two passes reaches 23e-6 K^{-1}, tin ~24e-6 K^{-1}, copper ~ 17e-6 K^{-1}, which is on average four times less than PC and eight times less for Pa6 and is in coincidence with literature data. Additionally for PA6 thermal expansion is very unstable and CTE varies in time, which was partially solved in

generation of polyamides i.e. Utramid Top 3000, characterized by very stable CTE of ~ 60e-6 K^{-1} in temperature range 293 – 353 K [165]. This difference in CTE according to rough equation for thermal stress [166] will result in enormous stresses, much higher than strength of the polymer materials:.

$$\sigma_{th} = E_c \Delta T(\alpha_c - \alpha_s) \tag{47}$$

Where: E_c – Young modulus of coating, ΔT – temperature difference, α_c – CTE of coating, α_c – CTE of substrate

This effect is responsible for spallation of the coatings directly after spraying process. The positive influence of interlayers might be explained following: deep embedded particles form semi graded coating (reducing difference in CTE), tin layers can deform easily reducing the stresses.

13.6.Thermogravimetric Analysis

Thermal stability of polymer substrate was checked using TGA method (Fig. 92). It might be seen that both polymer are stable in the temperature deposition range. The weight loss for polyamide 6 starts with melting temperature ~ 493 K (peak at the DTA line) and become significant at 672 K or even higher temperature depending on the heating rater. Polycarbonate significant weight loss begin at 718 K , this temperature is also shifted to higher ones for higher heating rates. Both polymers decomposed completely – 100 % weight loss might be noticed which means that inorganic additions like glass fibers were not present.

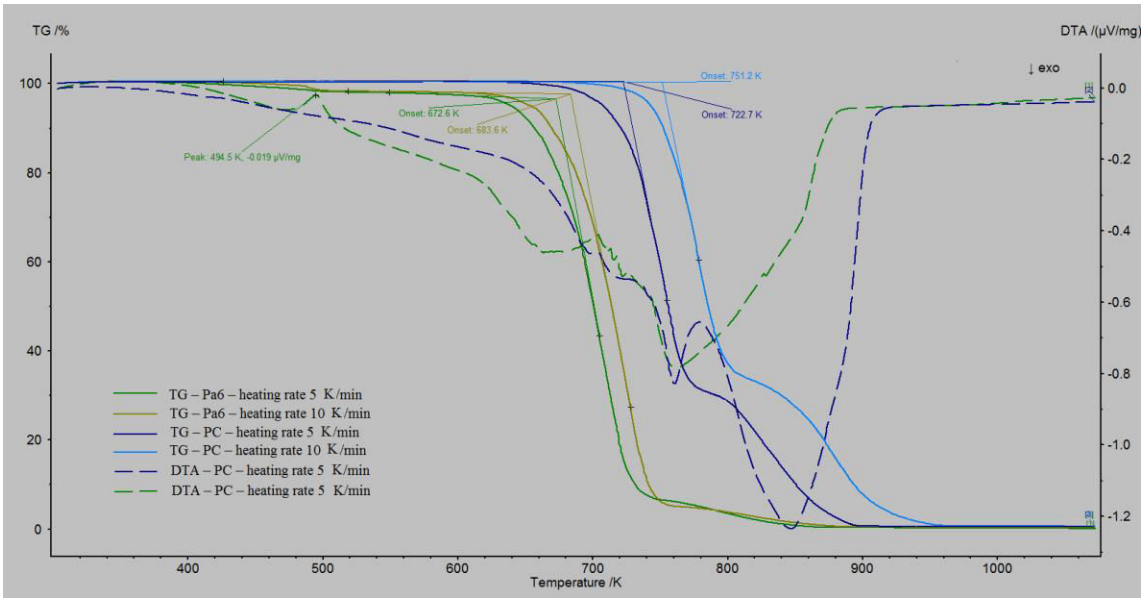

Fig. 92 TGA measurements for Pa6 and PC

13.7.Oxidation measurements

Oxygen content measurement in feedstock material and coatings are summarized in Fig. 93

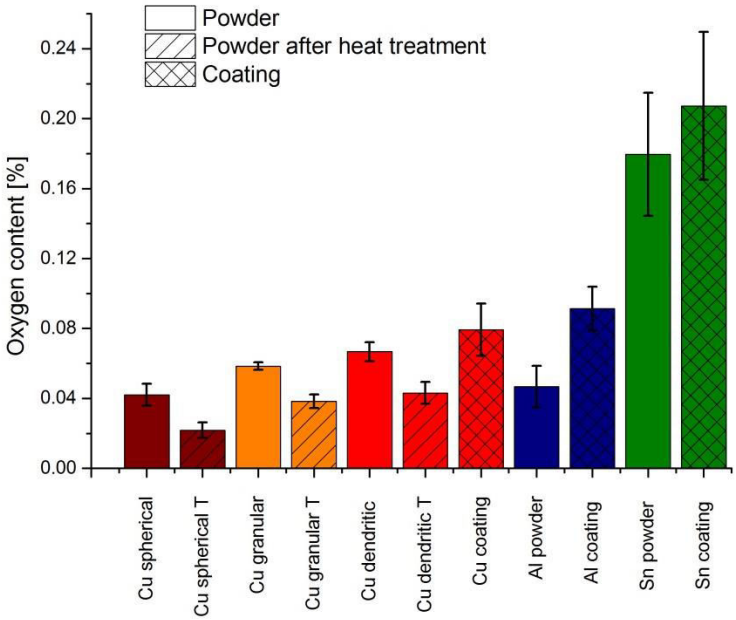

Fig. 93 Oxygen content in feedstock material and coatings

The highest oxygen content was noticed for tin powder 0.180 wt.%. The rest of the powders were less oxidized. Among copper powders oxygen content was lowest for spherical one - 0.042 wt.% and increased with irregularity of the powder morphology to 0.065 wt.%. For aluminum powder the value was about 0.047 wt. %. Copper powders after heat treatment in hydrogen and storing for one day in air exhibit about 1/3 lower oxidation. The value for dendritic copper was 0.043 wt.%. The oxidation level for dendritic powder stored one day in argon was even lower and amounted 0.033 wt.% ~1/2 of initial value. Initial oxide layer on copper, even at room temperature, forms rapidly. It was reported that after half an hour an initial oxide layer of 1 nm is formed, then oxide growth speed slows down and after 11 days the layer has thickness of about 4.5 nm [167] Similar values were observed for ion beam deposited films [168]. The changing of oxidation rates is prescribed to coalescence of initial oxide islands, which block surface diffusion routes; further oxide growth requires much slower bulk diffusion [169].

Initial oxide layer thickness equal to 1 nm might be recalculated for 20 µm spherical copper particle to 0.010 wt.% (taking copper oxide density ~6.14 g/cm^3) This oxygen content appears after half an hour contact with air so can be hardly avoided. Taking into account necessary milling and sieving of powder after heat treatment obtained values

seems to be correct. The oxygen content caused by initial oxidation decreases with increasing size of particle i.e. for 50 μm spherical copper 1 nm is 0.004 wt.%. Due to developed surface area copper amount in dendritic or globular powder are higher, which is also noted in the measurement. Powder properties after initial oxide formation will change slowly. Subsequent copper oxide formation obeys logarithmic law [168]. Such behavior was observed for dendritic copper particles by Ko et al [170]. Powder annealed in vacuum reached 60 % spraying efficiency which decreased to 40 % for two weeks air exposure and after was stable for 6 week period. Oxygen content after annealing was 0.066 wt.% [170]. Increase of critical velocity from 310 m/s to 550 m/s for oxygen content 0.02 to 0.14 wt.% was also reported by Li et al [62]. This might be explanation for coating formation when spraying with powder after deoxidizing the powder with hydrogen, but the difference of 0.02 wt % in oxygen content for heat treated and untreated powder is small. Kang et al [56] claimed that this relation is linear for aluminum powder. The lowest critical velocity values were estimated to be 721 m/s for 0.001 wt.%, and increased to 867 m/s for 0.045 wt.% oxygen content and are much higher than given by Schmidt [16]. Taking linear relation for data given by Li [62] increase of 0.02 wt.% will cause critical velocity increase at the level of 40 m/s. Additionally it must be noted that in case of low-pressure system air is used as spraying gas. This results in additional oxidation of powder particles despite the low temperature of the process. It was claimed that oxygen content in cold spray coatings is at the same level or even lower than feedstock material due to spallation of oxide layer during impact. This crushed oxide is partially removed and partially stays in formed coating [171]. However in this study oxygen amount in the coating was roughly two times higher than for powder material in case of aluminum and copper; the difference was smaller only for tin power which was oxidized heavily at the beginning. This additional oxidation is partially during spraying process and partially during cooling of the sample, so will affect also the deposition process. As it was shown for Ti particles only during presence in nozzle the oxide grow will be ~0.3 nm for 10 μm particle [172]. High amount of oxides in coatings might be also the result of low velocity which was insufficient to break them. Similar percent of oxygen content in al coating was reported by Li [37] however much higher spraying temperature was used 793 K.

Heat treatment of powder affects not only oxide layer but also hardness of the powder. It was noted that even heat treatment in air which causing additional oxidizing of the feedstock material increases spraying efficiency to certain degree. The increase of deposition efficiency was however higher for powder treated in vacuum [161] Benefits of

using heat treatment were extremely important for spraying copper coatings of polymers requires as it requires very narrow window of deposition and it was not possible to get the coating without powder treatment. Aluminum powder contain ~0.05 wt.%. The additional treatment was not applied as aluminum oxide is hardly reducible. The oxygen content might be the issue for high porosity of sprayed coatings, especially in connection with low velocity in low pressure cold spray method. Tin powder was highly oxidized - 0.180 wt. %, but this has limited influence of deposition efficiency as velocities obtained in the process were above critical velocity. The oxygen content recorded for coatings should have limited influence of electrical conductivity i.e. for copper oxygen content of ~0.20% decreased electrical conductivity value to 99% [104].

14. Impact simulation

The bonding mechanism was studied further with impact simulation in Abaqus software using Lagrange space. The particle was modeled as sphere with 20 μm diameter and the substrate as cylinder with 60 μm diameter and 80 μm height. One quarter of the model was model based on axial symmetry. The model was partitioned and meshed with 0.4 μm mesh size and C3D8RT mesh elements. The powder particle was modeled with Johnson-Cook material model which enables to predict large plastic deformation of the material, includes strain hardening and thermal softening of the material and it is given by following equation:

$$\sigma = \left[A + B \cdot \varepsilon^{n} \right] \cdot \left[1 + C \cdot ln(\dot{\varepsilon}^{*}) \right] \cdot \left[1 - T^{*m} \right] \tag{48}$$

Where: ε̇, A, B, C, n, m – material constants given in Tab. 15 and T* - temperature defined as follow:

$$T^{*} = \frac{T - T_{ref}}{T_{m} - T_{ref}} \tag{49}$$

Tab. 15 Johnson-Cook parameters

Plasticity model	**Cu**	**Sn**
A [MPa] – Yield stress	90	29
B [MPa] – Hardness Modulus	292	243
C – Constant	0.025	0.096
n – Hardening exponent	0.31	0.703
m – Constant	1.09	0.08
T_{melt} [K] – Melting temperature	1356	501
T_{ref} [K] – Reference temperature	298	298
$\varepsilon_{0\ ref}$ – Reference plastic strain rate	1	1
Material properties		
Density [kg/m3]	8960	7280
Young's Modulus [GPa]	124	45
Poisson's ratio	0.34	0.299
Thermal expansion coefficient [1/K]	16.6e-6	23.4e-6
Specific heat [J/kg*K]	383	220
Thermal conductivity [W/m* K]	401	67

For polyamide substrate model proposed by Pouriayevali [173] was chosen, which includes strain hardening and thermal softening and was calibrated with the strain rates up

to -3200/s. The model consists of two idealized mechanical groups of components connected in series (Fig. 94). First captures rate-depended reversible behavior and it includes hyperelastic element A which works together with visco-hyperelastic component B and viscous element denoted with viscosity element μ_{ve}. The second one is responsible for irreversible rate-dependent response and it is activated when the stress in the material exceeds yield value σ_c. It consists of two parallel elements – friction slider defines with σ_c and viscous element defined by coefficient μ_p [173, 174]. The detail description of the model might be find in [173, 174].

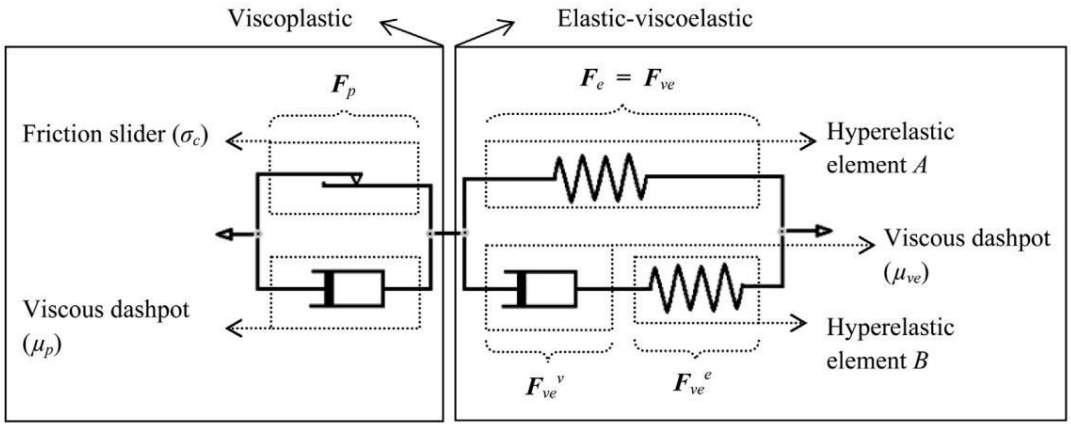

Fig. 94 Sketch of elastic-viscoelastic-viscoplastic model of semi-crystalline polymers proposed by Pouriayevali; *p, e, v,* ve stand for the plastic, elastic, viscous and viscoelastic components. [174]

The model was implemented in Abaqus as VUMAT using time integration procedure proposed by Pouriayevali [173]. Material data (Tab. 16) was taken for high compression from [173]

Tab. 16 Material data for PA6 [173]

Parameter	Value	Unit
$\mu_{ve}^{D\ \#}$	3.5e4	Pa·s
$\mu_p^{D\ \#}$	2.2e4	Pa·s
$G_{e_{10}}$	280.9	MPa
$G_{e_{01}}$	-215	MPa
$G_{e_{11}}$	52.07	MPa
D_{e_1}	1.2e4	MPa
${\sigma_u}^*$	35.0	MPa
H	10	MPa

$\Omega = \hat{\Omega}(\Theta)$	$7.198\, e^{-2.832\,\Theta/\Theta_0}$	$\Theta_0 = 298$ [K]
$\pi = \hat{\pi}(\Theta)$	$30945\, e^{-10.34\,\Theta/\Theta_0}$	$\Theta_0 = 298$ [K]
c	1700	J/kg K
α_{th}	5e-5	m/m K
ρ	1145	kg/m^3
Q	0.45	
ϑ	0.495	
ϒ	5	
ω	0.9	

Parameters identified with #, * are temperature-dependent and modified by multiplication with π and Ω respectively.

The model was calibrated using one element compression and tension. The obtained curves (Fig. 95) were compared to ones presented by Pouriayevali (Fig. 96) [173]. Good agreement was found and the implementation was recognized as correct.

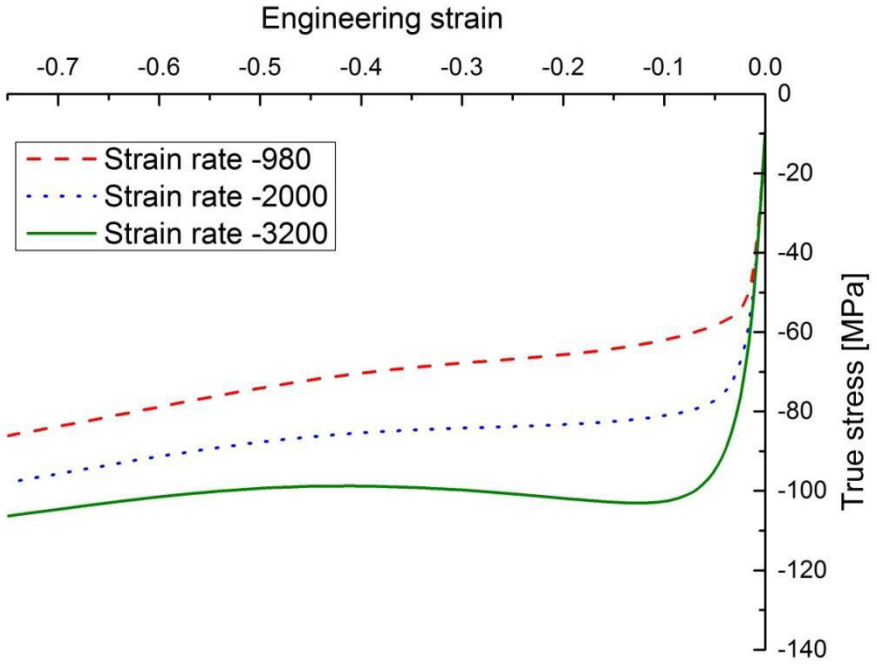

Fig. 95 Stress-strain curves obtained from the implemented model.

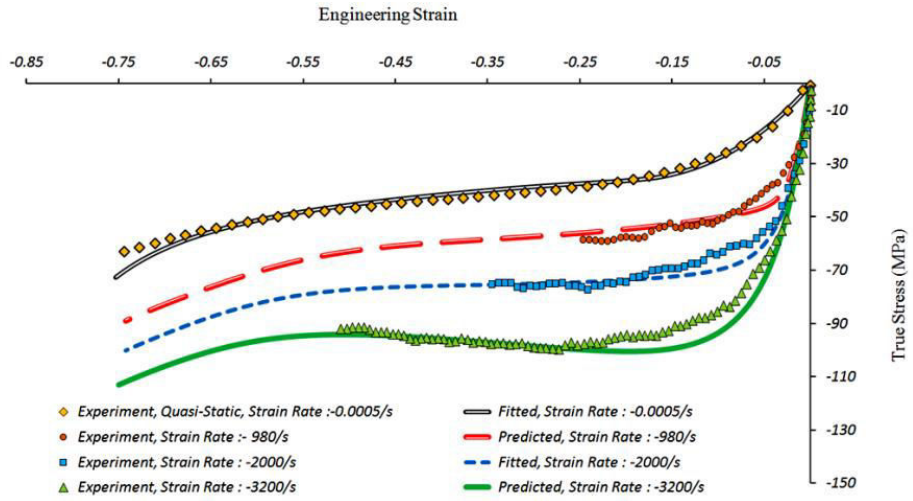

Fig. 96 Obtained stress-strain curves for different compression strain rates from [173]

Simulation parameters for cold spray process are summarized in Tab. 17

Tab. 17 Simulation parameters

No	Substrate material	Particle material	Substrate temperature [K]	Particle temperature [K]	Particle velocity [m/s]
1	Pa6	Cu	298	298	300
2			353	353	
3		Sn	298	298	
4			353	353	

The calculated stress and temperature field are presented in Fig. 98 and Fig. 99. The stress levels are unexpectedly high which might be caused by much higher strain rate than one used for calibration and lack of damage criteria. Therefore additional adjustment of the model is needed and the results might be treated rather as indication of occurring phenomena than absolute values. It might be seen that for room temperature much higher stress is generated under the surface of the substrate than for the temperature above glass transitions temperature. In case of semicrystalline polymers like PA6 below glass transition temperature the amorphous phase is in frozen state and material behave brittle (Fig. 97) [175]. Brittle behavior is also favorable for high strain rates [176]. In higher temperatures and lower strain rates molecules of amorphous part gain more mobility. Simultaneous presence of crystal phase causes that material behave tough elastic to hard [175]

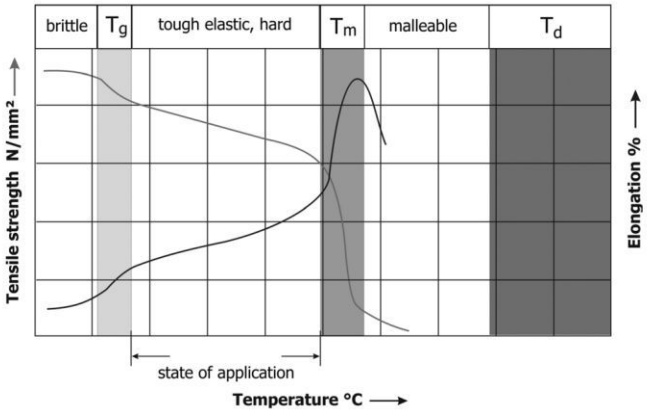

Fig. 97 Temperature behavior of semicrystaline polymers [175]

Based on this information it might be concluded that in case of room temperature probably fractures occurs under the particle after impact and it will be easily removable by incoming particle. Additionally there are "spring forces" which will cause bouncing of the particle [177], present in this model as hyperelastic element. Comparing tin and copper particle might be seen that copper particle impact will generate more stresses than tin particle. Additionally although both particles are embedment in substrate tin particle, due to low mechanical properties, is much more deformed in contact with polymer. The deformation ratio of copper particle is low. This might be the explanation possibility of deposition of tin coating in room temperature and impossibility of obtaining of copper coating observed by Lupoi when using non preheated gas [122].

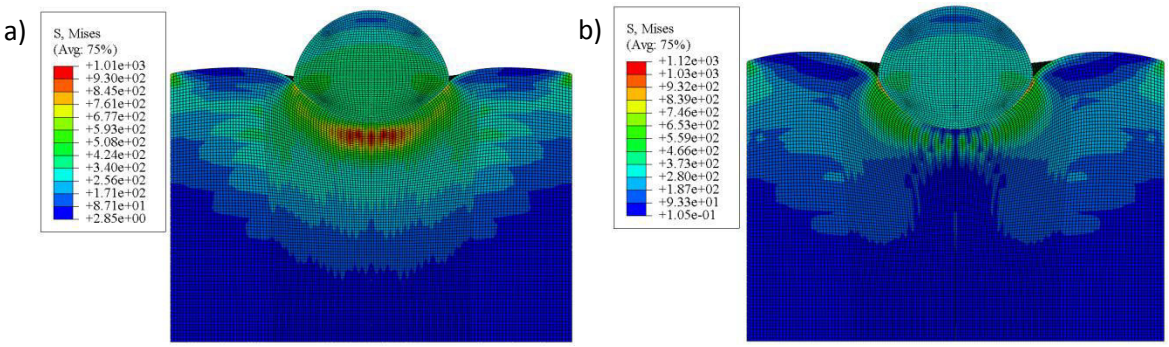

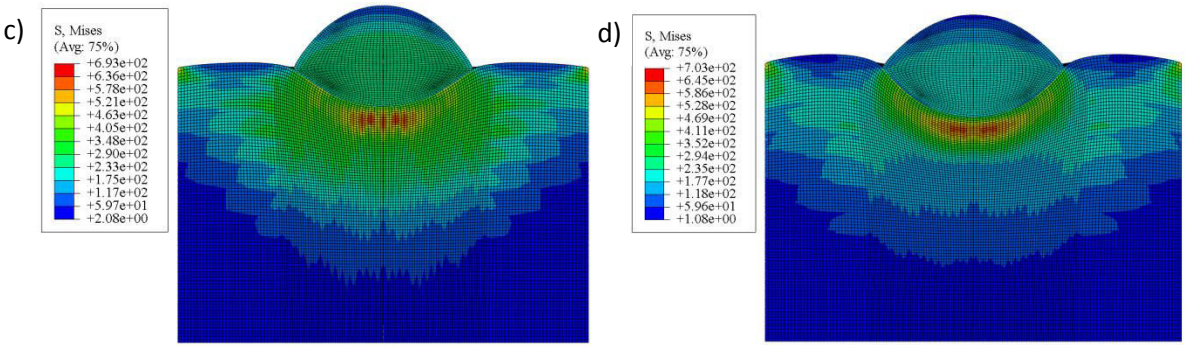

Fig. 98 Calculated stress field for simulation conditions: Cu -298 K (a) Cu-353 K (b) Sn -298 (c) Sn-353 (d) in highest deformation moment at higher deformation moment

The stress generated during impact is partially dissipated as heat causing thermal softening of polymer. This behavior might be observed especially for impact of copper particle and substrate preheated up to 353 K. In case of tin particle the stress and strain caused by impact is lower therefore the temperature rise is not so high and amounts to ~ 3K. Thermal softening favors plastic deformation and reduce present in the material stresses and therefore is beneficial. It is higher for higher material temperature because i.e. due to lower mechanical properties there higher strains observed in substrate material. It might be seen that in case of higher temperature of substrate the embedment of particle is higher and tin particle is well deformed. The copper particle however did not undergo notable deformation.

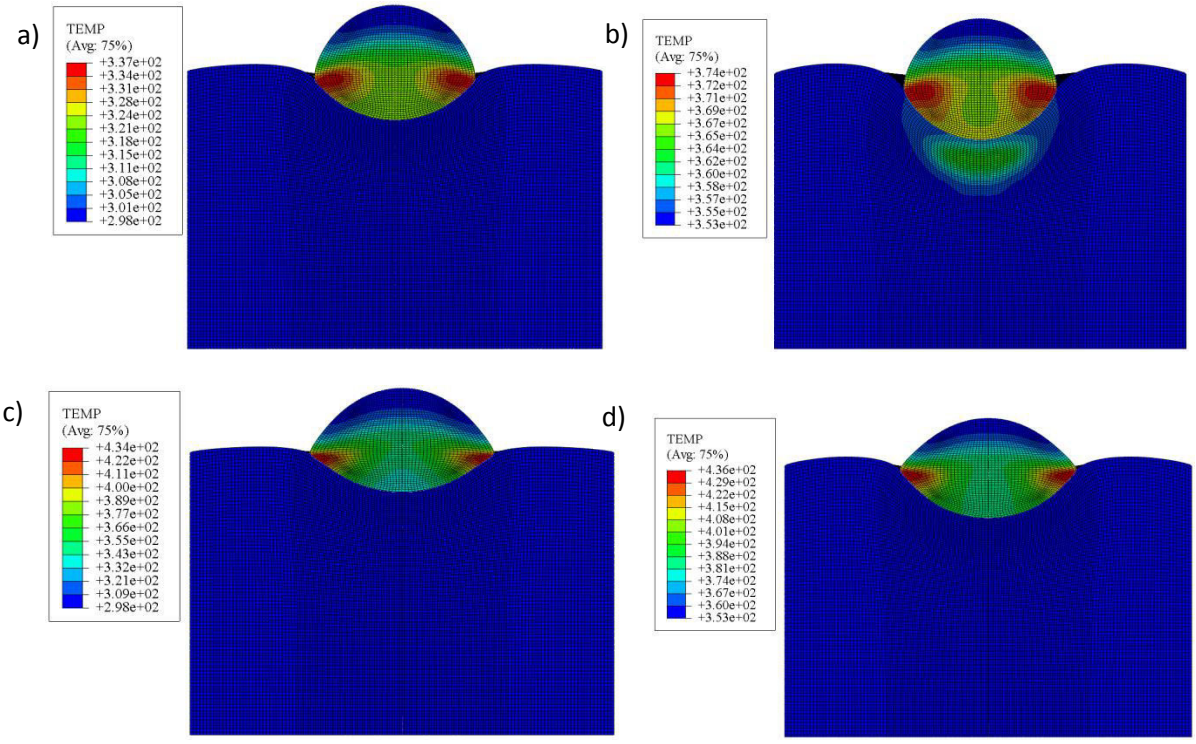

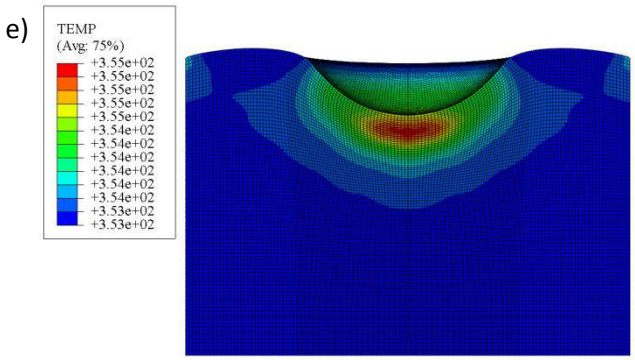

Fig. 99 Calculated temperature field for simulation conditions: Cu -298 K (a) Cu-353 K (b) Sn -298 (c) Sn-353 (d) Sn-353 – substrate only(e) at highest deformation moment

The partially hyperelastic behavior of PA6 especially visible in room temperature will cause that after deformation the substrate material will tend to recover and dissipate the stress. This is visible at Fig. 100. The simulation was done with coarse mesh as there were stability problems with higher deformation gradient. Used model does not take into account damage criteria therefore the recovery is almost complete. In reality due to high concentration of stress during impact polymer substrate will partially crack in contact place.

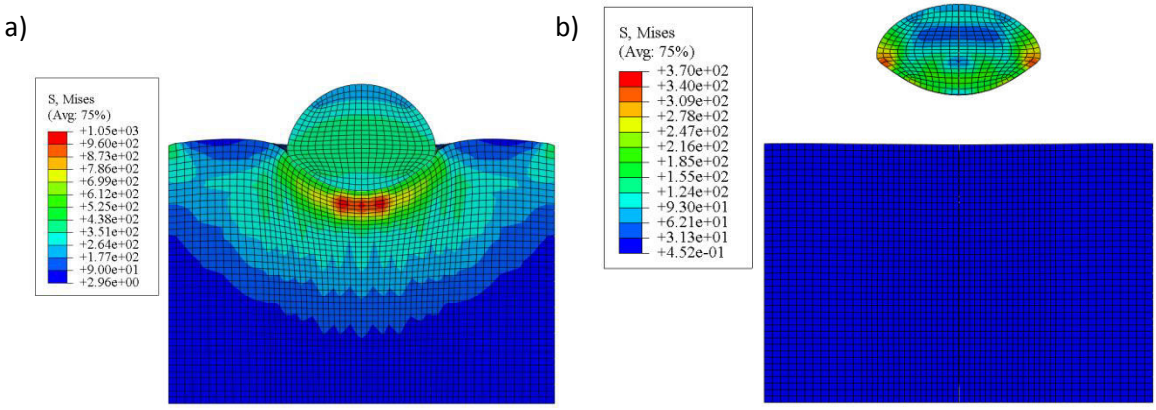

Fig. 100 Calculated temperature field for simulation conditions Cu -298 K : at highest deformation moment (a) after bouncing off (b)

The recovery will be suppressed totally after temperatures close to melting temperature and will be additional influencing by loading effect during spraying. Highly pressurized gas and particles present in the gas stream will constantly load the substrate in same place hence decrease its mechanical strength and partially block “spring forces”. In polymers hysteresis behavior for mechanical properties is observed with decreasing mechanical strength after cycling loading [176]. This effect might be and explanation for observed dependence of powder feed rate and forming the coating i.e. Ye et al observed no coating

formation for low feedrates [125]. As well as for higher bond strength of coating formed when using lower traverse velocity of spraying gun or higher feedrates.

Comparing simulation to experimental results might be see that there is almost no deformation of the copper particles. Additionally some squeezed polymers and cracks in the substrate might be observed (Fig. 101).

Based on the simulation it might be concluded that in case of pure copper coating the spraying temperature should be above T_g even close to T_m with low pressure however to avoid polymer flow. After successful deposition of first layer of spherical copper the whole coating might be build up with much higher pressures to reach critical velocity for given powder. This requires a nozzle with barrel shape in order to control fully the temperature as well precise temperature control unit. The commercially available Dymet 413 (Obninsk Center for Powder Spraying, Russia) set up is not adjusted for the metallization of polymers and should be modified.

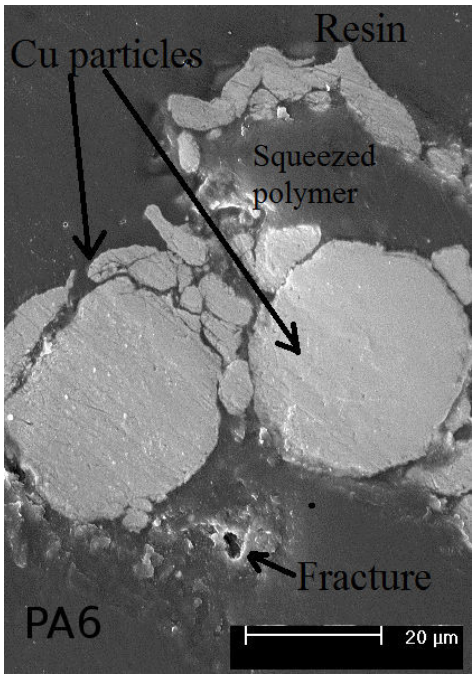

Fig. 101 Copper particles embedment in the PA6 substrate

15. Summary, conclusion and future work

Cold spray process is well-established thermal spraying process used for deposition metal and cermet coatings on metal substrates. Operating principle assures low temperature and high kinetic energy which results in i.e. low oxidation level, high bond strength, high electrical conductivity. These advantages cause constant development of the method and search for new application field.

In this work attempt of metallization of polymers with low pressure cold spray method was undertaken. Cold spray was chosen as low temperature process, relatively cheap and environment friendly which allows getting excellent coatings properties and local deposition in strictly defined places. Two thermoplastic substrates and five metal powders were studied. The substrates were amorphous polycarbonate and semicrystaline polyamide 6. The powder included: spherical, globular and dendritic copper, aluminum and tin. The deposition process on polymers turned out to be much more complex than in case of metal substrate. The problems included to name a few: low hardness of substrate, brittle behavior in low temperature, thermal softening already in very low temperatures.

The work started with calculation of velocity in the low pressure cold spray process. The calculated velocity value for all powders excluding tin was below critical one for parameters acceptable in view of deposition on polymers. First trials confirmed that the deformation of powder particles was insufficient. In case of copper it was impossible to obtain the coating. Additionally the bond strength was very low – the coatings delaminated spontaneously. Two ways have undertaken to improve the results: decreasing the critical velocity of powder and applying of the interlayers. Using both ways it was possible to obtain copper and aluminum coatings on PA6 and PC. Obtained mechanical and electrical properties were very low in compare to obtain for metal or ceramic substrate. The average bond strength does not exceed 5 MPa and the electrical resistivity was one order of magnitude higher than for bulk material. The results might have been improved for copper coating sprayed directly after deoxidizing and very fine spherical particles. Especially when using higher pressure.

It was assumed in the beginning of the thesis that it will be possible to obtain metal coatings on polymers having properties similar to the coatings deposited with presently used methods However, the properties of coatings obtained with low pressure cold spray method differ notably from the properties of coatings obtained with such methods as electroless deposition, electroplating or PVD. First of all they are much thicker and have higher electrical resistivity value which in case i.e. for electroless deposition approaches

value of bulk copper [178]. The increase in electrical resistivity in compare to bulk material is typical for thermal spraying methods due to structure defects and oxidation. The adhesion strength of coatings is at the similar level but can not be directly compared as there is huge difference in thicknesses [179]. Therefore much more reasonable is the comparison of the properties of obtained coatings with other thermal spraying methods. At this background obtained characteristic are similar or in some cases better than ones given in the literature [120, 123, 126]. The application of the manufactured coatings might find place in the area where well-established methods can be not used due to i.e. the dimensions of the parts or large effort for surface preparation. Additionally thick coatings might be easily manufactured which might be in desirable in some cases. It might be also assumed that the further development of the technology based on gained knowledge will result in notable increase in properties of coatings deposited on polymers.

On the base of the research and literature study following conclusion can be drawn:

- Even small amount of oxygen in copper powders increase notable critical velocity. Using partially deoxidized and heat treated powder it was possible to obtain continuous copper coating on PA6 and PC with interlayer.
- The bond strength of first metal layer is decisive for obtaining metal coating on polymers. Especially during spraying copper damage to the Sn+Al_2O_3 interlayer was observed due to high energy
- The texturing of the substrate has positive effect on the bond strength due to improved mechanical interlocking
- Detachment of the coatings took place between first deposited particles embedded in the polymer and the rest of the coating. It could be caused by: thermal coefficient mismatch, polymer squeezed during embedding of the particles preventing good bonding as well as spring response to impact by polymer substrate.
- The electrical conductivity is not related directly to the porosity of the coatings. Subsequent compaction of pores might only slightly improve properties of the coating and although pore is compressed there is still not good electrical contact.
- Substrate hardness plays very important role in the coatings formation allowing for proper deformation of the incoming particles.
- No anisotropy of elastic modulus was observed due to low deformation of coatings
- Microhardness values were low in compare to coating obtained on metal substrates.

- Deposition of coatings with increased numbers of passes has negative effect on bond strength due to thermal influence to substrate.

Conducted research allow for following practical conclusions:

- Thermoplastic polymers might be metallized with low pressure cold spray equipment and find the application i.e. as electric connection but further optimization is needed.
- The other field of application is using it as interlayer for abrasion resistance coatings.

To improve properties of obtained coatings further studies are needed.

- Mechanical behavior of polymers is correlated both with temperature and strain rate. With increasing strain rate and decreasing temperature polymers behave more brittle [physics of deformation]. This has negative e
- 3ffect on deposition process. For deep embedded interlayers which will increase bond strength seems that temperature above T_g for PA6 should be used with relatively low pressure to avoid unfavorable polymer flow. Instead of used ceramic for which bonding with metal is difficult larger metal powder should be used. To determine proper window of deposition it is necessary to run detailed simulations of particle impact with material model for polymer which incorporate temperature softening and strain hardening for polymers.
- Using graded coatings containing polymer and metal particles will decrease inadequacy of mechanical and thermal properties
- Using mixture of spherical-dendritic powders for spraying topcoat which might improve density of the coating or very small spherical powder which will decrease impact energy.
- Spraying coating with high pressure cold spray set up with optimized parameters
- Testing the possibility of metalizing thermoset polymer and polymer matrix composites
- Testing the possibility of using metalized polymers for soldering and brazing.

The French Embassy in Poland financed the stay of author in France with agreement co-tutelle.

16. References

1. Schmidt T, Gärtner F, Assadi H, Kreye H. Development of a generalized parameter window for cold spray deposition. Acta Materialia 2006;54:729–42. doi:10.1016/j.actamat.2005.10.005.
2. DIN EN 657: 2005-06. Thermisches Spritzen - Begriffe, Einteilung 2005: Beuth-Verlag, Berlin.
3. Siegmann S, Abert C. 100 years of thermal spray: About the inventor Max Ulrich Schoop. Surface and Coatings Technology 2013;220:3–13. doi:10.1016/j.surfcoat.2012.10.034.
4. Champagne VK. The cold spray materials deposition process: Fundamentals and applications. Cambridge, Boca Raton: Woodhead; CRC Press; 2007.
5. Pawłowski L. The science and engineering of thermal spray coatings. 2nd ed. Chichester, England, Hoboken, NJ: Wiley; 2008.
6. Maev R, Leshchynsky V. Introduction to Low Pressure Gas Dynamic Spray. Weinheim, Germany: Wiley-VCH Verlag GmbH & Co. KGaA; 2007.
7. Wen C. Surface Coating and Modification of Metallic Biomaterials: Elsevier Science; 2015.
8. Fauchais P, Vardelle A, Vardelle M, Fukumoto M. Knowledge concerning splat formation: An invited review: Journal of Thermal Spray Technology. J Therm Spray Tech 2004;13:337–60. doi:10.1361/10599630419670.
9. Smith RW, Knight R. Thermal spraying I: Powder consolidation—From coating to forming. JOM 1995;47:32–9. doi:10.1007/BF03221456.
10. Senderowski C, Bojar Z. Influence of Detonation Gun Spraying Conditions on the Quality of Fe-Al Intermetallic Protective Coatings in the Presence of NiAl and NiCr Interlayers: Journal of Thermal Spray Technology. J Therm Spray Tech 2009;18:435–47. doi:10.1007/s11666-009-9328-z.
11. Herman H, Sampath S, McCune R. Thermal Spray: Current Status and Future Trends. MRS Bull. 2000;25:17–25. doi:10.1557/mrs2000.119.
12. Kuroda S, Kawakita J, Watanabe M, Katanoda H. Warm spraying—a novel coating process based on high-velocity impact of solid particles. Sci. Technol. Adv. Mater. 2008;9:33002. doi:10.1088/1468-6996/9/3/033002.
13. Ang ASM, Sanpo N, Sesso ML, Kim SY, Berndt CC. Thermal Spray Maps: Material Genomics of Processing Technologies. J Therm Spray Tech 2013;22:1170–83. doi:10.1007/s11666-013-9970-3.

14. Bach F, Laarmann A, Wenz T. Modern Surface Technology. Weinheim, FRG: Wiley-VCH Verlag GmbH & Co. KGaA; 2006.
15. Irissou E, Legoux J, Ryabinin AN, Jodoin B, Moreau C. Review on Cold Spray Process and Technology: Part I—Intellectual Property. J Therm Spray Tech 2008;17:495–516. doi:10.1007/s11666-008-9203-3.
16. Schmidt T, Assadi H, Gärtner F, Richter H, Stoltenhoff T, Kreye H, Klassen T. From Particle Acceleration to Impact and Bonding in Cold Spraying: Journal of Thermal Spray Technology. J Therm Spray Tech 2009;18:794–808. doi:10.1007/s11666-009-9357-7.
17. Stoltenhoff T, Kreye H, Richter HJ. An analysis of the cold spray process and its coatings: Journal of Thermal Spray Technology. J Therm Spray Tech 2002;11:542–50. doi:10.1361/105996302770348682.
18. Stoltenhoff T, Voyer M., Kreye H. Cold spraying - state of the art and applicability. Proceedings of the ITSC 2002, Essen, Germany;2002.
19. Borchers C, Gärtner F, Stoltenhoff T, Assadi H, Kreye H. Microstructural and macroscopic properties of cold sprayed copper coatings. J. Appl. Phys. 2003;93:10064. doi:10.1063/1.1573740.
20. Dykhuizen R.C. and Smith M.F. Gas dynamic principles of cold spray.
21. Assadi H, Gärtner F, Stoltenhoff T, Kreye H. Bonding mechanism in cold gas spraying. Acta Materialia 2003;51:4379–94. doi:10.1016/S1359-6454(03)00274-X.
22. Grujicic M, Zhao C, DeRosset W, Helfritch D. Adiabatic shear instability based mechanism for particles/substrate bonding in the cold-gas dynamic-spray process. Materials & Design 2004;25:681–8. doi:10.1016/j.matdes.2004.03.008.
23. Ning X, Jang J, Kim H, Li C, Changhee Lee. Cold spraying of Al–Sn binary alloy: Coating characteristics and particle bonding features. Surface and Coatings Technology 2008;202:1681–7. doi:10.1016/j.surfcoat.2007.07.026.
24. Papyrin A. Cold spray technology. Amsterdam, London: Elsevier; 2007.
25. Villafuerte J. Current Trends in Cold Spray Technology: Looking at the Future. http://www.metalfinishing.com/view/6310/current-trends-in-cold-spray-technology-looking-at-the-future/. Accessed 1 Aug 2015.
26. Maev RG. Introduction to low pressure gas samic spray: Physics & technology. Weinheim: Wiley-VCH; 2007.

27. Irissou E, Legoux J, Arsenault B, Moreau C. Investigation of Al-Al2O3 Cold Spray Coating Formation and Properties: Journal of Thermal Spray Technology. J Therm Spray Tech 2007;16:661–8. doi:10.1007/s11666-007-9086-8.
28. Lee H, Yu Y, Lee Y, Hong Y, Ko K. Cold spray of SiC and Al2O3 with soft metal incorporation: A technical contribution: Journal of Thermal Spray Technology. J Therm Spray Tech 2004;13:184–9. doi:10.1361/10599630419355.
29. Maev RG, Leshchynsky V. Air gas dynamic spraying of powder mixtures: Theory and application: Journal of Thermal Spray Technology. J Therm Spray Tech 2006;15:198–205. doi:10.1361/105996306X108048.
30. Internet website of Cold Gas Technology GmbH:. http://en.dymet.net/coating-technology.html. Accessed 1 Aug 2015.
31. Schmidt T, Gaertner F, Kreye H. New Developments in Cold Spray Based on Higher Gas and Particle Temperatures. J Therm Spray Tech 2006;15:488–94. doi:10.1361/105996306X147144.
32. van Steenkiste TH, Smith JR, Teets RE. Aluminum coatings via kinetic spray with relatively large powder particles. Surface and Coatings Technology 2002;154:237–52. doi:10.1016/S0257-8972(02)00018-X.
33. Papyrin A., Klinkov S., Kosarev V. Effect of the substrate surface activation on the process of cold spray coating formation. Proceedings of the ITSC 2005, Basel, Switzerland;2005.
34. McCune RC, Donlon WT, Popoola OO, Cartwright EL. Characterization of copper layers produced by cold gas-dynamic spraying: Journal of Thermal Spray Technology. J Therm Spray Tech 2000;9:73–82. doi:10.1361/105996300770350087.
35. Shkodkin A, Kashirin A, Klyuev O, Buzdygar T. Metal particle deposition stimulation by surface abrasive treatment in gas dynamic spraying: Journal of Thermal Spray Technology. J Therm Spray Tech 2006;15:382–6. doi:10.1361/105996306X124383.
36. Gilmore DL, Dykhuizen RC, Neiser RA, Smith MF, Roemer TJ. Particle velocity and deposition efficiency in the cold spray process: Journal of Thermal Spray Technology. J Therm Spray Tech 1999;8:576–82. doi:10.1361/105996399770350278.
37. Li W, Zhang C, Wang H, Guo XP, Liao HL, Li C, Coddet C. Significant influences of metal reactivity and oxide films at particle surfaces on coating microstructure in cold spraying. Applied Surface Science 2007;253:3557–62. doi:10.1016/j.apsusc.2006.07.063.

38. Gärtner F, Stoltenhoff T, Schmidt T, Kreye H. The cold spray process and its potential for industrial applications: Journal of Thermal Spray Technology. J Therm Spray Tech 2006;15:223–32. doi:10.1361/105996306X108110.
39. Assadi H, Schmidt T, Richter H, Kliemann J, Binder K, Gärtner F, et al. On Parameter Selection in Cold Spraying. J Therm Spray Tech 2011;20:1161–76. doi:10.1007/s11666-011-9662-9.
40. Vidaller M. V. List A., Gärtner F., Klassen T., Dosta S., Guilemany J. M. Ti6Al4V cold gas sprayed coatings: impact morphologies, splat adhesion and correlations to coating microstructures. Proceedings of the ITSC 2013, Busan Republic of Korea May 13-15, 2013.
41. Wu J, Fang H, Yoon S, Lee C, Kim H. Critical Velocities for High Speed Particle Deposition in Kinetic Spraying. MATERIALS TRANSACTIONS 2006;47:1723–7. doi:10.2320/matertrans.47.1723.
42. Dykhuizen RC, Smith MF, Gilmore DL, Neiser RA, Jiang X, Sampath S. Impact of high velocity cold spray particles: Journal of Thermal Spray Technology. J Therm Spray Tech 1999;8:559–64. doi:10.1361/105996399770350250.
43. Li W, Liao H, Li C, Bang H, Coddet C. Numerical simulation of deformation behavior of Al particles impacting on Al substrate and effect of surface oxide films on interfacial bonding in cold spraying. Applied Surface Science 2007;253:5084–91. doi:10.1016/j.apsusc.2006.11.020.
44. Grujicic M, Saylor JR, Beasley DE, DeRosset WS, Helfritch D. Computational analysis of the interfacial bonding between feed-powder particles and the substrate in the cold-gas dynamic-spray process. Applied Surface Science 2003;219:211–27. doi:10.1016/S0169-4332(03)00643-3.
45. Heberlein JV, Fauchais P, Boulos MI. Thermal spray fundamentals: From powder to part. New York: Springer; 2014.
46. Li W, Zhang C, Li C, Liao H. Modeling Aspects of High Velocity Impact of Particles in Cold Spraying by Explicit Finite Element Analysis. J Therm Spray Tech 2009;18:921–33. doi:10.1007/s11666-009-9325-2.
47. Yin S, Wang X, Xu B, Li W. Examination on the Calculation Method for Modeling the Multi-Particle Impact Process in Cold Spraying. J Therm Spray Tech 2010;19:1032–41. doi:10.1007/s11666-010-9489-9.

48. Borchers C, Gärtner F, Stoltenhoff T, Kreye H. Microstructural bonding features of cold sprayed face centered cubic metals. J. Appl. Phys. 2004;96:4288. doi:10.1063/1.1789278.
49. Guetta S, Berger MH, Borit F, Guipont V, Jeandin M, Boustie M, et al. Influence of Particle Velocity on Adhesion of Cold-Sprayed Splats. J Therm Spray Tech 2009;18:331–42. doi:10.1007/s11666-009-9327-0.
50. King P, Bae G, Zahiri S, Jahedi M, Lee C. An Experimental and Finite Element Study of Cold Spray Copper Impact onto Two Aluminum Substrates: Journal of Thermal Spray Technology. J Therm Spray Tech 2010;19:620–34. doi:10.1007/s11666-009-9454-7.
51. Hussain T, McCartney DG, Shipway PH, Zhang D. Bonding Mechanisms in Cold Spraying: The Contributions of Metallurgical and Mechanical Components: Journal of Thermal Spray Technology. J Therm Spray Tech 2009;18:364–79. doi:10.1007/s11666-009-9298-1.
52. Price TS, Shipway PH, McCartney DG, Calla E, Zhang D. A Method for Characterizing the Degree of Inter-particle Bond Formation in Cold Sprayed Coatings: Journal of Thermal Spray Technology. J Therm Spray Tech 2007;16:566–70. doi:10.1007/s11666-007-9070-3.
53. Hussain T, McCartney DG, Shipway PH. Bonding between aluminium and copper in cold spraying: Story of asymmetry. Materials Science and Technology 2012;28:1371–8. doi:10.1179/1743284712Y.0000000051.
54. Li W, Zhang C, Li C, Liao H. Modeling Aspects of High Velocity Impact of Particles in Cold Spraying by Explicit Finite Element Analysis: Journal of Thermal Spray Technology. J Therm Spray Tech 2009;18:921–33. doi:10.1007/s11666-009-9325-2.
55. Li C, Li W, Liao H. Examination of the critical velocity for deposition of particles in cold spraying: Journal of Thermal Spray Technology. J Therm Spray Tech 2006;15:212–22. doi:10.1361/105996306X108093.
56. Kang K, Yoon S, Ji Y, Lee C. Oxidation dependency of critical velocity for aluminum feedstock deposition in kinetic spraying process. Materials Science and Engineering: A 2008;486:300–7. doi:10.1016/j.msea.2007.09.010.
57. Li WY, Zhang DD, Huang CJ, Yin S, Yu M, Wang FF, Liao HL. Modelling of impact behaviour of cold spray particles: Review. Surface Engineering 2014;30:299–308. doi:10.1179/1743294414Y.0000000268.

58. Binder K, Gottschalk J, Kollenda M, Gärtner F, Klassen T. Influence of Impact Angle and Gas Temperature on Mechanical Properties of Titanium Cold Spray Deposits: Journal of Thermal Spray Technology. J Therm Spray Tech 2011;20:234–42. doi:10.1007/s11666-010-9557-1.
59. Lee J, Shin S, Kim H, Lee C. Effect of gas temperature on critical velocity and deposition characteristics in kinetic spraying. Applied Surface Science 2007;253:3512–20. doi:10.1016/j.apsusc.2006.07.061.
60. Yin S, Wang X, Suo X, Liao H, Guo Z, Li W, Coddet C. Deposition behavior of thermally softened copper particles in cold spraying. Acta Materialia 2013;61:5105–18. doi:10.1016/j.actamat.2013.04.041.
61. Kim H, Lee C, Hwang S. Superhard nano WC–12%Co coating by cold spray deposition. Materials Science and Engineering: A 2005;391:243–8. doi:10.1016/j.msea.2004.08.082.
62. Li C, Wang H, Zhang Q, Yang G, Li W, Liao HL. Influence of Spray Materials and Their Surface Oxidation on the Critical Velocity in Cold Spraying: Journal of Thermal Spray Technology. J Therm Spray Tech 2010;19:95–101. doi:10.1007/s11666-009-9427-x.
63. Yin S, Wang X, Li W, Liao H, Jie H. Deformation behavior of the oxide film on the surface of cold sprayed powder particle. Applied Surface Science 2012;259:294–300. doi:10.1016/j.apsusc.2012.07.036.
64. Li C.-J., Li W.-Y., Wang Y. Y., Fukanuma H. Effect of Spray Angle on Deposition Characteristics in Cold Spraying. Proceedings of the ITSC 2003, Orlando, FL, USA May 2003:5–8.
65. Li W, Yin S, Wang X. Numerical investigations of the effect of oblique impact on particle deformation in cold spraying by the SPH method. Applied Surface Science 2010;256:3725–34. doi:10.1016/j.apsusc.2010.01.014.
66. Li C, Li W, Wang Y, Yang G, Fukanuma H. A theoretical model for prediction of deposition efficiency in cold spraying. Thin Solid Films 2005;489:79–85. doi:10.1016/j.tsf.2005.05.002.
67. Taylor K, Jodoin B, Karov J. Particle loading effect in cold spray: Journal of Thermal Spray Technology. J Therm Spray Tech 2006;15:273–9. doi:10.1361/105996306X108237.

68. Vlcek J, Gimeno L, Huber H, Lugscheider E. A systematic approach to material eligibility for the cold-spray process: Journal of Thermal Spray Technology. J Therm Spray Tech 2005;14:125–33. doi:10.1361/10599630522738.
69. Vlcek J., Huber H., Voggenreiter H., Fischer A., Lugscheider E. Kinetic Powder Compaction Applying the Cold Spray Process: A Study on Parameters. Proceedings of the ITSC 2001 28-30 May, 2001:417–22.
70. Zhang D, Shipway PH, McCartney DG. Cold gas dynamic spraying of aluminum: The role of substrate characteristics in deposit formation: Journal of Thermal Spray Technology. J Therm Spray Tech 2005;14:109–16. doi:10.1361/10599630522666.
71. Stoltenhoff T, Kreye H, Richter HJ. An analysis of the cold spray process and its coatings: Journal of Thermal Spray Technology. J Therm Spray Tech 2002;11:542–50. doi:10.1361/105996302770348682.
72. Koivuluoto H, Coleman A, Murray K, Kearns M, Vuoristo P. High Pressure Cold Sprayed (HPCS) and Low Pressure Cold Sprayed (LPCS) Coatings Prepared from OFHC Cu Feedstock: Overview from Powder Characteristics to Coating Properties: Journal of Thermal Spray Technology. J Therm Spray Tech 2012;21:1065–75. doi:10.1007/s11666-012-9790-x.
73. Stoltenhoff T, Borchers C, Gärtner F, Kreye H. Microstructures and key properties of cold-sprayed and thermally sprayed copper coatings. Surface and Coatings Technology 2006;200:4947–60. doi:10.1016/j.surfcoat.2005.05.011.
74. Sudharshan Phani P, Srinivasa Rao D, Joshi SV, Sundararajan G. Effect of Process Parameters and Heat Treatments on Properties of Cold Sprayed Copper Coatings: Journal of Thermal Spray Technology. J Therm Spray Tech 2007;16:425–34. doi:10.1007/s11666-007-9048-1.
75. Venkatesh L, Chavan N, Sundararajan G. The Influence of Powder Particle Velocity and Microstructure on the Properties of Cold Sprayed Copper Coatings: Journal of Thermal Spray Technology. J Therm Spray Tech 2011;20:1009–21. doi:10.1007/s11666-011-9614-4.
76. Kumar S, Bae G, Kang K, Yoon S, Lee C. Effect of powder state on the deposition behaviour and coating development in kinetic spray process. J. Phys. D: Appl. Phys. 2009;42:75305. doi:10.1088/0022-3727/42/7/075305.
77. Ganesan A, Affi J, Yamada M, Fukumoto M. Bonding behavior studies of cold sprayed copper coating on the PVC polymer substrate. Surface and Coatings Technology 2012;207:262–9. doi:10.1016/j.surfcoat.2012.06.086.

78. Sakaki K, Shinkai S, Ebara N., Shimizu Y. Effect of Geometry of the Gun Nozzle, the Increase in the Entrance Convergent Section Length and Powder Injection Point on Cold Sprayed Titanium Coatings. Materials Science Forum 2006;534-536:413–6.
79. Sakaki K, Huruhashi N, Tamaki K, Shimizu Y. Effect of nozzle geometry on cold spray process',. In: Lugscheider E., Berndt C C, editor. International Thermal Spray Conference; 4-6 March; Essen, Germany; 2002.
80. Li W, Liao H, Wang H, Li C, Zhang G, Coddet C. Optimal design of a convergent-barrel cold spray nozzle by numerical method. Applied Surface Science 2006;253:708–13. doi:10.1016/j.apsusc.2005.12.157.
81. Ascher H. Shapiro. The Dynamics and Thermodynamics of Compressible Fluid Flow. New York: The Roland Press Company; 1953.
82. Eklavya Calla. Cold Gas Spraying of Cold Gas Spraying of Copper and Tin onto Metallic and Non metallic substrates [Phd Thesis]: Univeristy of Nottingham; 2005.
83. Sutton GP, Biblarz O. Rocket propulsion elements. 7th ed. New York: John Wiley & Sons; 2001.
84. Katz J. Introductory fluid mechanics. New York: Cambridge University Press; 2010.
85. Levenspiel O. Engineering flow and heat exchange.
86. T. Al-Shemmeri. Engineering Fluid Mechanics: T. Al-Shemmeri & Ventus Publishing ApS; 2012.
87. Rajput RK. Engineering thermodynamics. 3rd ed. Sudbury, Mass.: Jones and Bartlett Publishers; 2010.
88. White FM. Fluid mechanics. New York, NY: McGraw-Hill Education; 2016.
89. Staniszewski B. Termodynamika. 4th ed. Warszawa: Państwowe Wydaw. Naukowe; 1986.
90. Ansys Fluent 14.5 User's Guide, Fluent Inc,Lebanon, NH.
91. Morsi SA, Alexande rA. An Investigation of Particle Trajectories in Two-Phase Flow Systems. J. Fluid Mech. 1972;55:193–208. doi:10.1017/S0022112072001806.
92. Ning X, Wang Q, Ma Z, Kim H. Numerical Study of In-flight Particle Parameters in Low-Pressure Cold Spray Process. J Therm Spray Tech 2010;19:1211–7. doi:10.1007/s11666-010-9548-2.
93. Grujicic M, Zhao CL, Tong C, DeRosset WS, Helfritch D. Analysis of the impact velocity of powder particles in the cold-gas dynamic-spray process. Materials Science and Engineering: A 2004;368:222–30. doi:10.1016/j.msea.2003.10.312.

94. Ng Ching Shan. Metallization of Engineering Plastics [MSc thesis]: The Hong Kong Polytechnic University; 2008.
95. Suchentrunk R. Kunststoff-Metallisierung: Mit 35 Tabellen. 3rd ed. Bad Saulgau: Leuze; 2007.
96. Lin Y, Liu H, Chen C. Plasma surface modification of polyimide films by air glow discharge for copper metallization on microelectronic flex substrates. Surface and Coatings Technology 2006;200:3775–85. doi:10.1016/j.surfcoat.2004.11.031.
97. Beil S, Horn H, Windisch A, Hilgers C, Pochner K. Photochemical functionalization of polymer surfaces for subsequent metallization. Surface and Coatings Technology 1999;116–119:1195–203. doi:10.1016/S0257-8972(99)00155-3.
98. Frerichs H, Stricker J, Wesner DA, Kreutz EW. Laser-induced surface modification and metallization of polymers. Applied Surface Science 1995;86:405–10. doi:10.1016/0169-4332(94)00431-5.
99. Teixeira LAC, Santini MC. Surface conditioning of ABS for metallization without the use of chromium baths. Journal of Materials Processing Technology 2005;170:37–41. doi:10.1016/j.jmatprotec.2005.04.075.
100. Domenech SC, Lima E, JR., Drago V, Lima JC de, Borges Jr., N. G, Avila AOV, Soldi V. Electroless plating of nickel–phosphorous on surface-modified poly(ethylene terephthalate) films. Applied Surface Science 2003;220:238–50. doi:10.1016/S0169-4332(03)00815-8.
101. Pinner SH, Simpson WG. Plastics: Surface and Finish: Elsevier Science; 2013.
102. Charbonnier M, Romand M, Goepfert Y, Léonard D, Bouadi M. Copper metallization of polymers by a palladium-free electroless process. Surface and Coatings Technology 2006;200:5478–86. doi:10.1016/j.surfcoat.2005.07.061.
103. Vossen JL. Thin Film Processes: Elsevier Science; 2012.
104. Davis JR, Committee A. Copper and Copper Alloys: ASM International; 2001.
105. Garg S, Thyssen JP, Uter W, Schnuch A, Johansen JD, Menné T, et al. Nickel allergy following European Union regulation in Denmark, Germany, Italy and the U.K. Br J Dermatol 2013;169:854–8. doi:10.1111/bjd.12556.
106. Lee CK. Structure, electrochemical and wear-corrosion properties of electroless nickel–phosphorus deposition on CFRP composites. Materials Chemistry and Physics 2009;114:125–33. doi:10.1016/j.matchemphys.2008.08.088.
107. Maurer C, Schulz U. Solid particle erosion of thick PVD coatings on CFRP. Wear 2014;317:246–53. doi:10.1016/j.wear.2014.05.016.

108. Schulz U. Review of modern techniques to generate antireflective properties on thermoplastic polymers. Appl. Opt., AO 2006;45:1608–18. doi:10.1364/AO.45.001608.
109. Yang J, Han Y, Choy J. TiO2 thin-films on polymer substrates and their photocatalytic activity: EMRS 2005 Symposium ESynthesis, Characterization and Applications of Mesostructured Thin Layers. Thin Solid Films 2006;495:266–71. doi:10.1016/j.tsf.2005.08.195.
110. Mattox DM. Handbook of Physical Vapor Deposition (PVD) Processing: Elsevier Science; 2010.
111. Bialojan W. GM. Vacuum Metallizing Plastic Parts. Products Finishing;October 1992.
112. Eich J. T., Weber E., Abell P., Wagner K. and Mack C. Opportunities for Functional Design Using Physical Vapor Deposition and UV-Curable Coatings. Plastics Decorating;October/November 2014:18–25.
113. Cha SC, Erdemir A. Coating Technology for Vehicle Applications: Springer International Publishing; 2015.
114. Voyer J, Schulz P, Schreiber M. Electrically Conductive Flame Sprayed Aluminum Coatings on Textile Substrates: Journal of Thermal Spray Technology. J Therm Spray Tech 2008;17:818–23. doi:10.1007/s11666-008-9228-7.
115. Knight, R., Ivosevic, M., Kalinidi, S., and Palmese, G. Microstructure and Properties of Thermally Sprayed Functionally Graded Coatings for Polymeric Substrates. Proceedings of the ITSC 2003;2003.
116. Sutter JK, Miyoshi K, Bowman C, Naik SK, Ma K, Sinatra R, et al. Erosion Coatings for Polymer Matrix Composites in Propulsion Applications. High Performance Polymers 2003;15:421–40. doi:10.1177/09540083030154003.
117. Liu A, Guo M, Zhao M, Ma H, Hu S. Arc sprayed erosion-resistant coating for carbon fiber reinforced polymer matrix composite substrates. Surface and Coatings Technology 2006;200:3073–7. doi:10.1016/j.surfcoat.2005.01.042.
118. Ganesan A, Yamada M, Fukumoto M. The Effect of CFRP Surface Treatment on the Splat Morphology and Coating Adhesion Strength: Journal of Thermal Spray Technology. J Therm Spray Tech 2014;23:236–44. doi:10.1007/s11666-013-0003-z.
119. Lopera-Valle A. MA. Use of Flame-Sprayed Coatings as Heating Elements for Polymer-Based Composite Structures. Proceedings of the ITSC 2015, Long Beach, USA May 11–14, 2015.

120. Ashrafizadeh H., Mertiny P., McDonald A. Evaluation of the Influence of Flame Spraying Parameters on Microstructure and Electrical Conductivity of Al-12Si Coatings Deposited on Polyurethane Substrates. Proceedings of the ITSC 2015, Long Beach, USA;May 11–14, 2015.
121. Robitaille F, Yandouzi M, Hind S, Jodoin B. Metallic coating of aerospace carbon/epoxy composites by the pulsed gas dynamic spraying process. Surface and Coatings Technology 2009;203:2954–60. doi:10.1016/j.surfcoat.2009.03.011.
122. Lupoi R, O'Neill W. Deposition of metallic coatings on polymer surfaces using cold spray. Surface and Coatings Technology 2010;205:2167–73. doi:10.1016/j.surfcoat.2010.08.128.
123. Zhou XL, Chen AF, Liu JC, Wu XK, Zhang JS. Preparation of metallic coatings on polymer matrix composites by cold spray. Surface and Coatings Technology 2011;206:132–6. doi:10.1016/j.surfcoat.2011.07.005.
124. Barletta M, Gisario A, Tagliaferri V. Electrostatic spray deposition (ESD) of polymeric powders on thermoplastic (PA66) substrate. Surface and Coatings Technology 2006;201:296–308. doi:10.1016/j.surfcoat.2005.11.120.
125. Ye H, Wang J. Preparation of aluminum coating on Lexan by cold spray. Materials Letters 2014;137:21–4. doi:10.1016/j.matlet.2014.08.119.
126. Affi J., Okazaki H., Yamada M., Fukumoto M. Fabrication of Aluminum Coating onto CFRP Substrate by Cold Spray. MATERIALS TRANSACTIONS 2011;52(9):1759–63. doi:10.11330/jtss.49.42.
127. Giraud D., Borit F., Guipont V., Jeandin M., Malhaire J.M., Metallization of a Polymer Using Cold Spray: Application to Aluminum Coating of Polyamide 66. Proceedings of the ITSC 2012, Houston, Texas, USA 21–24 May, 2012.
128. Burlacov I, Jirkovský J, Kavan L, Ballhorn R, Heimann RB. Cold gas dynamic spraying (CGDS) of TiO2 (anatase) powders onto poly(sulfone) substrates: Microstructural characterisation and photocatalytic efficiency. Journal of Photochemistry and Photobiology A: Chemistry 2007;187:285–92. doi:10.1016/j.jphotochem.2006.10.023.
129. Ganesan A, Yamada M, Fukumoto M. Cold Spray Coating Deposition Mechanism on the Thermoplastic and Thermosetting Polymer Substrates: Journal of Thermal Spray Technology. J Therm Spray Tech 2013;22:1275–82. doi:10.1007/s11666-013-9984-x.
130. Gonzalez R., McDonald A.G., Mertiny P. Damage Detection Method for Fiber-Reinforced Polymer Composites using AL-12SI Flame-Sprayed Coatings. Society of

Advancement of Material and Process Engineering (SAMPE) Conference Seattle, WA, USA, June 2014.

131. Vucko MJ, King PC, Poole AJ, Carl C, Jahedi MZ, Nys R de. Cold spray metal embedment: an innovative antifouling technology. Biofouling 2012;28:239–48. doi:10.1080/08927014.2012.670849.

132. Vucko MJ, King PC, Poole AJ, Jahedi MZ, Nys R de. Polyurethane seismic streamer skins: an application of cold spray metal embedment. Biofouling 2013;29:1–9. doi:10.1080/08927014.2012.741682.

133. Vucko MJ, King PC, Poole AJ, Carl C, Jahedi MZ, Nys R de. Cold spray metal embedment: an innovative antifouling technology. Biofouling 2012;28:239–48. doi:10.1080/08927014.2012.670849.

134. Shafaghi R., Pershin L., Mostaghimi J., Ringuette M. Surface Morphology and Bioactivity of Copper Alloy Coatings. Proceedings of the ITSC 2014, Bsrcelona, Spain 2014.

135. Gutierrez H, Portman T, Pershin V, Ringuette M. Evaluation of biocidal efficacy of copper alloy coatings in comparison with solid metal surfaces: generation of organic copper phosphate nanoflowers. J Appl Microbiol 2013;114:680–7. doi:10.1111/jam.12094.

136. Sharifahmadian O, Salimijazi HR, Fathi MH, Mostaghimi J, Pershin L. Study of the Antibacterial Behavior of Wire Arc Sprayed Copper Coatings. J Therm Spray Tech 2013;22:371–9. doi:10.1007/s11666-012-9842-2.

137. Oliver WC, Pharr GM. An improved technique for determining hardness and elastic modulus using load and displacement sensing indentation experiments. J. Mater. Res. 1992;7:1564–83. doi:10.1557/JMR.1992.1564.

138. Oliver WC, Pharr GM. Measurement of hardness and elastic modulus by instrumented indentation: Advances in understanding and refinements to methodology. J. Mater. Res. 2004;19:3–20. doi:10.1557/jmr.2004.19.1.3.

139. Sutherland's_law. http://www.cfd-online.com/Wiki/Sutherland's_law. Accessed 15.11.205.

140. Rathakrishnan E. Theoretical aerodynamics. Singapore: Wiley; 2013.

141. R. Shanthini. Thermodynamicsfor Beginnerswith worked examples. Peradeniya, Sri Lanka: Science Education Unit; 2009.

142. Koivuluoto H, Vuoristo P. Effect of Powder Type and Composition on Structure and Mechanical Properties of Cu + Al2O3 Coatings Prepared by using Low-Pressure Cold

Spray Process. J Therm Spray Tech 2010;19:1081–92. doi:10.1007/s11666-010-9491-2.

143. Winnicki M, Małachowska A, Dudzik G, Rutkowska-Gorczyca M, Marciniak M, Abramski K, et al. Numerical and experimental analysis of copper particles velocity in low-pressure cold spraying process. Surface and Coatings Technology 2015;268:230–40. doi:10.1016/j.surfcoat.2014.11.059.
144. Watanabe I, Kurtz KS, Kabcenell JL, Okabe T. Effect of sandblasting and silicoating on bond strength of polymer-glass composite to cast titanium. The Journal of Prosthetic Dentistry 1999;82:462–7. doi:10.1016/S0022-3913(99)70035-1.
145. Ajdelsztajn L, Schoenung J, Jodoin B, Kim G. Cold spray deposition of nanocrystalline aluminum alloys: Metallurgical and Materials Transactions A. Metall and Mat Trans A 2005;36:657–66. doi:10.1007/s11661-005-0182-4.
146. Yang S, Evans JRG. Metering and dispensing of powder; the quest for new solid freeforming techniques. Powder Technology 2007;178:56–72. doi:10.1016/j.powtec.2007.04.004.
147. http://www.matbase.com/material-categories/natural-and-synthetic-polymers/engineering-polymers/material-properties-of-polyamide-6-nylon-6-pa-6.html#properties. Accessed 19 Nov 2015.
148. http://www.matbase.com/material-categories/natural-and-synthetic-polymers/engineering-polymers/material-properties-of-polycarbonate-pc.html#properties. Accessed 19 Nov 2015.
149. Ivosevic M, Knight R, Kalidindi SR, Palmese GR, Sutter JK. Adhesive/Cohesive Properties of Thermally Sprayed Functionally Graded Coatings for Polymer Matrix Composites. Journal of Thermal Spray Technology 2005;14:45–51. doi:10.1361/10599630522765.
150. Marshall DB, Noma T, Evans AG. A Simple Method for Determining Elastic-Modulus–to-Hardness Ratios using Knoop Indentation Measurements. Journal of the American Ceramic Society 1982;65. doi:10.1111/j.1151-2916.1982.tb10357.x.
151. Luzin V, Spencer K, Zhang M. Residual stress and thermo-mechanical properties of cold spray metal coatings. Acta Materialia 2011;59:1259–70. doi:10.1016/j.actamat.2010.10.058.
152. Amateau M.F. ET. High- velocity particle consolidation technology. iMAST Quarterly;2000.

153. Antoni Roca,Aránzazu Villuendas,Ignacio Mejía,J.A. Benito,Núria Llorca-Isern,Jordi Llumà,Jordi Jorba. Can Young's Modulus of Metallic Alloys Change with Plastic Deformation? Materials Science Forum 2014;783-786:2382–7. doi:10.4028/www.scientific.net/MSF.783-786.2382.
154. Benito JA, Jorba J, Manero JM, Roca A. Change of Young's modulus of cold-deformed pure iron in a tensile test: Metallurgical and Materials Transactions A. Metall and Mat Trans A 2005;36:3317–24. doi:10.1007/s11661-005-0006-6.
155. Mott NF. CXVII. A theory of work-hardening of metal crystals. The London, Edinburgh, and Dublin Philosophical Magazine and Journal of Science 2010;43:1151–78. doi:10.1080/14786441108521024.
156. Villuendas A, Jorba J, Roca A. The Role of Precipitates in the Behavior of Young's Modulus in Aluminum Alloys: Metallurgical and Materials Transactions A. Metall and Mat Trans A 2014;45:3857–65. doi:10.1007/s11661-014-2328-8.
157. King PC, Zahiri S, Jahedi M, Friend J. Aluminium coating of lead zirconate titanate—A study of cold spray variables. Surface and Coatings Technology 2010;205:2016–22. doi:10.1016/j.surfcoat.2010.08.084.
158. Choi WB, Li L, Luzin V, Neiser R, Gnäupel-Herold T, Prask HJ, et al. Integrated characterization of cold sprayed aluminum coatings. Acta Materialia 2007;55:857–66. doi:10.1016/j.actamat.2006.09.006.
159. Winnicki M. Selected properties of tin and copper coatings deposited on aluminium substrate with low pressure cold spray method [Phd thesis]: Wroclaw University of Technology; 2015.
160. Liu Y, Li X, Zhang Q, Xu C. Study on Microstructure and mechanical properties of Cold Spraying Al coating on Magnesium Alloy. In: ; Dalian, China. doi:10.2991/ipemec-15.2015.43.
161. Ko KH, Choi JO, Lee H. Pretreatment effect of Cu feedstock on cold-sprayed coatings. Journal of Materials Processing Technology 2014;214:1530–5. doi:10.1016/j.jmatprotec.2014.02.020.
162. International AS, Lampman S. Characterization and Failure Analysis of Plastics: A S M International; 2003.
163. Sepe MP, Rapra Technology Limited. Thermal Analysis of Polymers: Rapra Technology Limited; 1997.
164. Olabisi O, Adewale K. Handbook of Thermoplastics: Taylor & Francis; 1997.

165. Bernhard Rosenau, Raquel Fernández Rodiles. Polyamides (PA). Kunststoffe international 2008:82–5.
166. H.M.Soliman A. Effect of Differential Thermal Expansion Coefficient on Stresses Generated in Coating. Journal of Materials Science & Technology 1999;15:457–62.
167. Suzuki S, Ishikawa Y, Isshiki M, Waseda Y. Native Oxide Layers Formed on the Surface of Ultra High-Purity Iron and Copper Investigated by Angle Resolved XPS. Materials Transactions, JIM 1997;38:1004–9. doi:10.2320/matertrans1989.38.1004.
168. Iijima J, Lim J, Hong S, Suzuki S, Mimura K, Isshiki M. Native oxidation of ultra high purity Cu bulk and thin films. Applied Surface Science 2006;253:2825–9. doi:10.1016/j.apsusc.2006.05.063.
169. Yang JC, Kolasa B, Gibson JM, Yeadon M. Self-limiting oxidation of copper. Appl. Phys. Lett. 1998;73:2841. doi:10.1063/1.122608.
170. Ko KH, Choi JO, Lee H, Lee BJ. Influence of oxide chemistry of feedstock on cold sprayed Cu coatings. Powder Technology 2012;218:119–23. doi:10.1016/j.powtec.2011.11.046.
171. Li W, Liao H, Li C, Bang H, Coddet C. Numerical simulation of deformation behavior of Al particles impacting on Al substrate and effect of surface oxide films on interfacial bonding in cold spraying. Applied Surface Science 2007;253:5084–91. doi:10.1016/j.apsusc.2006.11.020.
172. Małachowska A., Winnicki M., Pawłowski L., Pateyron B., Ambroziak A., Sokołowski P. Oxidation of titanium particles during cold gas dynamic spraying. Proceedings of COMSOL conference, Rotterdam, October 23-25, 2013.
173. Pouriayevali H. Describing large deformation of polymers at quasi-static and high strain rates [Phd thesis]: National University of Singapore; 2013.
174. H. Pouriayevali, S. Arabnejad, Y.B. Guo, V.P.W. Shim. A constitutive description of the rate-sensitive response of semi-crystalline polymers.
175. Klein R. Laser welding of plastics. Weinheim: Wiley-VCH; 2012.
176. Argon AS. The Physics of Deformation and Fracture of Polymers: Cambridge University Press; 2013.
177. Grujicic M, Pandurangan B, Bell WC, Daqaq M, Ma L, Seyr N, et al. A computational analysis and suitability assessment of cold-gas dynamicspraying of glass-fiber-reinforced poly-amide 6 for use indirect-adhesion polymer metal hybrid components. Applied Surface Science 2008;254:2136–45. doi:10.1016/j.apsusc.2007.08.077.

178.Radoeva M, Radoev B. Ohm resistivity of electroless copper layers as a function of their thicknesses. J Mater Sci;30:2215–9. doi:10.1007/BF01184563.

179.Gasparin A. L., Baumvol I. J. R., Umpierre A. P., Crespi A. E., Cemin F., Nunes R. C. R. and Giacomelli C. Adhesion measurement of Cu thin films on polyamide and polypropylene substrates. The International Conference on Advanced Materials (ICAM) 20-25 September 2009, Rio de Janeiro, Brasil.

Analiza procesu natryskiwania zimnym gazem oraz określenie wybranych właściwości powłok metalowych na polimerach

STRESZCZENIE

Celem niniejszej rozprawy doktorskiej była analiza możliwości metalizacji powierzchni tworzyw sztucznych za pomocą metody niskociśnieniowego natryskiwania zimnym gazem (z ang. Low-Pressure Cold Spraying – LPCS). Jako podłoże zastosowano dwa polimery: poliamid 6 (PA 6) i poliwęglan (PC). Powłoki zostały wykonane z użyciem proszków: cyny, aluminium i miedzi.

W ramach pracy obliczono prędkość oraz temperatura cząstek proszku podczas procesu natryskiwania. Na podstawie porównania otrzymanych wyników prędkości cząstek proszku do prędkości krytycznej dobrano wstępne parametry procesu. W przypadku bezpośredniego natryskiwania na tworzywo jedynie powłoki cynowe charakteryzowały się akceptowalnym właściwościami. Powłoki aluminiowe miały tendencje do samoistnego odspajania. W przypadku prób nanoszenia proszku miedzi nie udało się uzyskać ciągłej warstwy.

W dalszej kolejności zbadano wpływ morfologii i obróbki cieplnej proszku oraz zastosowania międzywarstw na proces formowania powłoki, co pozwoliło na uzyskanie powłok aluminiowych i miedzianych na powierzchni obydwu tworzyw sztucznych. Dla kompletu uzyskanych powłok (Sn, Al, Cu) przedstawiono zdjęcia mikrostruktury oraz wyniki pomiarów wyniki pomiarów przyczepności, rezystywności, mikrotwardości, modułu Younga, zawartości tlenu w proszku i powłoce.

Mechanizm wiązania cząstek proszku z materiałem podłoża przeanalizowano za pomocą symulacji uderzenia cząstek miedzi i cyny w podłoże poliamidowe w programie Abaqus. Wyniki z symulacji zostały porównane do rezultatów eksperymentalnych.

Całość pracy podsumowano wnioskami oraz przedstawiono możliwości dalszych badań.

Analysis of the cold gas spraying process and determination of selected properties of metallic coatings on polymers

ABSTRACT

The aim of this Phd thesis was to analyze the possibility of metallization of polymers surface using a Low-Pressure Cold Gas spraying method. Two polymers substrate: polyamide 6 (PA 6) and polycarbonate (PC) were investigated. The coatings were deposited using: tin, aluminium and copper powders.

Within the framework of this work powders particles velocity and temperature was calculated during spraying process. The obtained particle velocity was compared to the critical velocity to select initial spraying conditions. Direct spraying on polymers substrate brought acceptable properties only for tin powder. Aluminium coatings delaminated spontaneously after spraying process. In case of copper powder deposition of continuous layer was impossible.

Next, the influence of powder morphology, heat treatment of the feedstock material and the use of interlayers on the deposition process was investigated. Consequently, aluminium and copper coatings were obtained on both polymers. For a set of received coatings (Sn, Al, Cu) microstructure was observed and the results of adhesion, resistivity, micro-hardness, Young's modulus, and oxygen content in powders and coatings measurements were given.

The bonding mechanism of the powder particles with substrate material was investigated using simulation of impact of copper and tin particle on polyamide substrate in Abaqus program. The simulation results were compared to experimental results.

The dissertation was summed up with conclusion and possibilities of further research.

Résumé

Le but de cette thèse de doctorat état d'analyser la possibilité de la métallisation des couches des polymères à l'aide de la méthode de pulvérisation avec du gaz froid sous une basse pression.

La méthode de projection a froid a été invintée par les scientifques de l'Institut de la Mechanique Theorique et Appliquee dans la Section Siberienne de l'Academie Russie des Sciences (ITAM de RAS) à Novosibitsk en Russie dans les anées 80 [1]. Elle utilise la haute énergie kinetique des particules de poudre pour obtenir u dépôt sur le substrat. Le gaz chaud sous haute pression (Air, He, N) est accéléré dans une tuyère habituellement convergant-divergante [2,3]. Toutefois, il est également possible d'utiliser une autre forme, c'est-à-dire le tube convergant.. La poudre est injectée dans le flux de gaz via un injecteur séparée et accéléré suite à la force de résistance avant de forer le substrat.

La formation des revêtement est reliée à la vitesse des particules de poudre. Chaque matériau a une certaine vitesse critique vcr au-dessus de laquelle les particules sont suffisamment déformées plastiquement et collent avec le substrat, en formant un revêtement. Dans le cas de v_{cr} au-dessous, ont lieu surtout des usures et rebonds des particules [3,4]. L'efficacité du dépôt et force de liaison augment avec les particules de vitesse jusqu'a la vitesse d'usure v_{er} quand une autre usure a lieu. Ce schéma est valide seulement pour les matériaux ductiles. Dans le cas de l'usure céramique, elle est dominante indépendamment de la vitesse [2]. Les autres paramétérs importants qui influent sur la formation de liaison sont : l'oxydation des particules, leur taille, température, les propriétés de substrat et du matériau des revêtements [3, 6, 7]. Des nombreuses études numériques et empirique ont été faites pour expliquer la nature de liaison entre les particules des métaux et les substrats. De nos jours, on croit en général que les groupements des cisailles adiabiatiques, qui peuvent être détectées par le microscope, apparaissent dans des régions très déformées quand la vitesse des particules est plus grande que la vitesse critique. Le ramollissement thermique du matériau a aussi un rôle important [2, 8, 9].

Les outils de la projection à froid de la basse et haute pression sont disponibles. Les outils divergent selon le type de gaz de travail, sa pression et par le moyen d'alimentation en poudre [4, 10]. Selon le processus des paramétres (la température du gaz et la pression, la taille des particules de poudre, la forme de la tuyère et la distance de pulvérisation) et le gaz appliqué, les influences des particules de poudre, la vitesse peut être de 200 1200 m/s ou plus [11]. La taille de poudre est entre 5 à 150 µm [11]. Ce mémoire a été fait en utilisant le système de projection à froid sous une basse pression. Cette méthode (LPCS) est un processus dans lequel la pression ne dépasse pas d'habitude 1 MPa et la température varie entre la température ambiante et 873 K [12]. L'air ou le nitrogen sont d'habitude utilises comme des gaz de projection. Comme la vitesse des particules de poudre est assez basse, les matériaux de projection sont limités à Sn, Zn, Al, Cu et Ni. Typiquement, pour mener à l'augmentation de l'efficacité du dépôt du processus et de la force de liaison, il faut ajouter la poudre céramique (d'habitude Al_2O_3 ou SiC) [13-15]. La poudre est dirigée radialement. Le

pre-rechauffement du gaz est fait avec un appareil de chauffage place dans un pistolet de la projection [4, 15]. Les avantages principaux de la méthode LPCS sont le coût d'achat d'equiement très réduit, comme les coûts des gaz des processus et du système de mobilité.

L'origine du travail

La consomption des polymères dans l'industrie augmente suite aux nombreux avantages que par exemple les métaux n'ont pas. Il est plus facile de traiter les plastiques surtout dans la production des formes complexes. Les plastiques sont moins dures après la production, fournissent une densité plus basse et une meilleure résistance à la corrosion. Couvrir la surface du plastique avec une couche permet de combiner les avantages des plastiques avec ceux des métaux. On obtient des composants légers avec une surface plus dure et résistante à l'abrasion et la température. Les couches métalliques assurent une conductivité électrique additionnelle et permettent d'éviter l'accumulation de charge électrique. La littérature montre que la projection à froid pourrait être utilisée dans l'application des couches avec des qualités spécifiques sur la surface de polymères. C'est une technologie relativement nouvelle, dont les coûts d'achat et d'opération sont bas et la qualité est acceptable. L'usage de la projection à froid comme la solution pour l'impression directe est censé de simplifier ce procédé, réduire le temps de production et la surface occupée par les câbles. La technologie employée maintenant est l'utilisation des faisceaux de câbles. Le problème apparaît dans le cas de pièces testées dans les rotors. Les fils du capteur sont colles à la surface des polymères est souvent se décollent à cause de la force centrifuge et la basse énergie de surface de matrix de polymère qui réduit l'adhésion du colle. On croit que les couches pulvérisées auront une meilleure adhésion et une conductivité électrique suffisante.
Les exigences de base pour les couches sont les suivantes :
- Force de liaison suffisante
- Une bonne conductivité électrique
- Stabilité à long-terme
- Une bonne répétabilité des processus d'application des couches et le prix de la production réduit.

Les autres cas ou les polymères metalisses pourraient être utilises sont : les capteurs [16], dégivrage [17], la solution antifouling [18,19]. Il est aussi important, en ce qui concerne la méthode de pulvérisation à froid, qu'il est possible de métalliser les polymères difficiles pour l'application des couches avec des méthodes conventionnelles sans activation [20]. Il semble que même les polymères qui ont des particules de métal incorpores pourraient être utilises comme par exemple une méthode d'activation de surface, ou une surface avec des propriétés bactéricides et antifouling [21]. Par exemple, la méthode de projection à l'arc a été utilisée pour produire le revêtement en alliage Cu Ni Zn sur la surface des chaises dans la salle d'attente des hôpitaux dans le but de réduire le volume de la bactérie Gram-negative Escherichia coli (DH5ȷ) [22]. Il a été démontré que les couches ont un effet bactéricide. En revanche, les couches faites en alliage avec une composition similaire n'avaient pas ces propriétés [23,24].

La méthode de la projection à froid pour les polymères

La littérature mondiale témoigne de succès dans la création des couches à l'aide de la méthode de la projection à froid sur polymères, par exemple sur : l'étain sur PC/ABS, polypropylène, polystyrène et polyamide-6 [25], aluminium sur PEEK [26], cuivre sur PA66 [27] et l'aluminium sur le polycarbonate Lexan [20]. Ces couches avaient une grande densité et moindre porosité. Dans le cas où des doubles couches d'aluminium et cuivre ont été produites, un effet positif a été observé quand le cuivre a été appliqué comme deuxième couche. Comme c'était plus dense, cela a provoqué un compactage d'aluminium et donc une réduction de la porosité [26].L'influence des paramètres technologiques sur la déposition de poudre métallique sur les substrats en plastique a été abordée par Lupoi [25].Il a remarqué que dans le cas de la déposition du cuivre sur ABS et quand le composite a été renforcé avec des fibres de verre, la déposition dépendait des paramètres choisis. La pression du gaz était la plus importante et donc la vitesse des particules de poudre. La pulvérisation à basse pression (0.5 MPa) sans gaz qui chauffe était favorisée, ce qui a permis une déposition de couches de cuivre et d'étain. Quand la pression de 3 MPa a été utilisée sans le réchauffement qui augmenterait la vitesse des particules, surtout l'usure du substrat a été remarqué. Toutefois, il a été perçu [27], que dans le cas de cuivre, pendant que la première couche tendue a été mise, le restant de la déposition était fragmentaire.La plupart de la recherche qui a été faite porte sur les couches des métaux de transition – Al, Cu. Zhou et al [26] ont découvert l'épais Al et Al/Cu sur le polymère de haute performance PEEK450CA30. Affi at al [28] ont réalisé une couche intérmediare déposée par plasma pour obtenir une couche épaise projetée à froid de Al sur CFRP. Les couches obtenues avaient une plus grande conductivité éléctrique que celles deposée par plasma. Giraud et al [29] ont étudié les paramètres de déposition pour Al projeté à froid sur le polymère PA66. Ils ont vu que les couches ont commencé de se former quand la pression était de 1.5 MPa, le gaz avait la température de 473 K, mais les paramètres optimaux sont survenus à 2.5 MPa et 523 K. Il existe des études qui expliquent les différences entre l'interaction des particules de cuivre avec les polymères thermodurcissables et thermoplastiques. Les auteurs [30] ont observé que la déposition des métaux sur le thermodurcissable est plus difficile à cause de la plus grande fragilité. L'impact des particules en poudre provoque l'usure du substrat au lieu d'une déformation plastique. Ils ont réussi à obtenir une couche épaisse de cuivre sur PVC, polymère d'époxyde en utilisant des couches intermédiaires. Pour le PVC, ils ont d'abord projeté la première couche avec de la poudre sphérique. Ils ont en suite utilisé de la poudre dendritique pour obtenir un revêtement épais.

Le but du travail

En se basant sur l'étude de la littérature, la thèse suivant de travail a été formulée :

Il est possible d'utiliser la projection à froid à une basse pression pour faire directement les revêtements des métaux sur les polymères ayant des propriétés similaires aux revêtements depositiones avec des méthode utilisées à ce jour. Le but scientifique est de savoir plus sur les microstructures et les propriétés des revetements depositionnes.Qui plus est, le mécanisme de déposition du métal en poudre sur le substrat de polymère et l'influence des paramètres du processus devraient être connus. Le but pratique état le choix des paramètres de processus permettant la déposition des revêtements d'étain, aluminium, cuivre sur le polyamide 6 et le polycarbonate.

Résultats

Deux substrats thermoplastiques et cinq poudres métalliques ont été étudiés. Les substrats étaient le polycarbonate amorphe et le polyamide 6 semicrystalin. La poudre était : spherique, globulaire, dendrique cuivre, aluminium et étain. Le processus de déposition s'est avéré beaucoup plus complexe que dans le cas du substrat de métal. Les problèmes étaient, entre autres : faible dureté du substrat, comportement fragile dans les basses températures, l'amollissement thermique dans des températures très basses. Le travail a commencé avec un calcul de la vitesse dans une basse pression du processus de pulvérisation a froid. La vitesse calculée pour toutes les poudres sauf l'étain étaient au-dessous de la vitesse critique pour les paramètres acceptables en ce qui concerne la déposition des polymères. Les premières épreuves ont confirmé que la déformation des particules de poudre n'était pas suffisante. Dans le cas de cuivre, il était impossible d'obtenir le revêtement. En plus, la force de liaison était très faible - les revêtements étaient delaminés spontanément. Deux mesures ont été entreprises pour améliorer les résultats : réduire la vitesse critique de la poudre et insérer des couches intermédiaires. Avec ces deux moyens, il a été possible d'obtenir les revêtements en cuivre et alluminium sur PA6 et PC. En s'appuyant sur l'étude, des conditions optimales pour la déposition de revêtement ont été choisies pour la caractérisation. La caractérisation des revêtements a inclu : l'analyse structurelle avec le microscope à la lumière et électronique à balayage, mesure d'adhésion, mesures du module d'Young, résistivité électrique, mesures de micro-dureté, mesures de coefficient de dilatation thermique, mesures de contenu d'oxygène et la simulation FEM pour étudier le mécanisme de déposition.

a) Les mesures d'adhesion

La force d'adhésion des trois métaux - aluminium, cuivre, étain a été testée sur deux substrats - polyamide 6 (PA6) et polycarbonate (PC). Les valeurs de force de liaison des revêtements indépendants de matériau de substrat étaient au niveau similaire, mais il y avait une petite différence en faveur du polycarbonate. La force de liaison de tous les revêtements était au-dessous de 17% de résistance à la traction de polyamide 6 (45 MPa). Le plus grand résultat de force de liaison était pour le fin revêtement en étain - 6 MPa pour PA6 et 7.3 MPa pour PC. Ce résultat était attendu comme l'étain est le matériel le plus facilement

déformable parmi les choisis, mais la force d'adhésion est beaucoup plus basse que dans le cas de revêtement de cuivre sur le métal. En plus, les revêtements étaient fins ~ 100 µm. Dans le cas des revêtements de cuivre plus épais projetés avec un pistolet à vitesse traverse v=1000 mm/min à une fois, la force de liaison a été réduite à 4.3 pour PA6. Le revêtement en aluminium a été projeté sur : substrat non-traité, substrat après le sablage et le résultat était ~0.2 MPa, donc il n'y a pas eu de liaison. Un traitement additionnel (couche intermediaire de cuivre ou sablage à 400°C) avant la pulvérisation l'a augmenté jusque ~4.5 MPa pour PA6 et ~5.3 Mpa pour PC.
Cuivre était le troisième matériau de revêtement. Il a été projeté sur une couche intermediaire Sn+Al2O3 en prenant compte des difficultés déjà décrites concernant l'obtention du revêtement fin d'étain uniforme. La force de liaison des revêtements en cuivre était de 3.5 MPa pour PA6 et 3.4 MPa pour PC qui était au niveau de celles de l'aluminium. Koivuluto et al [32] a observé la force de liaison de cuivre dendrique projeté avec une pulvérisation de basse pression à froid (pression 0.6 MPa et température 813 K) de ~ 7.5 MPa. Elle a augmenté jusque ~17.5 MPa après l'ajout de 50% Al 2 O 3. La valeur obtenue était de ~ 50% de cela. La moindre différence dans la force de liaison sur PA6 et le substrat PC pourrait être attribuée aux propriétés physiques et mécaniques différentes [33, 34].

b) La résistivité électrique

La resistivité éléctrique des revêtements dépositionés sur PA6 et PC a été mesurée avec la méthode de sonde à quatre points. La résistivité de tous les revêtements était d'environ d'un ordre de grandeur plus élevée que le matériau de masse.La différence la plus petite a été obtenue pour les revêtements en étain sur PA6, environ 25% de matériau de masse, mais la valeur la plus basse absolue a été observé pour le revêtement d'Al sur PA6 - 15 µΩcm, ce qui donne 11% IASC.Dans le cas d'aluminium, on peut observer une baisse de résistivité en augmentant le nombre de pulvérisations. Les valeurs de résistivité pour le cuivre étaient proches de celles d'aluminium ou même plus grandes, ce qui était assez étonnant[36].

c) les mesures du module d'Young

Le module élastique a été déterminé avec la méthode d'empreinte de Marshal et al [35] utilisée en général pour les revêtements projetés thermiquement au dépit des difficultés liées à la mesure : microstructure poreuse et préparation de surface qui risque d'influencer assez fort les résultats [36].Cinq revêtements ont été mesurés : deux revêtements en aluminium sur un substrat sablonné pulvérisé en une et deux fois, un revêtement en aluminium projeté sur la couche intermédiaire en étain, le revêtement en cuivre projeté sur Sn+Al2O3 projeté sur le substrat PA6. Le revêtement Al projeté en une fois a obtenu ~ 80% de matériau de masse (données trouvées dans la littérature) ce qui coïncide avec [37]. Les valeurs obtenues pour le revêtement AL2 et Al avec une couche intermédiaire en étain sont

sur le niveau du matériau de masse, environ ~70 and ~67GPa respectivement.Pour le cuivre et l'étain,les valeurs des modules élastiques étaient environ de ~115 GPa and ~46 GPa chacun.

Les revêtements projetés thermiquement ont, d'habitude, des modules élastiques plus bas que les matériaux de masse. Ces résultats sont donc assez inattendus.
Il se peut que cela soit provoqué par le fait de mesurer dans la zone dense du revêtement et d'éviter l'impact de la porosité. Un comportement similaire a été observé dans [36]. La valeur des modules élastiques du revêtement en aluminium mesuré avec la méthode d'indentation était de 74±20 GPa. Toutefois, la technique d'excitation d'impulse a indiqué seulement 49.4 ± 0.2 GPa. Il peut être conclu que la méthode d'indentation risque de ne pas donner des valeurs correctes dans le cas de la porosité pour le revêtement entier, mais pour des zones locales. Ceci est confirmé par la grande valeur de la déviation standard, mais les valeurs restent grandes en comparaison avec les revêtements obtenus avec la méthode de projection à froid sous haute pression. Les mesures transversales en comparaison avec les mesures sur la surface ont apporté des résultats pareils.

d) La simulation

En comparant la simulation aux résultats empiriques, il a été observé que presqu'aucune déformation des particules de cuivre n'a eu lieu. De plus, des polymères serrés et des fissures sur le substrat sont apparus. En se basant sur la simulation, on peut conclure que dans le cas de revêtement en cuivre pur, la température de projection devrait être plus élevée que Tg, même plus rapprochée de Tm, mais avec une basse pression pour éviter le flux des polymères. Après la déposition avec succès de la première couche de cuivre sphérique, le revêtement en entier peut être construit avec les pressions beaucoup plus élevées pour obtenir la vitesse critique pour une poudre. Cela nécessite un vaporisateur en forme de tube dans le but de contrôler totalement la température et la température précise de l'unité de contrôle. Dymet 413 (Obninsk Center for Powder Spraying, Russia), une installation disponible pour vente, n'est pas adapté au processus de métalisation de polymères et devrait être modifiée.

Les conclusions

Il a été supposé au début de la thèse qu'il sera possible d'obtenir des revêtements en metal sur des polymères avec des propriétés semblables aux revêtements depositionés avec des méthodes d'aujourd'hui. Toutefois, les propriétés des revêtements obtenus avec la méthode de projection à froid sous basse pression sont très différentes des propriétés des revêtements obtenus avec des méthodes comme dépôt non-électrolytique, électrodéposition ou PVD.
Premièrement, ils sont beaucoup plus épais et ont une valeur de resisitivite électrique plus

élevée, ce qui dans ce cas, donc dans le cas de dépôt non-électrolytique s'approche de la valeur de cuivre de masse [38]. L'augmentation en resitstivité électrique en comparaison avec projetés thermiquement ont, d'habitude, des modules élastiques plus bas que les matériaux de de masse est typique pour les méthodes de pulvérisation thermique en raison des défauts structurels et d'oxydation. L'adhérence des revêtements est à un niveau similaire, mais ne peut être compare directement comme il y a une grande différence dans l'épaisseur [39]. Il est donc plus raisonnable de comparer les caractéristiques de revêtements obtenus avec d'autres méthodes de projection thermique. Les proprietés sont ici pareilles ou dans certains cas meilleures que celles dans la littérature [26, 28, 40]. L'application des revêtements frabriqués pourrait trouver lieu dans le domaine où les méthodes conventionnelles ne peuvent s'utiliser en raison de par exemple dimension de parties ou d'un grand effort dans la préparation de la surface. Qui plus est, des revêtements épais peuvent se produire facilement, ce qui peut être intéressant dans certains cas. On peut aussi supposer que l'avancement de la technologie basée sur le savoir acquis portera comme fruit une hausse dans les proprettes des revêtements depositionneés sur les polymères. En s'appuyant sur la recherche et l'étude de la littérature, on peut déduire les conclusions suivantes :

- La force de la liaison de la couche du premier matériau est décisive dans l'obtention des revêtements métalliques dans les polymères. Surtout quand on projété du cuivre sur la couche de $Sn+Al_2O_3$, l'usure a été observe en raison de la haute énergie

- La texturation du substrat a un effet positif sur la force de la liaison en raison du meuilleur positionnement mécanique

- Détachement de revêtement a eu lieu entre les particules desposités en premier dans le polymère et le reste du revêtement. Cela peut être occasionné par : non-concordance du coefficient thermique, polymère serré pendant la fixation des particules ce qui empêche une bonne adhérence et ressort comme réaction a l'impact du substrat de polymère

- La conductivité électrique n'est pas directement liée à la porosité des revêtements. Un compactage postérieur de pores pourrait améliorer légèrement les proprietes du revêtement et même si le pore est compressé, il n'y a toujours pas de bon contact électrique.

- La dureté du substrat joue un role tres important dans la formation des revêtements en permettant une bonne deformation des particules qui viennent.

- Les valeurs de microdureté etaient basse en comparaison avec le revetment obtenu dans les substrats metalliques.

- La deposition des revêtements a augementé le nombre de fois, et a un effet negative sur la force de liaison en raison de l'influence thermique de substrat.

Références

1. Irissou E, Legoux J, Ryabinin AN, Jodoin B, Moreau C. Review on Cold Spray Process and Technology: Part I—Intellectual Property. J Therm Spray Tech 2008;17:495–516. doi:10.1007/s11666-008-9203-3.
2. Schmidt T, Assadi H, Gärtner F, Richter H, Stoltenhoff T, Kreye H, Klassen T. From Particle Acceleration to Impact and Bonding in Cold Spraying: Journal of Thermal Spray Technology. J Therm Spray Tech 2009;18:794–808. doi:10.1007/s11666-009-9357-7.
3. Stoltenhoff T, Kreye H, Richter HJ. An analysis of the cold spray process and its coatings: Journal of Thermal Spray Technology. J Therm Spray Tech 2002;11:542–50. doi:10.1361/105996302770348682.
4. Champagne VK. The cold spray materials deposition process: Fundamentals and applications. Cambridge, Boca Raton: Woodhead; CRC Press; 2007.
5. Stoltenhoff T, Voyer M., Kreye H. Cold spraying - state of the art and applicability. Proceedings of the ITSC 2002, Essen, Germany;2002.
6. Borchers C, Gärtner F, Stoltenhoff T, Assadi H, Kreye H. Microstructural and macroscopic properties of cold sprayed copper coatings. J. Appl. Phys. 2003;93:10064. doi:10.1063/1.1573740.
7. Dykhuizen R.C. and Smith M.F. Gas dynamic principles of cold spray.
8. Assadi H, Gärtner F, Stoltenhoff T, Kreye H. Bonding mechanism in cold gas spraying. Acta Materialia 2003;51:4379–94. doi:10.1016/S1359-6454(03)00274-X.
9. Grujicic M, Zhao C, DeRosset W, Helfritch D. Adiabatic shear instability based mechanism for particles/substrate bonding in the cold-gas dynamic-spray process. Materials & Design 2004;25:681–8. doi:10.1016/j.matdes.2004.03.008.
10. Ning X, Jang J, Kim H, Li C, Changhee Lee. Cold spraying of Al–Sn binary alloy: Coating characteristics and particle bonding features. Surface and Coatings Technology 2008;202:1681–7. doi:10.1016/j.surfcoat.2007.07.026.
11. Papyrin A. Cold spray technology. Amsterdam, London: Elsevier; 2007.
12. Maev RG. Introduction to low pressure gas samic spray: Physics & technology. Weinheim: Wiley-VCH; 2007.
13. Irissou E, Legoux J, Arsenault B, Moreau C. Investigation of Al-Al2O3 Cold Spray Coating Formation and Properties: Journal of Thermal Spray Technology. J Therm Spray Tech 2007;16:661–8. doi:10.1007/s11666-007-9086-8.
14. Lee H, Yu Y, Lee Y, Hong Y, Ko K. Cold spray of SiC and Al2O3 with soft metal incorporation: A technical contribution: Journal of Thermal Spray Technology. J Therm Spray Tech 2004;13:184–9. doi:10.1361/10599630419355.
15. Maev RG, Leshchynsky V. Air gas dynamic spraying of powder mixtures: Theory and application: Journal of Thermal Spray Technology. J Therm Spray Tech 2006;15:198–205. doi:10.1361/105996306X108048.
16. Gonzalez R., McDonald A.G., Mertiny P. Damage Detection Method for Fiber-Reinforced Polymer Composites using AL-12SI Flame-Sprayed Coatings. Society of Advancement of Material and Process Engineering (SAMPE) Conference Seattle, WA, USA, June 2014.

17. Lopera-Valle A. MA. Use of Flame-Sprayed Coatings as Heating Elements for Polymer-Based Composite Structures. Proceedings of the ITSC 2015, Long Beach, USA May 11–14, 2015.
18. Vucko MJ, King PC, Poole AJ, Carl C, Jahedi MZ, Nys R de. Cold spray metal embedment: an innovative antifouling technology. Biofouling 2012;28:239–48. doi:10.1080/08927014.2012.670849.
19. Vucko MJ, King PC, Poole AJ, Jahedi MZ, Nys R de. Polyurethane seismic streamer skins: an application of cold spray metal embedment. Biofouling 2013;29:1–9. doi:10.1080/08927014.2012.741682.
20. Ye H, Wang J. Preparation of aluminum coating on Lexan by cold spray. Materials Letters 2014;137:21–4. doi:10.1016/j.matlet.2014.08.119.
21. Vucko MJ, King PC, Poole AJ, Carl C, Jahedi MZ, Nys R de. Cold spray metal embedment: an innovative antifouling technology. Biofouling 2012;28:239–48. doi:10.1080/08927014.2012.670849.
22. Shafaghi R., Pershin L., Mostaghimi J., Ringuette M. Surface Morphology and Bioactivity of Copper Alloy Coatings. Proceedings of the ITSC 2014, Bsrcelona, Spain 2014.
23. Gutierrez H, Portman T, Pershin V, Ringuette M. Evaluation of biocidal efficacy of copper alloy coatings in comparison with solid metal surfaces: generation of organic copper phosphate nanoflowers. J Appl Microbiol 2013;114:680–7. doi:10.1111/jam.12094.
24. Sharifahmadian O, Salimijazi HR, Fathi MH, Mostaghimi J, Pershin L. Study of the Antibacterial Behavior of Wire Arc Sprayed Copper Coatings. J Therm Spray Tech 2013;22:371–9. doi:10.1007/s11666-012-9842-2.
25. Lupoi R, O'Neill W. Deposition of metallic coatings on polymer surfaces using cold spray. Surface and Coatings Technology 2010;205:2167–73. doi:10.1016/j.surfcoat.2010.08.128.
26. Zhou XL, Chen AF, Liu JC, Wu XK, Zhang JS. Preparation of metallic coatings on polymer matrix composites by cold spray. Surface and Coatings Technology 2011;206:132–6. doi:10.1016/j.surfcoat.2011.07.005.
27. Barletta M, Gisario A, Tagliaferri V. Electrostatic spray deposition (ESD) of polymeric powders on thermoplastic (PA66) substrate. Surface and Coatings Technology 2006;201:296–308. doi:10.1016/j.surfcoat.2005.11.120.
28. Affi J., Okazaki H., Yamada M., Fukumoto M. Fabrication of Aluminum Coating onto CFRP Substrate by Cold Spray. MATERIALS TRANSACTIONS 2011;52(9):1759–63. doi:10.11330/jtss.49.42.
29. Giraud D., Borit F., Guipont V., Jeandin M., Malhaire J.M., Metallization of a Polymer Using Cold Spray: Application to Aluminum Coating of Polyamide 66. Proceedings of the ITSC 2012, Houston, Texas, USA 21–24 May, 2012.
30. Ganesan A, Yamada M, Fukumoto M. Cold Spray Coating Deposition Mechanism on the Thermoplastic and Thermosetting Polymer Substrates: Journal of Thermal Spray Technology. J Therm Spray Tech 2013;22:1275–82. doi:10.1007/s11666-013-9984-x.
31. Assadi H, Schmidt T, Richter H, Kliemann J, Binder K, Gärtner F, et al. On Parameter Selection in Cold Spraying. J Therm Spray Tech 2011;20:1161–76. doi:10.1007/s11666-011-9662-9.
32. Koivuluoto H, Vuoristo P. Effect of Powder Type and Composition on Structure and Mechanical Properties of Cu + Al2O3 Coatings Prepared by using Low-Pressure Cold Spray Process. J Therm Spray Tech 2010;19:1081–92. doi:10.1007/s11666-010-9491-2.
33. http://www.matbase.com/material-categories/natural-and-synthetic-polymers/engineering-polymers/material-properties-of-polycarbonate-pc.html#properties. Accessed 19 Nov 2015.

34. http://www.matbase.com/material-categories/natural-and-synthetic-polymers/engineering-polymers/material-properties-of-polyamide-6-nylon-6-pa-6.html#properties. Accessed 19 Nov 2015.
35. Marshall DB, Noma T, Evans AG. A Simple Method for Determining Elastic-Modulus–to-Hardness Ratios using Knoop Indentation Measurements. Journal of the American Ceramic Society 1982;65. doi:10.1111/j.1151-2916.1982.tb10357.x.
36. Luzin V, Spencer K, Zhang M. Residual stress and thermo-mechanical properties of cold spray metal coatings. Acta Materialia 2011;59:1259–70. doi:10.1016/j.actamat.2010.10.058.
37. Amateau M.F. ET. High- velocity particle consolidation technology. iMAST Quarterly;2000.
38. Radoeva M, Radoev B. Ohm resistivity of electroless copper layers as a function of their thicknesses. J Mater Sci;30:2215–9. doi:10.1007/BF01184563.
39. Gasparin A. L., Baumvol I. J. R., Umpierre A. P., Crespi A. E., Cemin F., Nunes R. C. R. and Giacomelli C. Adhesion measurement of Cu thin films on polyamide and polypropylene substrates. The International Conference on Advanced Materials (ICAM) 20-25 September 2009, Rio de Janeiro, Brasil.
40. Ashrafizadeh H., Mertiny P., McDonald A. Evaluation of the Influence of Flame Spraying Parameters on Microstructure and Electrical Conductivity of Al-12Si Coatings Deposited on Polyurethane Substrates. Proceedings of the ITSC 2015, Long Beach, USA;May 11–14, 2015.